THE NEUROSTRUCTURAL EFFECTS OF PRENATAL EXPOSURE TO METHAMPHETAMINE IN AN INFANT POPULATION IN THE WESTERN CAPE.

FLEUR LOUISE WARTON

SUPERVISOR: Ernesta M. Meintjes

CO-SUPERVISOR: Christopher M.R. Warton

Presented for the Degree of

DOCTOR OF PHILOSOPHY

Department of Human Biology

Faculty of Health Sciences

UNIVERSITY OF CAPE TOWN

April 2017

ABSTRACT

Prenatal methamphetamine exposure is associated with functional and neurostructural alterations, but neuroimaging investigations of these effects in infants are almost non-existent. Studies in neonates permit a degree of separation of drug exposure effects from potential confounders in the postnatal environment. Magnetic resonance imaging (MRI) was used to investigate the neurostructural effects of prenatal methamphetamine exposure on neonates recruited from a Cape Town community.

Mothers were recruited during pregnancy and interviewed regarding methamphetamine use. Women in the exposure group used methamphetamine at least twice per month during pregnancy, while control mothers did not use methamphetamine. MRI scans were acquired within the first postnatal month. Anatomical images were processed using FreeSurfer and subcortical and cerebellar structures manually segmented with Freeview. Volumes were regressed with methamphetamine exposure (days/month of pregnancy) and related confounding variables, including total brain volume, gestational age at scan, exposure to cigarette smoking and infant sex. Diffusion data were processed with FSL, and diffusion tensors and tensor parameters determined using AFNI. Probabilistic tractography defined white matter connections between target regions. For the first analysis, five major white matter networks (commissural, and bilateral projection and association networks) were defined between spherical targets. For the second analysis, regions traced in the anatomical study were used as targets. Averaged DTI parameters were then calculated for each connection, and multiple regression analysis determined associations between DTI parameters and methamphetamine exposure at network level and in the individual connections.

Methamphetamine exposure was associated with reduced caudate nucleus volume bilaterally, and in the right caudate following adjustment for confounders. Exposure was associated with

reduced fractional anisotropy in all major white matter networks, and in individual connections within the limbic meso-cortico-striatal circuit. Exposure was associated with increased radial diffusivity in a subset of these.

These results support findings in older children of methamphetamine-induced neurostructural damage, and demonstrate that such effects are already measurable in neonates. Corticostriatal circuit changes may underlie the impaired executive function observed in prenatally exposed children, and suggest a specific mechanism of damage in dopaminergic-related circuits that is consistent with the neurotoxic actions of methamphetamine.

ACKNOWLEDGMENTS

Personal financial support: NRF grantholder-linked bursary (2012); NRF Innovation Doctoral scholarship (2013, 2014) and extension funding (2015); the Duncan Baxter Scholarship through the University of Cape Town (2013); Grantholder-linked funding from NIH (R01HD071664) and NRF SARChI (2016).

This research was supported by NIH grants R01-AA016781, R21-AA020037, R21-AA020332, and R01-HD061485 to principal and collaborative investigators Ernesta M. Meintjes, Joseph L. Jacobson, Sandra W. Jacobson, Lilla Zöllei and Andre van der Kouwe; supplemental funding from the Lycaki/Young Fund, from the State of Michigan (SWJ and JLJ), and the South African Research Chairs Initiative (EM).

With thanks to Sandra Jacobson and Joseph Jacobson for their willingness to extend current studies of prenatal alcohol exposure and the associated established infrastructure in the Child Development Research Laboratory to permit the study of methamphetamine exposure; for design and recruitment, as well as conceptual and statistical guidance, and editing assistance.

Paul Taylor for tutelage, assistance and advice in DTI analysis;

Christopher Molteno and Nadine Lindinger for participation in infant scanning and data gathering;

Andre van der Kouwe, Lilla Zöllei and Pia Wintermark for technical advice;

Emma Ben-Avi for training in the use of FreeView software;

Aaron Hess and Azma Mareyam for their work in constructing the bird cage RF coil used in this study under the supervision of L. Wald, Director MRI Core, Martinos Center for Biomedical Imaging, Radiology, Massachusetts General Hospital;

Cape Universities Brain Imaging Centre radiographers N. Maroof and A. Siljeur;

UCT and WSU research staff M. September, B. Arendse, M. Raatz, P. Soloman and P. O'Leary.

Steven Randall, Marlie Greef, Stevie Biffen, Frances Robertson, Ali Alhamud, Jia Fan, Ken Mbugua and Keri Woods for administrative, software and/ or statistical advice.

With thanks to the Cape Town mothers and infants who participated in the study.

PREFACE

This thesis presents a multi-faceted MRI investigation into the effects of prenatal methamphetamine exposure on the central nervous system of neonates. Methamphetamine abuse is a significant issue in the Cape Flats region of the Western Cape, South Africa, and although some literature exists showing the effects of *in utero* exposure in older children, investigations during the neonatal period are almost non-existent.

This thesis contains three original articles, comprising chapters three to five. Each chapter is presented as an independent article which will be submitted for publication shortly. Each thus follows the traditional journal article format of introduction, methods, results and discussion, permitting the presentation and evaluation of each study. This dissertation format, however, necessitates a degree of repetition, particularly as regards aspects of the background and preliminary methodology in each study. Presented below is a description of each chapter and the contributions of co-authors to each study.

Chapter one is an in-depth introduction, providing a social context to the methamphetamine problem in the geographical region under study, followed by a presentation and analysis of the available literature on the neurostructural effects of methamphetamine use.

Chapter two provides background theory on the embryological development of the nervous system, the anatomical structure and connectivity of the basal ganglia, the mechanisms of action of methamphetamine, which includes a description of dopaminergic neurotransmission under physiological conditions, and the introductory principles of MRI. Chapter two also includes a more thorough description and explanation of some aspects of the methodology which fell outside the scope of the journal article format of chapters three to five.

Chapter three is an article describing a volumetric analysis of subcortical brain regions of neonates using structural MRI. I am the primary author of this article, with assistance from all

co-authors. My primary supervisor, Ernesta Meintjes, provided overall project supervision. Ernesta Meintjes and principal co-investigators Joseph Jacobson and Sandra Jacobson conceptualised the original study as a sub-set of an ongoing longitudinal cohort study investigating the effects of prenatal alcohol exposure in infants from the Cape Flats. As such, neonatal scanning of the infants investigated in this study was performed as part of the larger study and was supervised by Christopher Molteno following a protocol designed by Pia Wintermark. I assisted with the scanning of all infants, and performed the post-processing of each scan, following initial technical assistance from Andre van der Kouwe and Lilla Zöllei with data synthesis. My co-supervisor Christopher Warton provided expert anatomical guidance on manual segmentation. Nadine Lindinger independently retraced nine brains for inter-rater reliability purposes. Ernesta Meintjes, Joseph Jacobson and Sandra Jacobson gave guidance with statistical analysis. I drafted the manuscript, with co-authors providing editorial and technical input on later drafts.

Chapters four and five describe diffusion tensor imaging (DTI) analyses of white matter regions of the scanned neonates. Chapter four details a whole-brain approach, in which global white matter was investigated in five major networks (commissural fibres, and projection and association fibres bilaterally). Chapter five details the use of the regions traced in chapter three as seeds for tractographic analysis of cortico-striatal and mesolimbic white matter connections. As described for chapter 3, these studies formed part of the larger cohort study, and as such, the conceptual and technical contributions by Ernesta Meintjes, Sandra Jacobson, Joseph Jacobson and Christopher Molteno are as described above. Ernesta Meintjes provided overall project supervision. Paul Taylor provided guidance and technical assistance with pre-processing and data analysis, as well as statistical guidance for chapter 4 particularly. Christopher Warton assisted with anatomical analysis and interpretation. I drafted the

manuscripts for both chapters, with technical and editorial input on further drafts from Ernesta Meintjes, Christopher Warton and Paul Taylor.

Chapter six is a summary and evaluation of the findings in the light of previous literature, and discusses patterns and potential mechanisms of methamphetamine effects and the possible functional significance thereof.

CONTENTS

ABBREVIATIONS

AA: absolute alcohol

AD: axial diffusivity

ADHD: attention deficit/ hyperactivity disorder

CC: corpus callosum

CNS: central nervous system

COMT: catechol-*O*-methyl transferase

DAT: dopamine transporter

DT: diffusion tensor

DTI: diffusion tensor imaging

DW: diffusion weighted

DWI: diffusion weighted imaging

EPI: echo planar imaging

FACT: fiber assessment by continuous tracking

FACTID: fiber assessment by continuous tracking including diagonals

FID: free induction decay

FLASH: fast low angle shot

fMRI: functional magnetic resonance imaging

MAO: monoamine oxidase

MBP: myelin basic protein

MD: mean diffusivity

MRI: magnetic resonance imaging

MRS: magnetic resonance spectroscopy

MSN: medium spiny neuron

OFC: orbitofrontal cortex

PD: proton density

RF: radiofrequency

RD: radial diffusivity

ROI: region of interest

SNR: signal-to-noise ratio

TE: time to echo

TR: repetition time

VMAT-2: vesicular monoamine transporter 2

WM-ROI: white matter region of interest

CHAPTER 1

INTRODUCTION

Methamphetamine is one of the most widely used illicit drugs, with recent estimates suggesting that global amphetamine use is second only to cannabis[1]. Amphetamine dependency was determined in 2010 to have a global point prevalence of 0.25%[1], making it one of the two most common drug dependencies worldwide[2].

With the transition to democracy in the 1990s and the associated rapidly changing social and economic landscape, drug availability and abuse has become a significant societal pathology in South Africa[3,4]. The lifetime prevalence of substance use disorders in South Africa has been estimated at over 13%[5], which includes a high incidence of alcohol abuse and the use of illicit drugs such as marijuana, cocaine, amphetamines and opiates[4]. Prior to 2002, methamphetamine was relatively rarely used and unavailable, with only 0.2-0.7% of patients in substance abuse treatment centres in the greater Cape Town area reporting methamphetamine as their primary drug of abuse[6,7]. However, the rate of methamphetamine use has increased sharply since then. In 2006, the proportion of patients reporting methamphetamine as their primary drug of abuse was 52%[6], and another study suggested it to be as high as 59%[7]. The Western Cape province reports the highest incidence of methamphetamine use in South Africa[8], where it is particularly high in the 'Coloured' communities of the Cape Flats[3,4,8]. The term 'Coloured' is a demographic descriptive which originated in the apartheid era and is used to refer to individuals of mixed ancestry (African, European and/ or Asian)[8,9]. Methamphetamine use on the Cape Flats has been strongly linked with the pervasive and unique gang culture of the area[4], and is associated with increased interpersonal violence, mental health issues and sexual risk behaviours[10–12].

Methamphetamine is a psychostimulant, acting primarily to increase extracellular levels of the neurotransmitters dopamine, serotonin and norepinephrine in the central nervous system

(CNS)[13]. The mechanisms by which it modulates neurotransmitter levels are not fully understood, but are distinct from normal physiological transmitter release via secretory vesicle fusion[14], and appear to involve reverse transport of monoamines through membrane and vesicle transporters[15,16]. Although methamphetamine alters the release of several neurotransmitters, research has focused chiefly on the activity of methamphetamine in dopaminergic systems, given the fundamental role that this transmitter plays in cognition, motivation and reward[17].

A considerable body of literature provides cogent evidence that methamphetamine induces damage in the CNS. Structural magnetic resonance imaging (MRI) studies show that methamphetamine use is associated with volume alterations of striatal[18–20] and cortical[21,22] regions, as well as of the hippocampus and amygdala[23–25]. Diffusion tensor imaging (DTI) permits the visualisation and characterisation of white matter, and the determination of microstructural alterations in fibre bundles within the brain by means of analysis of water molecule diffusion in specific regions of interest[26,27]. DTI studies have revealed reduced microstructural integrity in frontal white matter and corpus callosum (CC)[28–31] in individuals who used methamphetamine, while investigations using magnetic resonance spectroscopy (MRS) show methamphetamine-associated alterations in neurometabolites in frontal white matter and basal ganglia[32–37]. Methamphetamine users have been shown to exhibit functional deficits in a range of domains, including poorer executive function[38,39], inhibition[40], cognitive control[29,41] and attention[42,43], and increased impulsivity[44,45], as well as increased incidence and severity of psychiatric symptoms[46–48]. Several studies additionally showed these functional deficits to correlate with specific structural changes, including reduced density of dopamine receptors[45] and transporters[47–49] in striatal and prefrontal regions, and functional MRI (fMRI) investigations of methamphetamine users have demonstrated reduced activation of prefrontal cortical regions in the performance of tests of executive function compared to controls[41,50–52].

Peak methamphetamine prevalence has been shown to occur between 20-35 years of age[1]. It is thus to be expected that a proportion of women will use methamphetamine while pregnant. In the United States, the incidence of pregnant women seeking treatment for methamphetamine abuse rose from 8% in 1994 to 24% in 2006[53]. Arria and colleagues determined that 5.2% of pregnant women in a 4-centre study in the United States had used methamphetamine during pregnancy[54]. Within the vulnerable social context of the Cape Flats, use of methamphetamine by pregnant women is not uncommon[8], particularly in the light of the increased incidence of sexual risk behaviours[6], including significantly reduced condom use[55], by methamphetamine-using women of child-bearing age. In one investigation of drug-using women on the Cape Flats, 92% of pregnant Coloured women reported methamphetamine as their drug of choice[56]. A significant number of children in this community are thus exposed to methamphetamine during prenatal development, making investigations into the effects of such exposure a matter of priority.

Methamphetamine use during pregnancy has been observed to be associated with increased risk of perinatal complications. It causes vasoconstriction and reduced blood flow to the placenta[57], with consequent restriction of oxygen and nutrient supply to the fetus[58]. These infants experience reduced intrauterine growth[59] and are more likely to be born early[60–62] and small for gestational age[63–66]. In the neonatal period they exhibit increased signs of stress and lower arousal[67–69].

In the light of these general physiological effects, and given the aforementioned neurotoxicity of methamphetamine in adult users, and its documented ability to cross the placenta[70,71] it is to be expected that exposure to methamphetamine during the prenatal period will result in similar damaging effects on the infants concerned. The CNS undergoes rapid growth and development during this period[72], with dopaminergic neurons and receptors appearing within the first few months of gestation[73]. Exposure to the neurotoxic insult of methamphetamine *in utero* may

thus induce long-term modifications in neuronal circuits which have been shown to be affected in adult users.

Investigation of the behavioural, psychological and cognitive characteristics of children with prenatal exposure to methamphetamine suggest that the effects are subtle but definite. Compared to unexposed controls, methamphetamine exposed infants display poorer quality of movement[67] and delayed motor development[74], and exhibit deficient fine motor performance in the first three postnatal years[74,75]. Poor psychomotor development and emotional adjustment was observed in methamphetamine exposed children at four years old[76], and a follow-up investigation of the same cohort noted aggressive behaviour at eight years of age[77], a finding which was similarly observed in a larger multi-site investigation of school-age children[78]. Methamphetamine exposure has also been associated with increased risk of affective problems such as anxiety and depression[79,80]. A number of investigations have demonstrated that children with prenatal exposure to methamphetamine have deficits in executive function[80–82], including poorer inhibitory control[83,84], and an increased incidence of the symptoms and clinical diagnosis of attention deficit/ hyperactivity disorder (ADHD) has been noted[79,85].

Given these functional outcomes, it is reasonable to assume that they might be underpinned by structural changes in the CNS, and there is a small but convincing body of literature which suggests that such changes do indeed occur following prenatal exposure to methamphetamine.

MRI provides non-invasive means for the investigation of structural, metabolic and functional characteristics of the CNS, and is thus a valuable tool for measuring potential neurological changes associated with prenatal drug exposure[26]. An fMRI study showed that children with prenatal methamphetamine exposure performed more poorly than controls in a verbal memory task, and activated more diffuse brain regions, including medial temporal, parietal and frontal cortex and the basal ganglia, in order to achieve a comparable level of performance to that of

the unexposed controls[86]. Exposed children were similarly shown to exhibit deficits in a task of working memory, and displayed reduced recruitment of the thalamus and left frontal cortex and basal ganglia compared to unexposed control children[87]. Altered levels of neurometabolites in the striatum and frontal white matter following methamphetamine exposure have been observed in several MR spectroscopy studies[88,89], suggesting that such exposure is associated with alterations in metabolism in these regions.

The neuroimaging literature investigating the structural changes associated with prenatal methamphetamine exposure is extremely limited. A handful of DTI studies have demonstrated that such exposure is associated with white matter changes, but the results are not unanimous as to the exact nature of these changes. Reduced fractional anisotropy (FA) and increased diffusion have been observed in white matter connections traversing striatal, limbic and frontal regions of 6-7 year-olds with prenatal methamphetamine exposure[82]. Similar changes were noted in the corona radiata of methamphetamine- and tobacco- exposed infants in the first four postnatal months[90]. Other research, by contrast, found methamphetamine exposure to be associated with increased FA and reduced diffusivity in the genu and splenium of the CC, frontal and parietal white matter, and basal ganglia of 3-4 year-olds[91], and with higher FA in the genu, corona radiata and internal and external capsules of 9-11 year old children[92].

Methamphetamine exposure *in utero* has been shown in a small number of anatomical MRI studies to be associated with volume changes of specific brain regions. In children with concomitant methamphetamine and alcohol exposure, volumes of the striatum, thalamus and left parieto-occipital and right anterior prefrontal cortices were reduced, while anterior and posterior cingulate, ventral and medial temporal lobes and bilateral perisylvian cortices were increased in volume compared to unexposed control children, with volume changes in the methamphetamine and alcohol exposed subjects more severe than those observed in the cohort with alcohol exposure alone[93]. Reduced volumes of putamen and pallidum, with a trend

towards reduction in the volumes of the caudate, thalamus, hippocampus and cerebellum, were observed in another study of methamphetamine exposed children of a similar age, and the pallidal, putamenal and hippocampal changes correlated with poorer performance on tasks of sustained attention, verbal memory and visual motor integration[94]. In a study of 3-5 year-old children with prenatal methamphetamine and tobacco exposure, caudate volumes were significantly reduced and orbitofrontal and perisylvian cortical volumes were increased, with the former inversely related to a measure of cognitive flexibility[95]. In contrast to these findings, however, one study found increased striatal volumes in methamphetamine-exposed 6-year-olds[96].

A coherent body of research thus demonstrates that exposure to methamphetamine in utero has considerable and persisting effects on the brain, with effects repeatedly being observed in dopaminergic regions such as the basal ganglia and fronto-striatal circuitry, as well as in certain non-dopaminergic areas such as the hippocampus, thalamus, and cerebellum. The literature is, however, extremely sparse, and somewhat equivocal as to the exact direction of the observed changes. As Chang and colleagues observed, further detailed morphometric studies of the neurostructural changes associated with prenatal methamphetamine exposure are imperative in order to determine more clearly the alterations exhibited by these children[88]. Furthermore, investigations of prenatal drug exposure are inherently confounded by the effects of post-natal environment. The latter is likely to be suboptimal for a child born to a mother using methamphetamine[59,60,65,81], and this itself will exert a strong effect on neural development that is distinct from the effects of prenatal drug exposure but may be difficult to quantify. These issues can largely be mitigated by investigations during the neonatal period. Studying neonates permits the separation of the effects of prenatal exposure from potential confounding effects in the postnatal environment. To our knowledge, however, only one study has investigated white

matter changes during the neonatal period[90], and no research has examined potential volumetric changes in neonates following prenatal exposure to methamphetamine.

The aim of the following studies was therefore to explore the neurostructural changes in neonates who were exposed to methamphetamine *in utero*, as compared to unexposed control infants, in a study sample drawn from the Cape Flats region of the Western Cape. The first study investigated potential volumetric changes in subcortical regions by means of manual segmentation of anatomical MR images. The second and third studies used DTI to investigate white matter alterations, in three major white matter classes, and specific fronto-striatal circuits, respectively.

CHAPTER 2

BACKGROUND

2.1 EMBRYONIC DEVELOPMENT OF THE CENTRAL NERVOUS SYSTEM

(See Refs[97–104])

2.1.1 Neurulation and proliferation

At the end of the third week of gestation the embryo is a three-layered disc, consisting of the endoderm, the intermediate mesoderm and the ectoderm. Within the ectoderm are the neuroectodermal stem cells located along the rostro-caudal midline in a region referred to as the neural plate. Primary neurulation, or development of the neural tube, begins in weeks 3-4 of gestation, and involves invagination and dorsal closure of the neural plate. The neural tube will ultimately form the CNS, with the spinal cord arising from the caudal aspects of the neural tube and the rostral region giving rise to the brain. Following the closure of the neural tube, cell proliferative areas are formed in the ventricular and subventricular zones surrounding the developing ventricular system. From these proliferative regions all the cells of the CNS are derived: the ventricular zone gives rise chiefly to neurons, while the subventricular zone produces both neurons and glial cells, with neural progenitor cells developing mainly between weeks 3 and 23 and glial cells from week 18 onwards. Cell proliferation in the rostral region of the neural tube results in the formation of three initial vesicles, the prosencephalon, or forebrain, the mesencephalon (midbrain), and the rhombencephalon (hindbrain). The forebrain and hindbrain vesicles later divide to form the telencephalon and diencephalon, and the metencephalon and myelencephalon, respectively (see Table 2.1).

2.1.2 Neuronal migration

From the third gestational month, neuronal migration occurs. Most neurons migrate actively in a radial pattern along a scaffold of glial cells, with earlier neurons finding their final location

Table 2.1. Major subdivisions of the embryonic central nervous system with their associated mature structures.

Three-vesicle stage	Five-vesicle stage	Mature structures
Forebrain (prosencephalon)	Telencephalon	Cerebral cortex, basal ganglia, hippocampus, amygdala, olfactory bulb
	Diencephalon	Thalamus, hypothalamus, subthalamus, epithalamus, retina, optic nerves/ tracts
Midbrain (mesencephalon)	Mesencephalon	Midbrain
Hindbrain (rhombencephalon)	Metencephalon	Pons and cerebellum
	Myelencephalon	Medulla

(Adapted from Ref[99])

in deeper layers of cortex and those of later generations settling in the more superficial layers. The earliest neurons to migrate form the preplate, which is the first recognisable cortical layer and which is present from about week 5 to week 8. The preplate then develops to form the cortical plate, which is bounded by the marginal zone superficially and the subplate on its inner side. The subplate plays an essential role in the organisation of the cerebral cortex and its connections. Differentiation of neurons occurs to some extent during migration, but the sprouting of axonal and dendritic processes takes place chiefly once the cells have reached their final location. The subplate provides a temporary waiting region for afferent fibres projecting from the thalamus, brainstem nuclei, basal forebrain and ipsilateral and contralateral hemispheres, and may also be involved in guiding cortifugal axonal projections. As the target neurons in the cortex mature, the afferent fibres relocate to the cortical plate and the subplate neurons undergo apoptosis. The subplate begins to regress in the third trimester of gestation and is gone by the sixth postnatal month.

2.1.3 Synaptogenesis

Cellular differentiation and organisation of the cortex occurs with increasing synaptogenesis. Once a neuron has reached its final position, it develops connections with other neurons. Developing axons are guided by their terminal growth cones, which respond to chemoattractor or chemorepellent cues, to form short projections, as in the case of interneurons, or significantly lengthier connections, such as those found in the monoaminergic systems, CC or corticofugal pathways. Formation of the latter leads to the development of long-distance bundles. Dendritic tree development occurs relatively slowly through the first two trimesters, and accelerates during the third trimester, with those of the subplate and deep cortical neurons maturing earlier than the more superficial cortical dendrites. As the dendritic and axonal connections develop,

synaptogenesis increases. The first synapses form in the spinal cord during the sixth gestational week, and in the cortex at around 7 weeks. Synaptic density increases homogeneously in the cortex until around 22 weeks, after which it rapidly accelerates in a region-specific manner until well after birth. Maximum synaptic density in the primary sensory areas occurs at 3 postnatal months, while in the prefrontal cortex maximum density is not reached until 15 months of age.

2.1.4 Neural regression

An important aspect of neurodevelopment is the orchestrated loss of neural elements. This consists of two main regressive phenomena intended to shape the structure and connectivity of the CNS, each of which are sensitive to exogenous factors to some extent. Programmed cell death, or apoptosis, is a process whereby cells undergo regulated cellular and molecular events which culminate in their death, and is essential in controlling the population of both neurons and glial cells. Significant numbers of cells in all brain regions are eliminated in this manner, with neural apoptosis occurring chiefly during the prenatal period while glial cell death occurs over a more protracted period that is predominantly postnatal. The second regressive process is synaptic pruning, which follows an initial vigorous overproduction of synaptic connections. This involves axonal retraction and elimination of a substantial proportion of connections and is essential for shaping local connectivity.

2.1.5 Glial cells

Glial cells surround and provide support for neurons in the CNS, and include two main forms: microglia and macroglia. Microglia infiltrate the brain during the fifth week of gestation and progressively colonise and cluster in different regions over the following weeks. They are

macrophages and fulfil essential immune functions within the brain, but are additionally involved in neurogenesis and synaptogenesis, the establishment of brain vasculature, and support of myelination during neurodevelopment.

The two main forms of macroglial cells are astrocytes and oligodendrocytes. The latter are responsible for the myelination of axons in the CNS, while astrocytes have a range of functions which include extracellular regulation, neurotransmitter removal and modulation of synaptic structure and function. Macroglia arise from neural progenitor cells, with astrocytes developing after neurons but prior to oligodendrocytes in any given region of the CNS. Oligodendrocytes mature in four stages, namely, early and late oligodendrocyte progenitors, and immature and mature oligodendrocytes.

2.1.6 Myelination and formation of white matter tracts

Myelination, or the ensheathment of axons in myelin, is the final stage of white matter development and occurs subsequent to axonal development and pruning. During the pre-myelinating phase, oligodendrocyte precursors proliferate and migrate, and form initiator processes which align themselves along axons. This is followed by the true myelination phase. Oligodendrocyte processes elongate and wrap around the axon, ultimately effecting several spiral turns that produce a more compact sheath. The myelin sheath matures in three stages. The premyelin sheath consists of immature oligodendrocytes and contains no myelin basic protein (MBP), an essential constituent of the mature myelin sheath. This is followed by the development of a transitional sheath, which contains MBP in some layers. The mature myelin sheath consists of mature oligodendrocytes and is characterised by MBP in all layers.

Myelination is a predominantly postnatal process, although it occurs from the second half of pregnancy. The oligodendrocyte progenitors form during the embryonic phase (the first eight

weeks following conception), but only begin to proliferate and transform into oligodendrocytes in the 20th gestational week. Myelination of fibre tracts is significantly regionally asynchronous, and appears to follow the hierarchy of processing needs within the cortical connections, with regions responsible for low-level processing maturing earlier than those involved in higher functions. Despite the protracted development and maturation of the myelin sheath, however, all major white matter fibre systems are in place and identifiable at term.

2.1.7 Neurotransmitters

Neurotransmitters and neuromodulators play a significant part in the migration and differentiation of neural cells, and are essential for the modulation of synaptic connections. The presence and activity of transmitters ensure the survival of synapses, as neurons which do not release neurotransmitters undergo apoptosis following synaptogenesis. Environmental cues are important in the determination of neurotransmitter type for precursor neurons.

The major neurotransmitters are present from early in the embryonic period. Catecholaminergic neurons are generated around the time of the formation of the telencephalic vesicle, and these neurotransmitters appear to be involved in gene regulation, and the regulation of the development, migration and maturation of cortical neurons. Dopaminergic cells are detectable in the spinal cord, medulla, pons, mesencephalon and hypothalamic region from the 6th gestational week, while noradrenergic cells are identifiable in the pons, medulla and locus coeruleus at the same age. Two weeks later monoaminergic fibres make contact with the cortical anlage, and by 13 weeks they have reached the cortical plate. Dopaminergic and noradrenergic connections become detectable throughout the cerebral cortex between 20 and 24 weeks, and by this stage their pattern of innervation resembles that of the adult brain, although dopaminergic innervation continues to develop for many years postnatally.

Serotonergic cells appear between the 5th and 12th gestational weeks, but serotonin is detectable long before that and is involved in the early development of the heart and craniofacial structures. Serotonergic neurons project to the forebrain during development and appear to play a role in the differentiation of neuronal progenitor cells and particularly in the detailed development of the sensory cortex and hippocampus. Serotonergic axons project throughout the cortex at birth, but their distribution declines significantly within the first postnatal month.

Cholinergic neurons innervate the cortex around week 20, and appear to play an important role in cortical development and plasticity. Markers of acetylcholine are present earlier in the brainstem region, however. The amino acid transmitters, glutamate, aspartate, GABA and glycine, are suggested to be involved in neuronal wiring and cellular architecture.

2.2 FUNCTIONS AND CONNECTIVITY OF THE BASAL GANGLIA CIRCUITS

(See Refs[17,99,105–107])

2.2.1 Anatomical components of the basal ganglia

The cerebral hemispheres are derived from the embryonic telencephalon, and make up the largest part of the brain. They include the cerebral cortex and underlying white matter, as well as several subcortical structures: the basal ganglia, the amygdala and the hippocampus. The basal ganglia work synergistically with the cortex to plan and execute motivated behaviours that require limbic, cognitive and motor functionalities. They are associated with many aspects of goal-directed behaviour leading to motor output, including emotion, motivation and cognition and the involvement of these elements in the control and production of movement. Within the basal ganglia, different regions are structurally and functionally involved in circuits subserving each of these modalities. Ventral regions are significant in reward and

reinforcement, while the central regions play a role in cognitive functions including memory and learning. The dorsolateral aspect of the basal ganglia functions in the control of movement.

The basal ganglia consist of the striatum, the globus pallidus, the substantia nigra, and the subthalamic nucleus. The striatum can be divided into three regions: the caudate nucleus, the putamen, and the ventral striatum. The latter denotes that portion of the striatum which extends ventrally, and includes the nucleus accumbens, the medial and ventral parts of the caudate and putamen, and the olfactory tubercle. At its lateral and dorsal borders the ventral striatum merges with the dorsal striatum. The nuclei of the dorsal striatum, the caudate and the putamen, are divided by the internal capsule, a prominent area of white matter fibres connecting the thalamus and cerebral cortex. The globus pallidus and substantia nigra give rise to the major basal ganglia output projections. The globus pallidus is divided into the internal and external segments, while the substantia nigra consists of the pars reticulata and pars compacta. The pars compacta is continuous medially with the ventral tegmental area.

2.2.2 Functional connections within the basal ganglia

The striatum receives all major inputs to the basal ganglia, including excitatory glutamatergic afferents from the cortex and thalamus (see Fig. 2.1). The majority of neurons within the striatum are GABA-ergic medium spiny neurons (MSNs). These are both the targets of the input from the cortex, and the projection neurons responsible for all striatal output. The internal pallidum and the substantia nigra pars reticulata are the output nuclei of the basal ganglia. Their projections are GABA-ergic and exert a tonically inhibitory effect on target nuclei in the thalamus and brainstem. Two parallel pathways modulate the basal ganglia output: the direct and indirect pathways. In the direct pathway, the internal pallidum and substantia nigra pars reticulata receive inhibitory afferents directly from the striatum. In the indirect pathway, the

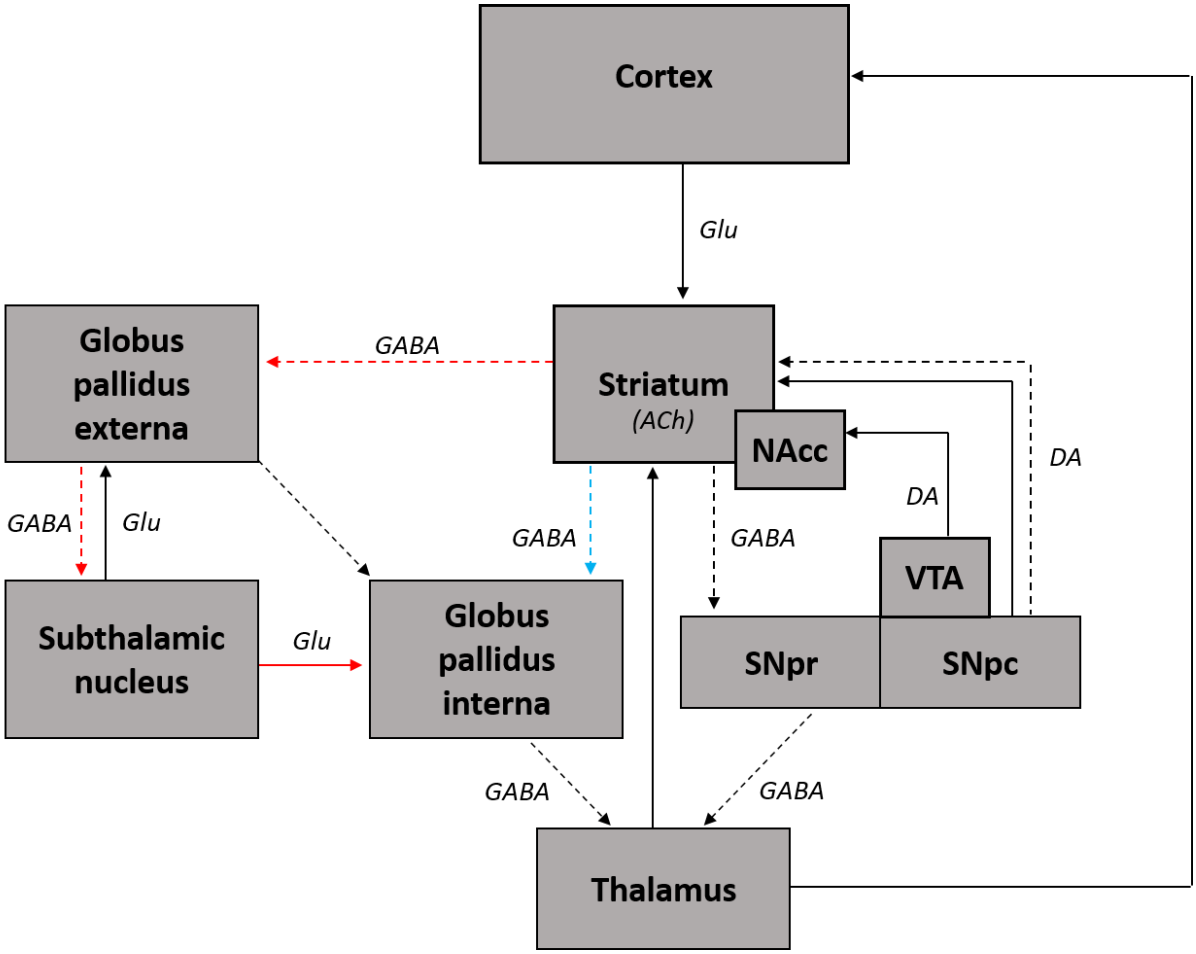

Figure 2.1. Diagrammatic representation of the major connections of the basal ganglia. Solid lines indicate excitatory connections; dashed lines indicate inhibitory connections. The direct pathway is indicated by blue lines, while the indirect pathway is depicted by red lines. DA: dopamine; Glu: glutamate; Ach: acetylcholine is the neurotransmitter produced by striatal interneurons. (Adapted from Ref[112]).

---

striatum sends projections to the globus pallidus pars externa, which in turn projects to the subthalamic nucleus. The subthalamic nucleus then sends excitatory glutamatergic projections to the output nuclei. The thalamus completes the circuit by sending excitatory projections to the cortex. Activation of the direct pathway results in disinhibition of the thalamus and consequent activation of the thalamocortical neurons, while activation of the indirect pathway inhibits the thalamus and reduces thalamocortical neuronal firing.

2.2.3 Connections of the midbrain dopamine system

The substantia nigra pars compacta and ventral tegmental area consist largely of dopaminergic cell bodies. The former give rise to fibres which synapse with MSNs of the dorsal striatum, in what is called the nigrostriatal pathway. Striatal MSNs can be divided into those which express D_1 dopamine receptors, and those which express D_2 receptors; these form part of the direct and indirect pathways respectively. Broadly speaking, D_1 receptors have an excitatory effect on their associated MSNs, while D_2 receptors are inhibitory. Neurons of the nigrostriatal projection thus facilitate activation of the direct pathway, or inhibit the indirect pathway. It has been suggested that the direct and indirect pathways may act synergistically under the influence of dopamine. In this model, the direct pathway rapidly primes a range of potential actions in several parallel pathways; the indirect pathway then inhibits those with weak reward association, to select the most appropriate or desirable response based on current physiological needs[107].

Dopaminergic cells of the ventral tegmental area give rise to fibres which project primarily to the ventral striatum, and in particular the nucleus accumbens – the mesolimbic pathway. Dopaminergic fibres in the mesocortical pathway project from the ventral tegmental area and substantia nigra pars compacta to a number of cortical regions, with synapses in layer 1 of cortex acting as general cellular modulators while synapses in layers V and VI directly modulate corticostriatal and corticothalamic connections. The midbrain receives modulatory inputs from the cortex, striatum and globus pallidus.

A fourth dopaminergic pathway, the tuberoinfundibular pathway, projects from the arcuate nucleus of the hypothalamus to the median eminence and is involved in the inhibition of prolactin release from the pituitary.

2.2.4 Parallel corticostriatal circuits

The frontal cortex drives the basal ganglia, with several topographically and functionally distinct pathways responsible for controlling the components of goal directed behaviour. It can be divided into several anatomical and functional regions: the medial and orbitofrontal cortex (OFC), responsible for motivation and reward; the dorsolateral prefrontal cortex, responsible for executive functions; and the premotor and motor regions, responsible for planning and execution of motor function. The corticostriatal pathways preserve a distinct topographical organisation throughout each circuit. Projections from motor cortex terminate chiefly in the dorsolateral putamen; those from caudal premotor regions project to an adjacent putamenal area and slightly into the caudate nucleus, while the rostral premotor cortex sends fibres to both the putamen and caudate. Projections from somatosensory parietal cortex also synapse in these regions of the dorsal striatum, enabling sensorimotor integration and planning. The dorsolateral prefrontal cortex projects chiefly to the rostral striatum. The lateral OFC sends afferents to the central and lateral ventral striatum, while the medial OFC projects to the medial wall of the caudate and into the nucleus accumbens. The ventral striatum also receives afferents from the hippocampus and amygdala.

2.3 METHAMPHETAMINE: PHARMACOLOGY AND MECHANISMS OF ACTION

2.3.1 Dopamine neurotransmission

(See Refs[99,105,108–112])

Dopamine is a relatively slow-acting catecholaminergic neurotransmitter which functions generally to modulate glutamatergic and GABA-ergic neuronal activity. Under normal conditions, it is synthesised in the neuronal cell body by the sequential hydroxylation and decarboxylation of tyrosine by the enzymes tyrosine hydroxylase and dopa decarboxylase (see

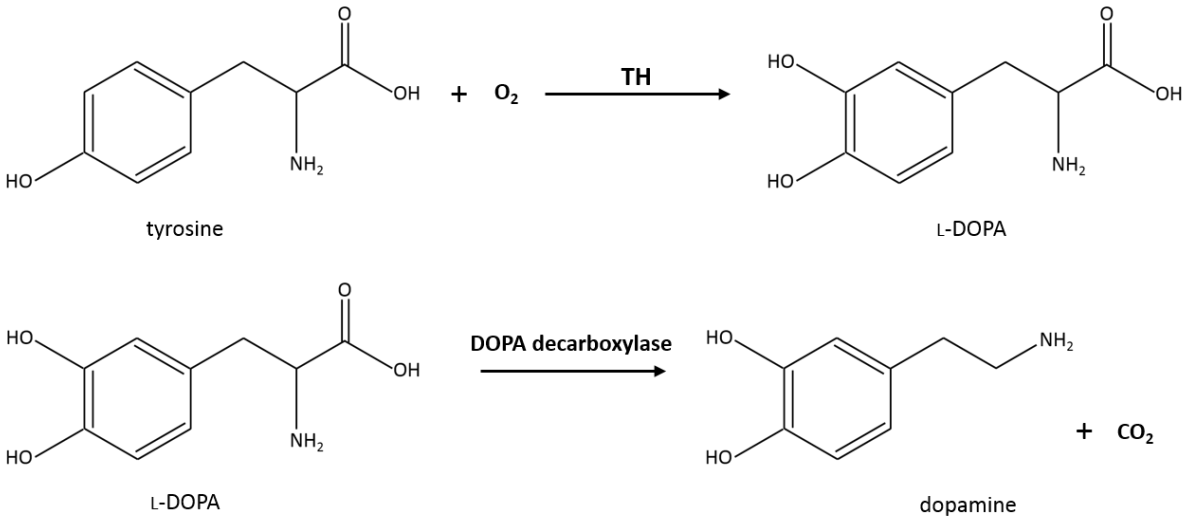

Figure 2.2. Synthesis of dopamine from the amino acid tyrosine. (Adapted from Ref[99]).

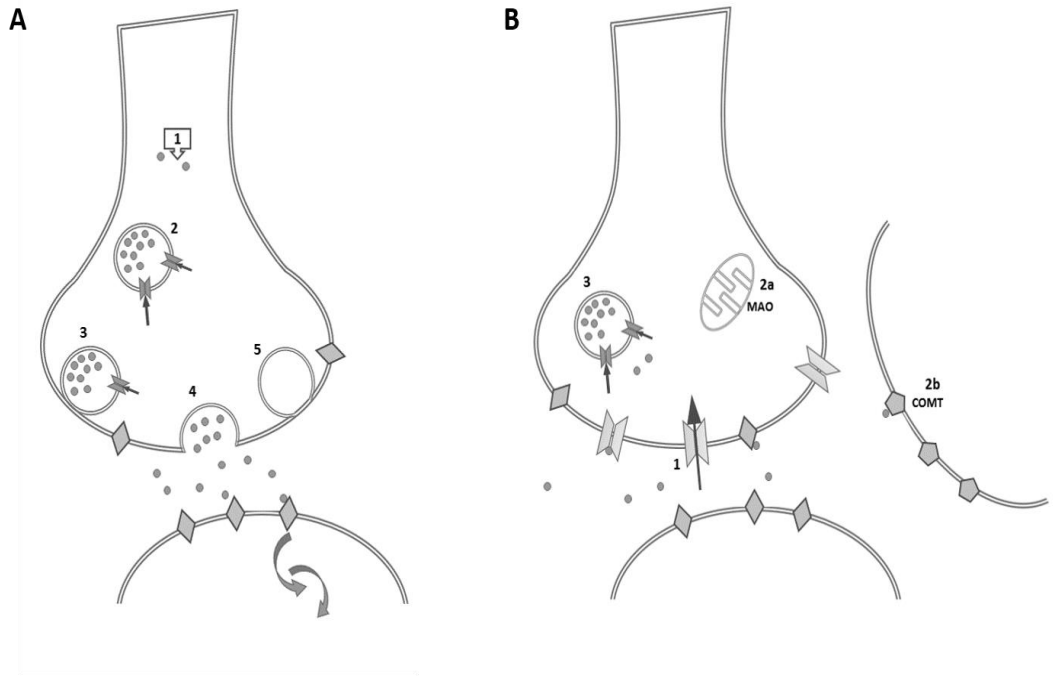

Figure 2.3. **Dopamine neurotransmission**. **A**. Secretion and release of dopamine. 1) Dopamine is synthesised in the neuronal cytoplasm and 2) transported into the synaptic vesicles by vesicular monoamine transporters (VMAT-2). 3) The vesicles are trafficked to the axon terminals where they are docked and primed on the presynaptic membrane. 4) The vesicles fuse with the axon membrane and release dopamine by exocytosis. The dopamine in the synaptic cleft can then bind with dopamine receptors on the post-synaptic membrane to induce enzymatic cascades in the post-synaptic neuron. 5) The vesicle is retrieved from the membrane and recycled. **B**. Removal of dopamine. 1) Reuptake through dopamine transporter (DAT) molecules; 2) Metabolic breakdown by a) monoamine oxidase (MAO) or b) catechol-*O*-methyl transferase (COMT); c) sequestration into vesicles via VMAT-2. (Adapted from Ref[112])

Fig. 2.2 and Fig. 2.3A). It is transported from the cytoplasm into synaptic vesicles by means of the membrane transporter vesicular monoamine transporter-2 (VMAT2), where it accumulates in readiness for synaptic release. The acidic internal environment of the vesicles permits the maintenance of a pH gradient across the vesicle membrane, which provides the energy for dopamine transport. Vesicle acidity additionally results in the protonation and consequent sequestration of the basic neurotransmitter molecules. Vesicles are trafficked to presynaptic release sites in axon terminals and then to a docking site on the presynaptic membrane, where they are primed for fusion. The arrival of an action potential at the axon terminal activates a large influx of Ca^{2+} ions into the terminal. This results in the fusion of the vesicles with the axon membrane, and the release of the neurotransmitter via exocytosis into the synaptic cleft. The vesicles are then retrieved from the axon terminal membrane and recycled to form new vesicles.

Dopamine released into the synaptic cleft exerts its effects by binding to receptor sites on the postsynaptic membrane. Dopamine receptors are G-protein coupled, or metabotropic, receptors, which trigger enzymatic cascades in the post-synaptic neuron when bound to dopamine. There are five dopamine receptors, which are divided into two main groups, D_1- and D_2-type receptors, based on their differing pharmacological, biochemical and structural properties. D_1-type (D_1 and D_5) are excitatory and expressed exclusively on the post-synaptic membrane of dopamine-receptive neurons, such as MSNs in the striatum. D_2-type (D_2, D_3 and D_4), by contrast, are inhibitory, and are expressed on both the post-synaptic dopamine target cell and on the presynaptic neuron. Receptors located on the presynaptic neuron are designated autoreceptors, and play an important role in regulating neuronal firing and neurotransmitter synthesis and release by the presynaptic neuron in response to extracellular dopamine levels.

If neurotransmitters were allowed to remain in the synaptic cleft, the receptors would be desensitised and the synapse would become refractory. Removal of the transmitter is thus

essential to ensure continued functioning of the synapse. There are several mechanisms by which dopamine is removed from the synaptic cleft (see Fig. 2.3B). Diffusion into the extracellular space passively removes a fraction of all transmitters. The majority of dopamine is, however, removed by means of reuptake through dopamine transporter (DAT) molecules in the presynaptic membrane. DAT is a 12-membrane-spanning molecule that undergoes several conformational changes during the reuptake of dopamine. Its initial outward-facing state permits the recognition of dopamine molecules, as well as Na^+ and Cl^- ions which are cotransported down their concentration gradients. These are taken up by DAT and translocated across the membrane. The transporter assumes an inward-facing conformation and releases the dopamine and ions into the neuronal cytoplasm, and then returns to its outward-facing state. DAT is thus responsible for terminating the transmission activity by the dopamine molecule, as well as for recycling dopamine for reuse or degradation. A subset of the dopamine molecules are metabolised in the neuronal cytoplasm by the mitochondrial membrane-associated enzyme monoamine oxidase (MAO). Dopamine is also catabolised by the extraneuronal enzyme catechol-*O*-methyl transferase (COMT). Dopamine which is not metabolised is recycled by re-sequestration in synaptic vesicles via VMAT-2 for reuse in neurotransmission.

2.3.2 Chemistry and pharmacology of methamphetamine

(See Refs[13,14,109,113–117])

N-methyl-1-phenylpropan-2-amine, or methamphetamine, is the *N*-methyl derivative of its parent compound, amphetamine (see Fig.2.4A). It is a psychostimulant synthesised by the reduction of ephedrine or pseudoephedrine, and is stereoisomeric, with the d-isomer being the more biologically active and illicitly available enantiomer. It is available as a white powder or in a purer crystalline form, and is consumed orally, intranasally, intravenously or by vapour

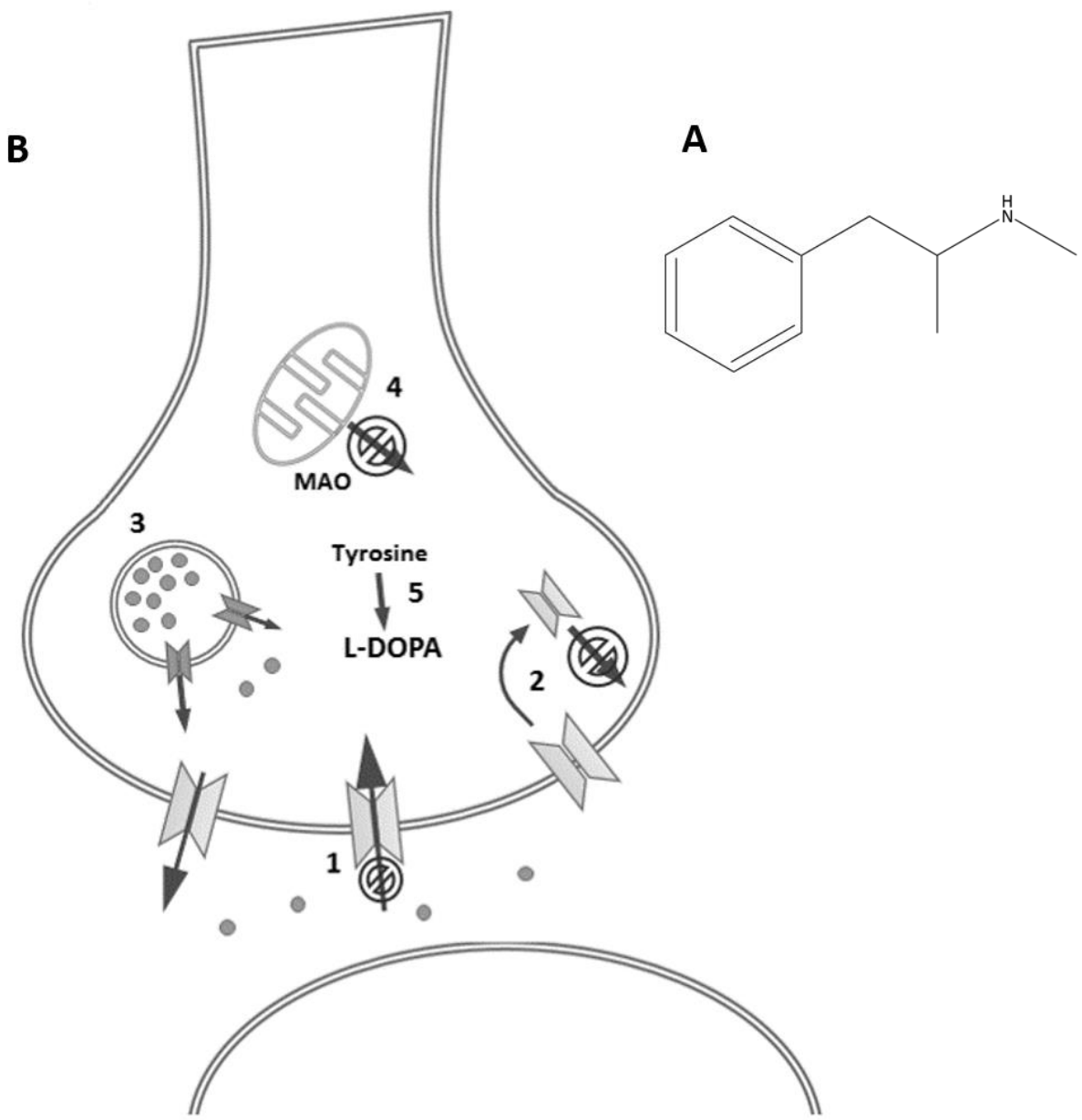

Figure 2.4. **A**. Chemical structure of methamphetamine. **B**. Actions of methamphetamine to increase dopamine availability: 1) blockade of and promotion of reverse transport through DAT; 2) promotion of DAT internalisation; 3) redistribution of dopamine from vesicular to cytosolic stores; 4) inhibition of MAO; 5) enhanced dopamine synthesis. (Adapted from Ref[13]).

---

inhalation (smoking). In South Africa, the primary route of consumption is by smoking of the crystalline form, known locally as 'tik'[58].

Methamphetamine has potent effects on both the central and peripheral nervous systems. Its sympathomimetic activity induces elevations in heart rate and blood pressure via vasoconstriction and bronchodilation, while vasodilation in skeletal muscles and hyperglycaemia enhance muscle activity. Levels of the stress-related hormones cortisol and ACTH are increased following methamphetamine consumption. Centrally, the acute effects of a low to moderate dose of methamphetamine include cognitive alterations such as increased arousal and improved attention and concentration. Affective changes are also observed, such as elevated mood and confidence, heightened libido and reduced appetite. Higher doses may result in anxiety, agitation and restlessness, as well as peripheral symptoms of excessive sympathetic activity.

Methamphetamine acts primarily to increase extracellular levels of the monoamine neurotransmitters. Addiction to methamphetamine is believed to be underpinned by impairments in the corticostriatal circuits mediating executive function and impulse control. Methamphetamine-induced alterations in dopamine neurotransmission within the striatum result in dysregulated basal ganglia output, and are thus a dominant factor in the development and maintenance of drug dependence. Methamphetamine enhances dopamine release in several ways (see Fig.2.4B). Predominant, however, is its role in modulating the activity of two membrane transporters: DAT on the presynaptic membrane, and VMAT-2 on the vesicles.

Methamphetamine functions primarily at DAT to promote reverse transport of dopamine from the cytosol into the synapse. The exact mechanisms whereby this is accomplished are not fully understood, but two primary mechanisms have been proposed. The facilitated exchange diffusion model involves the translocation of methamphetamine by DAT into the neuronal cytosol. The accompanying conformational change increases the availability of the DAT binding site to internal dopamine, which is then transported into the synapse. A second mechanism is the channel-like mode model, in which methamphetamine induces a

conformational change in DAT that permits an influx of ions, chiefly Na^{2+}. The increase in cytosolic sodium ion concentration promotes the reverse transport of dopamine. It has also been suggested that methamphetamine promotes the internalisation of DAT, removing it from the plasma membrane and thereby reducing its availability to reduce synaptic dopamine, although this has not been conclusively demonstrated *in vivo*.

The second primary mechanism by which methamphetamine increases dopamine levels is by redistribution of the neurotransmitter to the cytosol from vesicular stores. As with DAT, there is evidence for several means by which this is accomplished, which are not mutually exclusive. One putative mechanism, VMAT-2 competition, involves direct binding of methamphetamine to the vesicular transporter. This prevents the sequestration of dopamine via VMAT-2, so that it remains in the cytosol. Another proposed mechanism relies on methamphetamine's chemical properties as a lipophilic weak base: in the acidic environment of the synaptic vesicle, it is protonated, becomes less membrane permeable, and accumulates. This results in a pH increase within the vesicle. Under normal conditions, the pH gradient provides the energy required for dopamine transport into the vesicle; the methamphetamine-induced gradient collapse thus reduces vesicular uptake of dopamine. Additionally, competition for protons occurs between dopamine and methamphetamine. An increased concentration of unprotonated dopamine molecules within the vesicle permits their passive diffusion into the cytosol. As with DAT, there is some evidence that methamphetamine causes a redistribution of VMAT-2 away from the vesicle membrane, which would further reduce dopamine transport. Increased levels of non-sequestered dopamine are thus available within the axon terminal for reverse transport into the synapse.

There are several additional putative mechanisms by which methamphetamine may influence neurotransmitter availability. One such is the inhibition of MAO, which would reduce dopamine catabolism. Methamphetamine has also been shown to enhance dopamine synthesis,

which may be accomplished by promoting the activity of tyrosine hydroxylase. Non-dopaminergic dependent mechanisms also appear to play a role: methamphetamine targets other monoaminergic transporters, such as those on noradrenergic neurons in the prefrontal cortex, which indirectly increase dopamine levels in the basal ganglia through their modulating influence on glutamatergic neurons in the corticostriatal pathways.

2.4 MAGNETIC RESONANCE IMAGING

2.4.1 Basic principles and terminology

(See Refs[99,118,119])

MRI makes use of the magnetic properties of tissue to extract information about the structure and function of the anatomical region under consideration. This is accomplished by measuring signals from the hydrogen nuclei of water molecules in the tissue. The hydrogen nucleus is

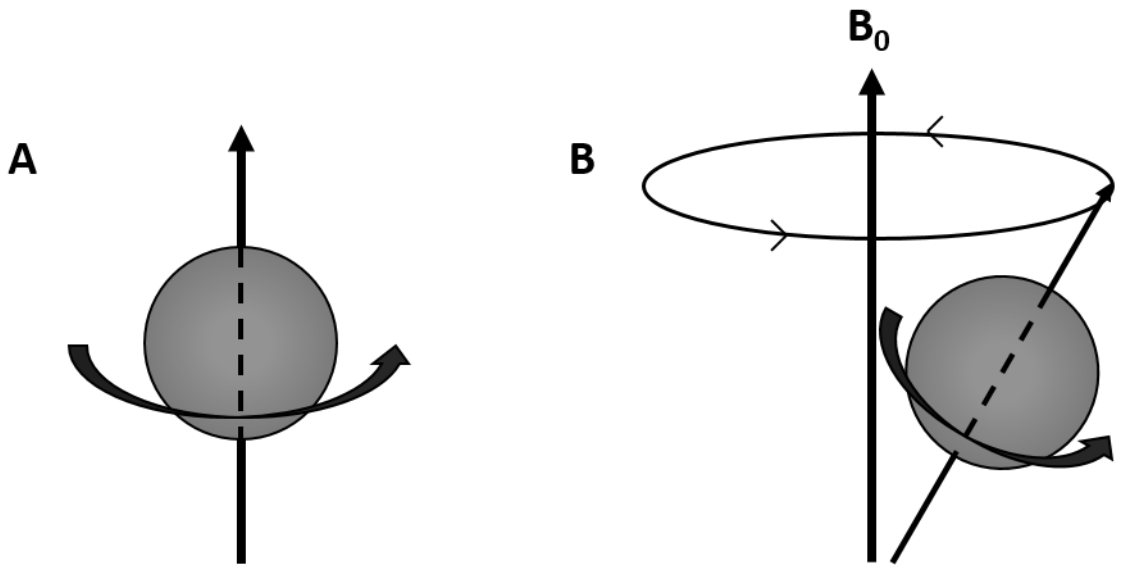

Figure 2.5. **A**. A proton rotating about its own axis generates a magnetic field. **B**. In an external magnetic field B_0, a proton rotates about its own axis and also precesses about the axis of B_0. (Adapted from Ref[118]).

composed of a single, positively charged proton, which spins about its axis and generates a magnetic field, or magnetic dipole moment (see Fig.2.5A). Under physiological conditions, the magnetic fields of the protons within the tissue are randomly directed so that the tissue as a whole has no net magnetisation.

If the protons are placed in an external magnetic field B_0, they experience a torque causing them not only to spin about their own axes, but also to rotate, or precess, around the axis of the external magnetic field (the z-axis of a three-dimensional system), resulting in a net magnetisation parallel to B_0 (see Fig. 2.5B). The protons precess about B_0 at a characteristic frequency γB_0, where γ is the gyromagnetic ratio, known as the Larmor precession frequency.

If a radiofrequency (RF) pulse is now transmitted along an axis perpendicular to the direction of B_0, the x-axis for example, a second magnetic field (B_1) is generated in this direction (see Fig. 2.6A). If the RF pulse has a frequency that exactly matches that with which the protons

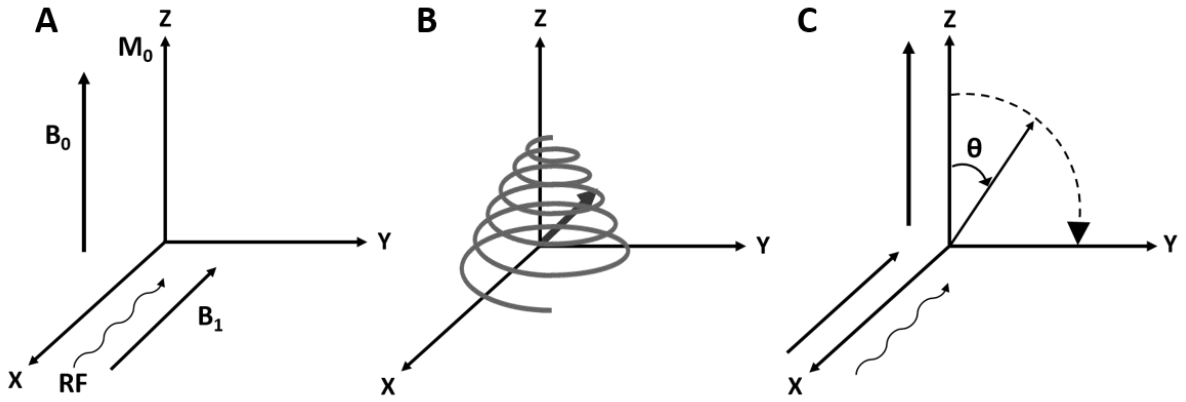

Figure 2.6. **A**. If a radiofrequency (RF) pulse is transmitted along an axis perpendicular to B_0, a second magnetic field, B_1, is generated in this direction. **B.** The net magnetisation rotates away from B_0 into the transverse plane. **C.** The angle that M_0 makes with the z axis following the RF pulse is called the flip angle (θ). (Adapted from Ref[118]).

are precessing, they will begin to precess additionally about the axis of B_1, causing the net magnetisation to rotate away from an alignment parallel to B_0 into the transverse plane (see Fig. 2.6B). This change of direction of the net magnetisation vector is called 'flipping', and the angle that M_0 makes with the z-axis following the RF pulse is called the flip angle (see Fig. 2.6C). The flip angle is determined by the duration and amplitude of the RF pulse. M_0 consists of two vector components: M_z, which is the component parallel to the B_0 field, and M_{xy}, the component in the x–y plane. If, following the RF pulse, the magnitude of M_{xy} equals the magnitude of M_0, the flip angle is 90° and the magnetisation has been completely flipped into the transverse plane.

Once the RF pulse is switched off, the proton spins dephase and realign with the B_0 axis, in a process called relaxation. During this process, the M_{xy} vector decreases rapidly owing to spin-spin dephasing, while the M_z component recovers to its equilibrium state owing to spin-lattice relaxation, where the energy absorbed during excitation is returned to the lattice. Both of these processes are exponential. The time constant of the M_z recovery rate is called the longitudinal relaxation time, or T1. The transverse relaxation time, or T2, characterises the rate of decay of M_{xy} (see Fig. 2.7). These time constants are inherent properties of tissues and are thus fixed for a particular tissue at a given field strength.

A coil is a device that can generate a magnetic field (gradient coils), or transmit or receive an RF pulse (RF coil). The RF coil detects a changing magnetic field as an induced electric current. As the flipped protons precess, their net magnetisation induces an oscillating current in the RF coil. The signal decays once the RF pulse is switched off as the protons dephase and relax. The received signal from one RF pulse is called a free induction decay (FID).

A single FID is a composite of all the protons in the patient, and gives no information about the signal location. Gradients are thus used to specify the coordinates of the signal. Gradient

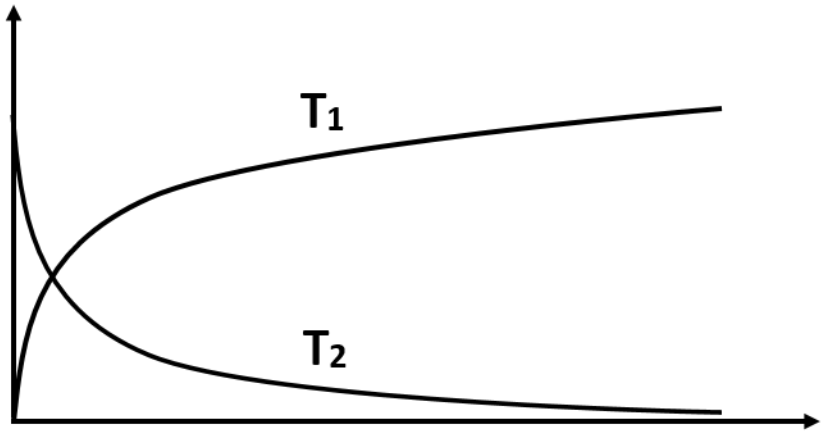

Figure 2.7. T1 represents the growth of magnetisation along the z axis, while T2 represents the decay of magnetisation in the x-y plane. The rate of decay of transverse magnetisation (T2) is several times greater than the rate of recovery of longitudinal magnetisation (T1). (Adapted from Ref[118]).

---

coils produce an organised change in the homogeneity of the external magnetic field, thereby spatially encoding the signal. They consist of three orthogonal coils, each representing one of the gradients: the slice-select gradient (G_z), the phase-encoding gradient (G_y) and the frequency-encoding gradient (G_x), which are applied at different times during image acquisition.

The time between the application of one RF pulse and the next is called the repetition time, or TR. If TR is less than the time taken for M_z to recover completely along the T1 curve, all successive FIDs will be reduced in magnitude compared to the first FID, as there will be less longitudinal magnetisation to flip, and smaller M_{xy}s will be produced. After a pulse is applied, a period of time elapses before the measurement is taken; this period is called the time to echo, or TE. If the measurement was taken immediately after the pulse was applied, there would be no decay in the signal, and the maximum FID would be measureable. However, during TE some signal decay occurs according to the T2 curve. Thus the received signal will be a combination of the influence of T1 and T2. By manipulating TR and TE, the effects of T1 and T2 can be differentially enhanced or reduced in order to give better contrast between different tissues in an image (see Fig. 2.8). Increasing TR reduces the effect of T1, while increasing TE

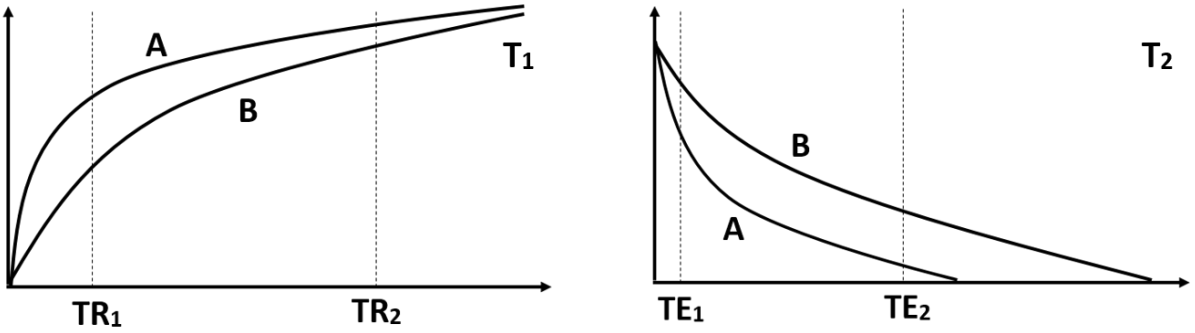

Figure 2.8. Increasing TR reduces the effect of T1, while increasing TE increases the effect of T2. Short TR and TE will produce a T1-weighted image; long TR and TE will produce a T2-weighted image. (Adapted from Ref[118]).

---

enhances the T2 effect. Thus by increasing TR and TE, a T2-weighted image can be obtained, in which the effect of T1 is mostly eliminated. By contrast, shorter TR and TE will produce a T1-weighted image. Different tissue types within the brain also have different proton densities (PDs), producing different relative intensities of signal, and different 'brightness' (see Table 2.2).

2.4.2 Diffusion tensor imaging

(See Refs[101,118,120–128])

DTI uses magnetic imaging techniques to measure the diffusion of water. In a completely unrestricted environment, water molecules exhibit random translational movements, known as Brownian motion, as a consequence of their thermal energy. Various factors influence this diffusional motion. In the complex structural environment of tissue such as the brain, the movement of water molecules is significantly restricted. DTI is based on the fundamental principle that water diffusion in the nervous system is anisotropic; that is, it is not equal in all directions. In an environment where the restrictions are not directionally coherent, diffusion will be more isotropic than in one with highly organised and directionally cohesive barriers, and thus different tissue subtypes can be identified and characterised on the basis of the nature

Table 2.2. Relaxation times and appearance of central nervous system tissues in different MR images.

			T1-weighted		T2-weighted	
	T1	**T2**	**Adult**	**Infant**	**Adult**	**Infant**
White matter	Intermediate	Intermediate	Bright	Intermediate	Dark	Intermediate
Gray matter	Intermediate	Intermediate	Intermediate	Bright	Intermediate	Dark
CSF	Long	Long	Dark	Dark	Bright	Bright

(Adapted from Refs[118,177])

of water diffusion within them. Within the CNS, white matter fibre bundles provide a significant level of organisation and directional coherence, with water molecule movement occurring preferentially along the length of axons and restricted by barriers such as neuronal membranes and the myelin sheath in a direction perpendicular to the axon.

In diffusion weighted imaging, pulsed gradients provide a linearly varied magnetic field. The received signal is reduced by water movement in the direction of the gradient. Most simply, a single gradient pulse is followed by a second of equal magnitude but opposite direction, to rephase the proton spins. However, displacement of the water molecules before the refocusing phase results in incomplete spin recovery, and thus an attenuated signal. The *b*-value, which encapsulates the strength and timing of the gradient pulses used in the sequence, determines the sensitivity of the sequence to diffusion. In a completely isotropic environment, the rate of diffusion of water molecules can be adequately described by a single scalar parameter, namely, the diffusion coefficient *D*. DTI is an advanced form of diffusion MRI which investigates and characterises anisotropy. In an anisotropic environment, a single scalar is not sufficient to characterise diffusion. A minimum of 6 gradient pulses with non-zero *b* values (typically of the order of 700 – 1000 s/mm^2) are applied in different directions in addition to a reference non-diffusion weighted acquisition (b = 0 s/mm^2)). The diffusion in any given direction can

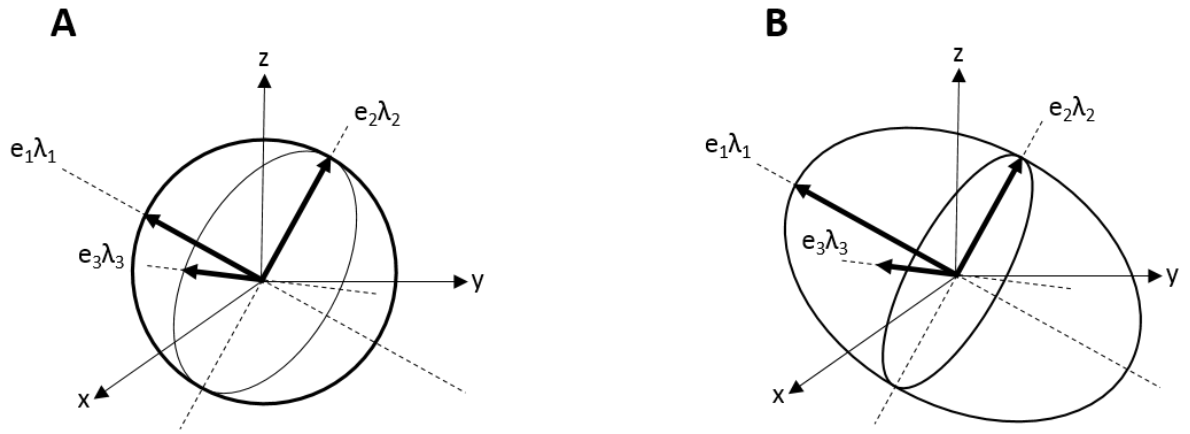

Figure 2.9. The diffusivity in three dimensions is modelled as an ellipsoid whose orientation is characterised by the eigenvectors e_1, e_2 and e_3, and whose shape is defined by the eigenvalues λ_1, λ_2 and λ_3. Completely isotropic diffusion within a voxel is modelled by a perfect sphere (**A**), while anisotropy is shown by the eccentricity of the ellipsoid (**B**). (Adapted from Ref[193]).

---

then be determined by measuring the signal attenuation following diffusion weighting compared to the signal emitted with no diffusion weighting. D_x, D_y and D_z, represent diffusion along the principal axes. Three additional off-diagonal elements, D_{xy}, D_{xz} and D_{yz}, make up the tensor matrix, **D**.

From the different components, the average diffusion or degree of anisotropy can be determined for each voxel. Additionally, the directionality and value of diffusion in each voxel can be calculated. The principal direction is titled the principal eigenvector (e_1), with the diffusion coefficient in that direction known as the principal eigenvalue (λ_1). This corresponds to the direction of greatest diffusivity. The two orthogonal eigenvectors, e_2 and e_3, with associated diffusivities λ_2 and λ_3, represent the lesser diffusion directions. These values and directionalities can be visualised by means of diffusion ellipsoids, which provide a 3-dimensional representation of diffusion in each voxel of an image (see Fig. 2.9). The long axis of the ellipsoid represents the principal eigenvalue, while the radii indicate the second and third eigenvalues. The eccentricity of the ellipsoid is a visual indication of the degree of anisotropy

in the voxel, such that a perfectly spherical ellipsoid would be representative of complete isotropy.

The diffusion tensor (DT) provides three main types of data which can be analysed in several ways to characterise the tissue under examination: diffusion, anisotropy, and orientation. Mean diffusivity (MD) characterises the overall displacement of molecules and presence of obstacles within each voxel without taking into account the directional variation. The degree of anisotropy is most commonly represented by FA; this is the normalised standard deviation of the three eigenvalues, and provides a measure of how they vary. This is complemented by examining the diffusivity along the principal axis (axial diffusivity, AD) and the diffusion in orthogonal directions, or contributions of λ_2 and λ_3 (radial diffusivity, RD). A third type of information that can be extracted from DTI images is related to the 3-dimensional orientation of the tissue structure. Based on the assumption that the principal eigenvalue represents movement of water along the white matter fibre length, the principal eigenvector is taken to indicate the 3-dimensional orientation of the fibres within the voxel.

2.4.2i Strategies of analysis

Once information has been extracted regarding each voxel, it can be analysed in several ways, as the precise anatomical locations of the diffusion variations are chiefly of interest. There are two main ways in which diffusion data can be analysed: voxel-based or regional analysis, and tractography.

Whole brain voxelwise analysis examines specific diffusion measures in every voxel in the brain. This is particularly useful when there are no *a priori* hypotheses as to locations of significant interest. Spatial normalisation is used to align individual brains to a template so that the same structures are compared across the sample. Following this, voxels which meet a threshold value are individually processed and the results are statistically analysed for group

differences or correlation with some measure of interest. Limitations of this approach are that the normalisation process frequently results in distortion of brain images, particularly in clinical populations, and that the need arises to correct for multiple comparisons. A variation of this approach is Tract-based Spatial Statistics (TBSS), which creates a group mean FA skeleton by aligning the images of all subjects in a study into a common space. The FA skeleton is a representation of the centre of the fibre bundles common to all subjects. The FA data from each subject is then projected onto the skeleton and the FA value from the centre of the nearest relevant tract is used. Voxels selected in this way are then statistically analysed in the same way as for a whole brain voxelwise analysis. A drawback to this approach is that it excludes the peripheral voxels of white matter and may thus miss variations in those regions.

Region of interest (ROI) analysis relies on selection of specific structures or regions where changes in diffusion measures are hypothesised to occur. These regions are defined, by manual delineation or automated segmentation, and only the voxels located within the regions are statistically analysed. An advantage of this method is that the reduced number of voxels increases the statistical power of the analysis, in contrast with whole brain approaches which must statistically correct for multiple comparisons. Manual segmentation provides the additional advantage that individual subject structural variation is taken into account and no distortion is necessary. However, it is time-consuming and labour-intensive. Automated segmentation is less laborious, but morphological distortion following normalisation is again a risk associated with this technique.

Tractographic analysis involves the reconstruction of fibre tracts by the sequential connection of neighbouring voxels. The orientation of the fibres within a voxel are assumed from its principal eigenvector. This can then be extrapolated to connect to neighbouring voxels, and from this the fibre bundles can be reconstructed. Equivalent connections can thus be compared across subjects, and connections between anatomical ROIs can be investigated. Diffusion

measures can be averaged across tracts or segments of tracts for additional characterisation. Seeds, or defined ROIs, are used in tractography to define a location from where a tract will originate. Target regions are anatomical locations through which the fibres of a tract must pass. These ROIs may be defined manually or automatically, as described above.

There are two chief methods of determining the trajectory of white matter bundles: deterministic and probabilistic tractography. Deterministic tractography assumes a single primary fibre direction in each voxel and connects neighbouring voxels based on their principal diffusion directions, or eigenvectors. Successive voxels are connected in this way until the tract terminates by reaching voxels unlikely to be located in the tract. Deterministic tractography has distinct limitations in voxels where fibre bundles cross. In such voxels the principal diffusion direction may no longer represent the fibre of interest and the continuing trajectory of the constructed tract may be incorrect. Probabilistic tractography does not assume a single orientation in a voxel based on the principal diffusion direction. Rather, variation and uncertainty in diffusion measures are taken into account and whole brain tractography is run with multiple iterations, with voxel parameters altered slightly each time. The result is a probability distribution for each voxel showing the most likely locations of white matter connections between the defined ROIs. This method permits the identification of a number of white matter pathways in areas where fibres cross.

2.4.3 MR Imaging of neonates

MRI is a non-invasive technique which does not involve ionising radiation, and is thus safe for use in infants. It is valuable for imaging subtle structural alterations which may not be visible using other modalities. MR imaging in neonates, however, does not simply involve the application of adult acquisition and post-processing protocols to the infant context. A variety

of factors must be taken into account when imaging neonates in order to achieve optimal visualisation.

The neonatal brain is not merely an adult brain in miniature. The water content of the infant brain is much higher than that of an adult brain. Although the basic structures of the adult brain are present in the infant, they are significantly immature. Fibre bundles are chiefly in place, but myelination is incomplete. T1 and T2 relaxation rates are much longer in neonates, and the tissue contrasts in T1-weighted and T2-weighted images are very different in infants from those of adult brains. In the neonate, the contrasts are reversed, with T1-weighted images showing lower white matter than grey matter intensity, while T2-weighted images show higher grey than white matter signal intensity. However, given the incomplete myelination of the neonatal brain, the contrast is not merely an anatomical reversal of adult images; regional asynchrony of maturation results in some fibre bundles having the appearance of grey matter, while others are visualisable as white. As a result, the definition of boundaries between grey and white matter is not always very clear. Additionally, automated segmentation of anatomical MR images depend on previously defined atlases, of which the majority are based on adult brains, to which neonatal brains do not normalise well or accurately.

DTI is a useful tool for imaging white matter in neonates, and well suited to gathering information which may not be measurable via other MR modalities. Although the neonatal brain is incompletely myelinated, the fibre bundles are well organised, leading to intrinsic anisotropy based on high parallel and low perpendicular diffusivity. The lack of myelin in many areas, however, makes it necessary to use a lower FA threshold for tractography than would be the case in adult images[129].

2.5 METHODOLOGY: ADDITIONAL DETAILS

2.5.1 Recruitment

(See Refs[58,130–132])

These studies form part of a larger cohort study investigating the effects of alcohol and methamphetamine consumption during pregnancy. The women whose infants were investigated were recruited from 3 midwife obstetric units located in the Cape Coloured communities in Cape Town. Following their first antenatal visit to the clinic (at approximately 20 weeks gestational age), the women were interviewed about their alcohol and drug use, at recruitment and at time of conception. The interviewer used a time-line follow-back approach to determine alcohol consumption and patterns (see below). Women who reported drinking at least 1.0 oz absolute alcohol/ day (AA/d; approximately 2 standard drinks) or who participated in binge drinking (≥ 2.0 oz AA/ occasion) were invited to join the study. Women who did not drink or drank < 1.0 oz AA/d and did not binge drink were invited to join the study as control subjects. Women from the same community who used methamphetamine but reported minimal alcohol use (with the same criteria as for the controls), were invited to participate in the methamphetamine group. Exclusion criteria for the mothers in the study were as follows: age < 18 years old, multiple pregnancy, HIV+ status, and on medication for diabetes, epilepsy, hypertension and/ or cardiac illness. For the infants, the exclusion criteria were neural tube defects, seizures and chromosomal abnormalities. Women who reported drinking during pregnancy were counselled to stop drinking or to reduce their alcohol intake; those who agreed were referred for treatment.

2.5.1i Timeline follow-back

The first time-line follow-back interview was conducted at recruitment. The women were asked about their drinking during each day in a typical 2-week period around the conception date,

using specific daily activities and times to assist recall. If a woman's drinking patterns or quantity had changed during the pregnancy, the same process was followed regarding the previous two weeks and when the change had occurred. Two further interviews were performed, at approximately 4 and 12 weeks post-recruitment, where the follow-back approach was used to assess her alcohol, drug use and cigarette smoking for the previous two weeks, as well as for any weeks where she had consumed more alcohol than usual. Volume was recorded for each type of alcohol being consumed (wine, beer, liquor, cider) and converted to oz AA, to produce 3 measures of alcohol consumption across pregnancy: oz AA per day, oz AA per occasion, and frequency of drinking. Methamphetamine was recorded as number of days used per month of pregnancy. Smoking was recorded as cigarettes smoked per day. Other drugs of abuse (marijuana, cocaine, and methaqualone) were measured as number of days used/ month. To confirm the maternal report, urine samples were collected from a subset of the women and tested with the AccuTest^{TM} 6+2 drugs of abuse panel test (DTA Pty Ltd, Cape Town, South Africa), which measures drug metabolites of amphetamines, opiates, tetrahydrocannabinol, cocaine and methaqualone). Of the women who reported no methamphetamine use, none tested positive for methamphetamine. None of the women tested positive for cocaine or opiates.

2.5.2 Post-processing and manual segmentation of anatomical scans

(See Refs[133])

2.5.2i Post-processing of anatomical MRI with FreeSurfer

Two acquisitions of a motion navigated multiecho gradient echo sequence were used for the volumetric study, with flip angles of 5° and 20° respectively. Using FreeSurfer (http://surfer.nmr.mgh.harvard.edu/), a composite image was then synthesised from the two with an optimised flip angle for contrast. Each image was converted from dicom format to mgz

format using mri_convert. The 8 echoes from each were then split by selecting successive frames. Tissue parameters were estimated using mri_ms_fitparms, which takes all echoes from both acquisitions, estimates the T1 and PD values for each voxel, and creates T1 and PD volumes. Using mri_synthesize, these were then used to synthesize an optimally weighted volume with TR = 20ms, flip angle = 24° and TE 0ms.

2.5.2ii Manual segmentation using Freeview software

Freeview is a visualisation tool forming part of the FreeSurfer software package (FreeSurfer image analysis suite http://surfer.nmr.mgh.harvard.edu/). It is used to visualise and analyse anatomical images in three planes (sagittal, coronal and axial). For manual segmentation, the anatomical scan is opened and size, contrast and brightness are adjusted for optimal visualisation of ROIs. A new volume is then created to layer over the original. Each volume can be viewed in a range of colour maps; for manual tracing purposes, the original volume is viewed in greyscale (i.e. a standard anatomical MRI view), while the segmentation volume is viewed in colour. Freeview assigns each ROI a unique colour to assist in easy identification and visualisation of individual structures. Each ROI is additionally assigned a unique integer value for later analysis. The opacity of the segmentation volume can be adjusted for optimised viewing of the underlying structures. Each volume view can be "smoothed" for more anatomical realism; for the purposes of this study, the original volume was smoothed, while the segmentation volume was not.

Manual segmentation was performed with a stylus on a Lenovo ThinkPad X220 tablet. Using the Freehand tool in Freeview, an outline of each ROI was created in the segmentation volume on a slice by slice basis. This was then filled using the Fill tool. Regions were traced in the following order: caudate nucleus, putamen and globus pallidus, nucleus accumbens, thalamus, hippocampus and amygdala, vermis, and cerebellar hemispheres. Where structures are

bilateral, both hemispheres were completed for that structure before the next was traced. Voxels traced in one plane in Freeview are automatically visible in all three; tracings were completed chiefly in the coronal plane, with guidance from the sagittal and axial planes where necessary.

Caudate nucleus and nucleus accumbens

An oblique line from the inferior tip of the lateral ventricle to the midpoint of the inferior boundary of the internal capsule was drawn to separate the caudate and nucleus accumbens, while a line descending from the middle of the inferior border of the anterior limb of the internal capsule was considered to define the boundary between the putamen and the nucleus accumbens. The caudate and accumbens were traced as one structure and separated later.

Posteriorly, the caudate diminishes in size and eventually becomes difficult to define as the tail reaches the point where it curves inferiorly posterior to the thalamus. For this reason the posterior and inferior portions of the caudate were not traced.

Putamen

The junction of putamen and pallidum was generally most clearly seen in axial sections, so that tracing was done in the axial or coronal planes on a slice by slice basis.

Pallidum

The pallidum was traced by the addition of its inferior border to the tracing of the putamen in each slice. Globus pallidus externa and interna were indistinguishable from one another and so were not separated.

Thalamus

The thalamus lies medial to the posterior limb of the internal capsule. Its medial and superior borders are visible where the thalamus meets the cerebrospinal fluid of the lateral and third ventricles or within the horizontal fissure superiorly. Where the left and right thalami meet in

the midline, they were separated by an appropriate line in the median sagittal plane. The lateral border of the thalamus is formed by the medial boundary of the internal capsule. Inferiorly, it is bounded by the subthalamus, with the medial lemniscus between the two structures. In posterior slices the internal capsule disappears and the thalamus descends to form the medial and lateral geniculate bodies.

Hippocampus

The hippocampus was traced chiefly in the coronal plane, with considerable guidance from views in the sagittal plane. It can be seen in sagittal sections within the temporal lobe as a sausage-shaped structure. More anteriorly in the coronal plane the hippocampal head appears, and the structure becomes large and rounded.

Amygdala

The amygdala is located anterior to the head of the hippocampus. It is bounded in its anterior, inferior and lateral aspects by white matter, and postero-inferiorly by the hippocampus and the tip of the lateral ventricle. The tracings of the amygdala were done in all three planes, as it was difficult to see in its entirety in any one plane. The amygdala is difficult to define clearly, which may reflect on the reliability of the tracing volumes generated.

Cerebellum and Vermis

The cerebellar hemispheres were primarily traced in sagittal and coronal planes. The two hemispheres are anatomically separated by the vermis. In the coronal and axial planes, the vermis is distinguished from the hemispheres by means of vertical lines which taper slightly posteriorly (in the axial plane) and inferiorly (in the coronal). By convention of the Infant Brain Segmentation Manual (see Ref[134]), the vermis is present in no more than five slices in and adjacent to the midline in the sagittal view. Once the vermis was delineated, the hemispheres

were traced. In the infant brain, subdivision of the hemispheres into lobules is very difficult and so was not attempted in this study.

2.5.2iii Determinations of volumes and interrater reliability

To compute the volumes of the segmented structures, compute_label_volumes.csh in FreeSurfer was used. This script produced an output of voxel count and volume (mm^3) for each structure.

For interrater reliability, 9 of the brains were also segmented by an independent, trained investigator. The degree of overlap was determined using compute_interrater_variability in FreeSurfer. The Dice overlap measure was used, which is defined as follows:

Dice = 2*nshared/(nvox1+nvox2) where

nshared = intersection of the 2 ROIs

nvox1 = number of voxels in ROI1

nvox2 = number of voxels in ROI2

Dice coefficients were determined for each ROI as well as for the entire segmentation.

2.5.3 Pre-processing of Diffusion Tensor images

2.5.3i Data processing
(See Refs[118,135–138])

Artefacts in diffusion weighted images have a considerable impact on the accuracy of the data obtained. A significant aspect of data processing prior to tractographic analysis is removal of such artefacts. Subject motion is almost inevitable in neonatal studies; to an extent, this can be managed by applying diffusion weighting gradients along more than 6 directions to create a

degree of redundancy, and discarding individual volumes in which motion is detectable. This is done manually as a first step in data processing. There is a limit to how many volumes can be discarded, however. In the current study, 30 diffusion-weighted (DW) volumes (or directions) were acquired, in addition to the non-weighted volumes. Any subject in which fewer than 12 volumes remained was discarded. Eddy currents are another source of artefact, and arise when the gradients are rapidly switched on and off. These, and more subtle motion artefacts, are corrected by applying affine registration to the $b = 0$ reference images, using the fsl tool eddy_correct. In the current study, 4 $b = 0$ images were acquired, and the DW images were registered to the mean of these. Susceptibility distortion is an additional problem. The ability of a substance to be magnetised when placed in an external magnetic field is termed magnetic susceptibility. Different substances have different susceptibilities, and in MRI these differences can produce artefacts at interfaces between such substances, such as between tissue and air. Echo planar imaging (EPI), which is typically used in DTI, is particularly sensitive to susceptibility distortion. This issue can be overcome by performing two DTI acquisitions with the phase-encoding gradient directions switched (anterior to posterior, and posterior to anterior, respectively). These images will have nearly identical distortions along the anterior-posterior axis but in opposite directions, and can thus be combined to produce a DT map in which the distortion is reduced. This is done using the topup tool in fsl, which estimates the field that most accurately represents both volumes. It is worth noting that, in practice, these distortions often occur simultaneously to some degree. Therefore, while the application of the various "correction" techniques can greatly reduce their effects, they can never fully be removed from the data.

2.5.3ii Mini-probabilistic tractography

(See Ref[135])

In order to perform tractographic analysis, seed and target ROIs must be placed in appropriate locations with white matter connections. To determine these locations, a mini-probabilistic approach was used to highlight regions within the three networks of interest: commissural, projection and association. Mini-probabilistic tractography combines the valuable aspects of both deterministic and probabilistic tractography; it incorporates the uncertainty of the probabilistic algorithm, but is faster and generates tract structure, in line with the deterministic approach. A small number of brute force, whole brain tractography iterations are performed, each time perturbing the tensor properties based on their uncertainties as estimated during the previous iteration. The current study used FATCAT software in AFNI for this purpose[127]. Once the whole-brain tractography had been performed, a primary target ROI was placed within a central network of interest, followed by the placement of additional targets in locations along the tracts passing through the primary target region.

2.5.3iii Tractographic propagation: FACTID

(See Ref[139])

Propagation of tracts in tractography may be accomplished via a number of algorithms. One such technique is FACT (**f**iber **a**ssessment by **c**ontinuous **t**racking)[140]. In this approach, test tracts initiate at each location where FA is greater than a given threshold (in adults, FA > 0.2 is predominantly used), and each tract propagates in the 'forward' and 'negative' direction of the direction of the voxel's greatest diffusion (see Fig. 2.10A). Upon reaching the edge of a voxel, the tract terminates if the FA in the new voxel is sub-threshold or if the turning angle of propagation is too large (this parameter is set to minimize the existence of tracts with extremely sharp bends that are deemed unphysical; for studies at standard voxel resolution of approx. 2 mm isotropic voxels, this parameter is commonly in the range 45-60°); otherwise, the test tract

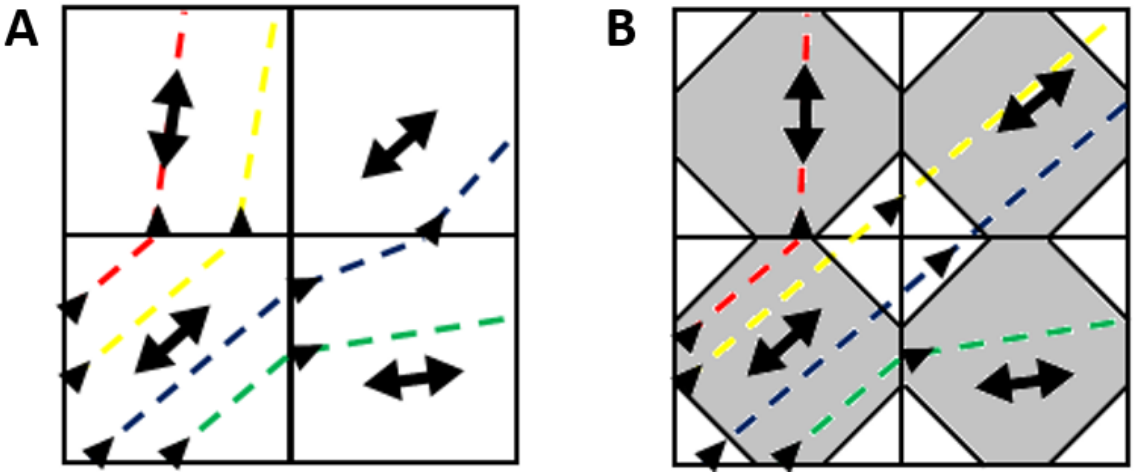

Figure 2.10. **A**. An example of the propagation of test tracks in two dimensional FACT, where tracks cross from edge to edge of the lower left voxel and pass to face-wise neighbouring voxels. **B**. The same test tracks in the FACTID approach, where tracks can propagate to the octagon surface in each voxel (the gray areas). Bold arrows represent the orientations of principal eigenvectors. (Adapted from Ref[139]).

---

propagates by passing into the new voxel and being redirected to follow a trajectory parallel to its direction of greatest diffusion. It is important to highlight that in this approach, tract propagation to a neighbouring voxel can only occur through voxel 'faces'; this means that a tract traversing the voxel diagonally through a voxel matrix may often be diverted from its underlying trajectory due to the neighbourhood definitions of the voxels. Additionally, rotation of either the coordinates or the tensor ellipsoids will have a significant effect on the output of the propagation algorithm, as a slight perturbation of direction could result in tract propagation orthogonal to the anatomical direction.

While the FACT approach has been shown to reproduce several known, major tract bundles reliably across populations, the FACTID (**f**iber **a**ssessment by **c**ontinuous **t**racking **i**ncluding **d**iagonals) was developed to address the aforementioned issues of potential grid-neighbour bias by permitting tracts to propagate diagonally between voxels (see Fig. 2.10B). Thus instead of tracts only propagating through six boundary faces, they may propagate through any of the 26 neighbouring voxels that share either a face, edge or node. Tracts reaching a voxel boundary

near an edge or corner 'test propagate' to determine whether their trajectory carries through a corner, edge-region or voxel face. A tract passing through a voxel diagonally is now able to follow its trajectory through successive voxels. FACTID has been shown to provide more reproducible results than FACT when data are acquired on rotated grids or as signal-to-noise ratio (SNR) is decreased, and results of the former converge to high-resolution values more quickly than FACT. Thus, the simple change in FACTID produces more robust results.

CHAPTER 3

PRENATAL METHAMPHETAMINE EXPOSURE IS ASSOCIATED WITH REDUCED CAUDATE VOLUMES IN NEONATES

3.1 INTRODUCTION

Methamphetamine is one of the most widely used recreational drugs[65] and there is considerable evidence that exposure during pregnancy has marked effects on the infant[58–60,141,142]. Given the dopaminergic activity of methamphetamine and its documented neurotoxicity in adult users[88,93], it was expected that prenatal exposure would induce similar damaging effects on the infants concerned, considering the rapid development and growth of the CNS that occurs during this period[72]. Neuropsychological and behavioural alterations have been observed in studies of children with prenatal methamphetamine exposure, including low arousal and lethargy[67,68], poor fine motor skills[75], poor psychomotor and emotional adjustment[76] and aggressive behaviour[77]. Deficits in visuomotor integration[88], inhibitory control[84], and executive function and working memory[81] have also been observed in children with *in utero* methamphetamine exposure. In view of these findings, it is of interest to determine whether these deficits reflect structural alterations in the brain related to prenatal methamphetamine exposure, and whether these alterations can already be detected in the newborn.

MRS, DTI and fMRI have shown a range of metabolic, microstructural and functional alterations as a consequence of prenatal methamphetamine exposure[82,86–89,91,92,143]. In children with prenatal methamphetamine and alcohol exposure, reductions in volume in the thalamus, striatum, and left parieto-occipital and right anterior prefrontal cortices, and increased volumes of several cortical regions, were observed compared to controls and to children with alcohol exposure only[93]. Putamen and globus pallidus volumes were reduced in methamphetamine exposed children, with a trend towards volume reductions of the caudate, thalamus,

hippocampus and cerebellum[94]. A number of these reductions were related to poorer cognitive function[94].

Prenatal methamphetamine exposure has been shown to have considerable, persistent effects on dopaminergic regions of the brain such as the fronto-striatal circuits, as well as certain non-dopaminergic regions. The neuroimaging literature, however, is sparse. To date, no anatomical studies have been conducted with neonates. Such an investigation in neonates is highly warranted, not least because of the sub-optimal postnatal environment into which these children are often born[59,60,65,81]. The aim of this study was thus to investigate the volumetric changes in subcortical areas and cerebellum of the brains of neonates with prenatal methamphetamine exposure. We hypothesized that increased exposure to methamphetamine would be associated with reduced volume of the striatal structures.

3.2 METHODS

3.2.1 Study sample

The cohort consisted of 39 infants born to women in the Cape Coloured (mixed ancestry) community of Cape Town, South Africa, who are participating in a larger prospective longitudinal study of prenatal alcohol and drug exposure on infant development[58,132,135]. The rate of methamphetamine abuse in this community is the highest in South Africa[3], with 35-43% of drug treatment patients reporting it as their primary drug of abuse[7,144]. Rates of use among women in this community have been reported to be as high as 58%[55].

Pregnant mothers were recruited following initial antenatal care visits at midwife obstetric care units serving the community. The mothers were interviewed, once at recruitment and twice more before delivery, regarding their alcohol consumption using a time-line follow-back approach[130,131], and about the frequency of use (days per month) of methamphetamine,

cigarettes and other drugs (marijuana, methaqualone, and cocaine) during pregnancy. The present study consists of infants born to women in the cohort who reported using methamphetamine at least twice per month during pregnancy. The control group, recruited from the same community, comprises infants whose mothers abstained from alcohol and other drugs of abuse or who consumed no more than 2 drinks on 2 or fewer occasions during pregnancy. Exclusion criteria for pregnant women were as follows: < 18 years of age, HIV positive, treatment for medical conditions such as hypertension, epilepsy, diabetes or heart disease, and multiple pregnancy. Infant exclusion criteria were neural tube defects, major chromosomal anomalies, very low birth weight (< 1500g), gestational age < 32 weeks, and seizures[58]. Urine samples were collected and tested to confirm the validity of drug use (reported elsewhere as part of the larger cohort study[58]).

Informed consent was obtained from each mother at recruitment and at the Child Development Research Laboratory and neuroimaging visits. Approval for this study was obtained from the ethics committees at Wayne State University and the Faculty of Health Sciences at the University of Cape Town.

3.2.2 Scanning

Nonsedated infants were scanned between 1 and 4 weeks after birth, with the exception of two infants born prior to 34 weeks who were scanned at 7 and 9 weeks of age, respectively.

Infants were brought to the Cape Universities Brain Imaging Centre (CUBIC) a minimum of 1 hour prior to scanning. During this period they were weighed and head circumference and crown-to-heel length were measured. Neonatal behavioural characteristics[145] were assessed by a trained developmental paediatrician. Following this, the infant was swaddled firmly and placed in a VacFix® vacuum cushion (S&S Par Scientific, Houston, TX) for later use in

immobilising the infant's head in the coil, in accordance with an adapted protocol for neuroimaging assessment of nonsedated newborns[146]. Earplugs were used to protect the infant from the noise of the scanner. The infant was then fed by the mother and allowed to fall asleep.

MRI scanning was performed using a Siemens 3 T Allegra scanner. A custom-built circularly polarised birdcage coil, designed for use with neonates, was used for transmission and reception of the signal. Several sequences were acquired during the protocol. For this study a motion navigated multiecho gradient echo sequence was used, with the following protocol parameters: FOV 114 mm, 128 slices, TR 20 ms, TE 1.46/ 3.14/ 4.82/ 6.5/ 8.18/ 9.86/ 11.54/ 13.22 ms, 1 mm^3 isotropic resolution. The sequence was acquired twice, with flip angles of 5° and 20°, respectively.

The sleeping infant was positioned in the scanner and immobilised by means of the VacFix® cushion. An oxygen saturation and pulse monitor probe was secured to the infant's foot, and this was monitored during the scanning period.

3.2.3 Data synthesis

The individual echoes from the two flip angle acquisitions were split, tissue parameters estimated and an image volume synthesised using FreeSurfer[147]. A flip angle of 24° was chosen as that which produced optimal contrast.

3.2.4 Manual segmentation

ROIs were viewed and manually delineated using Freeview software (FreeSurfer image analysis suite http://surfer.nmr.mgh.harvard.edu/) run on a Lenovo ThinkPad X220 tablet. The following structures were traced bilaterally: caudate nucleus, nucleus accumbens, putamen,

pallidum, thalamus, hippocampus, amygdala and cerebellar hemispheres, as well as the cerebellar vermis. Tracing protocols for each section followed the Infant Brain Segmentation Manual developed by the HST/MGH Athinoula A. Martinos Center for Biomedical Imaging[134], where training in the use of Freeview software and manual tracing of infant MRI scans was received. Tracings were rendered chiefly in the coronal plane, with guidance from the axial and sagittal planes where region boundaries were indistinct in a coronal view. The volumes of the traced regions were then calculated. Total brain volume was determined by extracting the brain from the anatomical T1-weighted volumes using an in-house script. Nine brains were independently retraced for inter-rater reliability purposes. Both tracers were blind to the exposure status of the infant brains.

3.2.5 Statistical analysis

Statistical analysis was performed using SPSS (version 22; IBM, Armonk, NY). Nine variables were considered as potential confounders: maternal age at delivery, educational status (number of years), parity, maternal marijuana use (days per month during pregnancy), smoking (number of cigarettes per day during pregnancy), alcohol use (oz of absolute alcohol consumed per day during pregnancy), infant sex and gestational age at scan (weeks), and total brain volume.

T-tests or chi-square tests for categorical variables were used to compare sample characteristics between exposed and control groups. The methamphetamine use and smoking variables both contained outliers, which were recoded to 1 unit greater than the next highest value (see[148]). Prenatal alcohol use was skewed and was therefore logged for multivariable analyses.

Pearson correlation was used to analyse the relation between methamphetamine exposure and ROI volume. Following this, regions showing significant association with methamphetamine exposure were analysed by means of hierarchical multiple linear regression using a best

estimate approach. Methamphetamine was entered first into the regression; the potential confounders described above which were at least weakly related to volume ($p < 0.20$) were then entered successively according to the strength of their association with the ROI volume. Variables that did not alter β by 10% or more were excluded.

3.3 RESULTS

3.3.1 Sample characteristics

Data is reported for 39 infants (18 methamphetamine exposed and 21 controls). Demographic and substance exposure characteristics of the infants are summarised in Table 3.1. Maternal education differed between groups, with controls achieving a higher level of education than the methamphetamine group.

The sample consisted of 18 male and 21 female infants. Infants exposed to methamphetamine were born earlier, which is consistent with previous studies[58,141]. Although the methamphetamine group weighed less at birth, there was no between-group difference in terms of gestational age at scan (calculated as gestational age at birth + age in weeks).

Mean methamphetamine, smoking, marijuana and alcohol use by mothers of the exposed group was higher than in the control group. Although control mothers did not use methamphetamine, 62% reported smoking, 9.5% used marijuana and 4.8% (1 mother) drank alcohol, although this was within the acceptable limits set for inclusion in the cohort. By contrast, all of the mothers in the exposed group reported smoking, 55.6% ($n = 10$) reported using marijuana and 55.6% ($n = 10$) reported drinking alcohol during pregnancy.

Table 3.1. Sample characteristics (*N* = 39)

	Methamphetamine (*n*= 18)			Control (*n* = 21)				
	Mean	**SD**	**Range**	**Mean**	**SD**	**Range**	**χ^2 or *t***	***p***
Maternal								
Age at delivery (years)	27.0	4.2	19.8 - 34.0	26.7	5.9	18.8 - 36.4	-0.19	0.850
Education (years)	9.3	1.4	7.0 - 12.0	10.5	1.4	7.0 - 12.0	2.60	0.013
Parity	2.2	1.6	0 - 5	1.4	1.3	0 - 4	-1.70	0.098
Socioeconomic status[a]	20.2	4.7	11.0 – 27.0	22.1	7.2	8.0 – 34.5	0.96	0.342
Infant								
Sex (% male)	33			57			2.21	0.137
Birth weight (g)	2804.2	498.9	1370.0 - 3590.0	2915.7	541.7	1940.0 - 4200.0	0.67	0.510
Head circumference (cm)	32.9	1.9	27.0 – 35.0	33.3	2.0	31.0 – 38.0	0.67	0.509
Crown-to-heel length (cm)[b]	47.6	3.5	41.0 – 53.0	48.8	3.4	40.0 – 53.0	1.08	0.287
Gestational age at birth (weeks)	37.6	2.7	31.0 - 41.3	39.1	2.0	33.7 - 42.1	2.01	0.052
Gestational age at scan (weeks)	40.5	2.1	36.7 - 44.0	41.6	1.9	37.6 - 44.6	1.65	0.107
Total intracranial volume (mm^3)	491044	41631	395900 - 549600	516805	69236	428700 - 660700	1.38	0.177
Substance use								
Methamphetamine (days/month)	6.1	3.8	0.7 - 12.0	0.0	0.0	0.0 - 0.0	-7.34	<0.001
Smoking (number cigarettes/day)	6.5[c]	4.5	2.0 - 20.0	3.5[d]	3.4	0.0 - 10.3	-2.42	0.021
Marijuana (days/month)	5.8[e]	8.4	0.0 - 30.5	0.0[f]	0.1	0.0 - 0.2	-3.18	0.003
Alcohol (oz AA /day)	0.2[g]	0.4	0.0 - 1.4	0.0[h]	0.0	0.0 - 0.1	-2.15	0.038

[a]Hollingshead (2011) Four Factor Index of Social Status Scale; [b]n = 17 for methamphetamine group; [c]18/18 (100%) and [d]13/21 (62%) smoked; [e]10/18 (56%) and [f]2/21 (10%) used marijuana; [g]10/18 (56%) and [h]1/21 (5%) used alcohol.

Table 3.2. Volumes and interrater reliability measures

ROI	Volume (mm^3)		Dice Coefficients	
	Methamphetamine (n=18) Mean ± SD	Control (n=21) Mean ± SD	Median	Range
Overall	-	-	88.5	84.7 - 99.6
Left caudate	1241 ± 201	1300 ± 197	84.6	83.2 - 88.8
Right caudate	1175 ± 159	1264 ± 156	86.6	84.4 - 89.9
Left putamen	1679 ± 256	1806 ± 322	81.5	76.7 - 87.3
Right putamen	1720 ± 242	1798 ± 328	84.0	73.2 - 86.5
Left pallidum	650 ± 111	685 ± 123	66.8	37.7 - 76.1
Right pallidum	594 ± 91	626 ± 131	69.8	49.8 - 81.1
Left nucleus accumbens	150 ± 29	148 ± 41	38.3	18.0 - 63.4
Right nucleus accumbens	158 ± 41	147 ± 41	43.1	28.1 - 66.2
Left thalamus	4344 ± 352	4435 ± 713	90.3	85.3 - 92.1
Right thalamus	4264 ± 360	4470 ± 708	90.8	86.4 - 92.9
Left hippocampus	1187 ± 148	1149 ± 151	80.8	63.2 - 85.1
Right hippocampus	1173 ± 109	1144 ± 140	79.7	73.4 - 86.3
Left amygdala	383 ± 116	370 ± 74	64.2	44.6 - 75.6
Right amygdala	406 ± 124	374 ± 79	67.5	54.0 - 74.5
Vermis	1957 ± 383	1986 ± 386	84.7	71.4 - 89.7
Left cerebellar cortex	10207 ± 1500	10365 ± 1949	92.4	91.7 - 96.0
Right cerebellar cortex	10188 ± 1447	10501 ± 1820	93.3	88.6 - 95.8

3.3.2 Inter-rater reliability of manual tracing

Volumes of traced regions and inter-rater reliability measures are reported in Table 3.2. Interrater reliabilities are reported as the median and range of the Dice coefficients calculated for 9 brains. A threshold median value of 75.0 was set, falling below which any traced region was regarded as too unreliable to include in further analyses. Following these criteria, right and left pallidum, right and left nucleus accumbens, and right and left amygdala were discarded from further analyses.

Table 3.3. Association between prenatal methamphetamine exposure and volume of subcortical structures (*N* = 39)

Volume (ROI)	Methamphetamine exposure	
	r	***p***
Left caudate	**-0.31**	**0.059**
Right caudate	**-0.48**	**0.002**
Left putamen	-0.13	0.430
Right putamen	-0.10	0.550
Left thalamus	-0.17	0.297
Right thalamus	-0.26	0.107
Left hippocampus	-0.06	0.702
Right hippocampus	0.10	0.563
Vermis	-0.07	0.654
Left cerebellum	-0.18	0.275
Right cerebellum	-0.22	0.188

r is the Pearson correlation between methamphetamine exposure and volume. Boldface denotes significant findings.

3.3.3 Relation of methamphetamine exposure to subcortical regional volumes

The associations between methamphetamine exposure and the subcortical regions are shown in Table 3.3. Pearson correlation analyses showed that heavier methamphetamine exposure was associated with reduced left and right caudate volumes (Fig. 3.1). No association was observed between methamphetamine exposure and the other regions. Infants with heavier methamphetamine exposure also tended to have reduced total brain volume (r = -0.28, p = 0.08).

Potential confounding variables (Table 3.4) were included in the subsequent regression analyses if they showed a correlation with ROI volume at $p < 0.20$. Total brain volume, cigarette smoking, infant sex, gestational age at time of scan, and parity were associated with

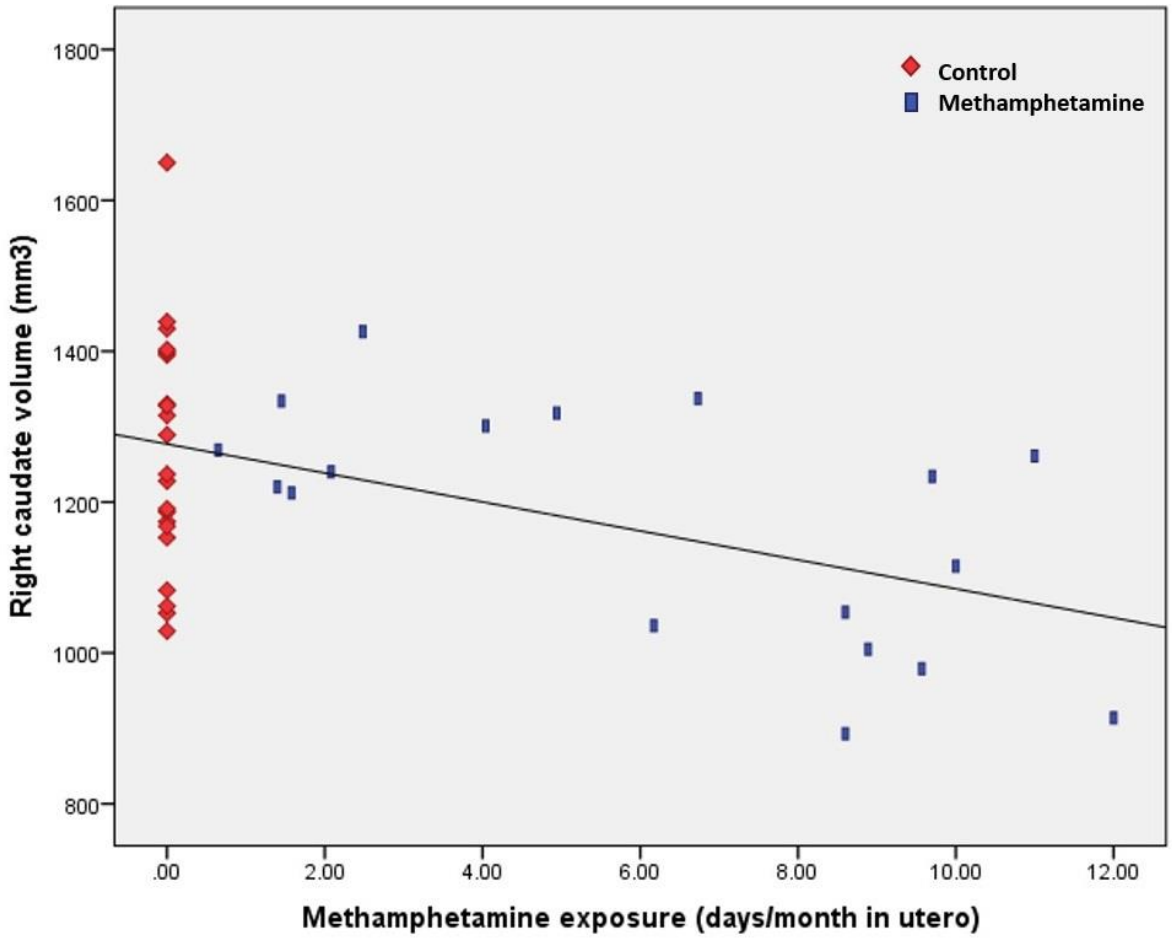

Figure 3.1 Relation of prenatal methamphetamine exposure across pregnancy to volume of the right caudate nucleus.

---

left and right caudate volumes, while maternal education was also associated with right caudate volume. Left and right caudate volume were then each regressed with methamphetamine, followed by total brain volume, and finally maternal cigarette smoking and infant sex for left and right caudate volumes respectively. Prenatal exposure to methamphetamine was associated with reduced volume in the right caudate even after controlling for total brain volume (β = -0.33, p = 0.01) and the potential confounder (infant sex; β = -0.28, p = 0.03). The association of methamphetamine exposure with left caudate volume did not persist when total brain volume and maternal smoking were included (β = -0.07; $p < 0.20$).

Table 3.4. Association of potential confounding variables with volumes of regions showing significant associations with methamphetamine

	Maternal age (years)	**Education (years)**	**Parity**	**Marijuana (days/month)**	**Smoking (number of cigarettes/ day)**	**Alcohol (oz AA/day)**	**Infant sex**	**Gestational age at scan (weeks)**	**Total brain volume (mm^3)**
Left caudate	-0.03 (0.840)	0.21 (0.208)	**-0.24 (0.145)**	-0.02 (0.898)	**-0.49 (0.002)**	0.16 (0.337)	**-0.42 (0.008)**	**0.25 (0.128)**	**0.55 (<0.001)**
Right caudate	-0.18 (0.271)	**0.24 (0.170)**	**-0.35 (0.032)**	0.02 (0.924)	**-0.37 (0.020)**	0.19 (0.237)	**-0.49 (0.002)**	**0.43 (0.006)**	**0.59 (<0.001)**

Values are Pearson *r* (*p*). Results with a trend towards association ($p < 0.20$) are shown in boldface.

3.4 DISCUSSION

This study is the first to investigate the neurostructural effects of prenatal exposure to methamphetamine in neonates. As hypothesised, changes were observed in the left and right caudate nuclei, as well as in total brain volume, with reduced volume observed in all three as a consequence of prenatal methamphetamine exposure. Although the association in the left caudate did not persist when confounding variables were included in the analysis, the effect of methamphetamine on the right caudate remained significant, even after controlling for reduction in total brain size.

These results are consistent with those obtained in previous studies in which volumetric effects of prenatal methamphetamine exposure on the caudate were observed in older cohorts. In a study of children aged between 5 and 15 years, the striatum was smaller in children exposed to both methamphetamine and alcohol prenatally, with the volume reduction more severe than in children exposed to alcohol alone[93]. Similarly, a study of 3-5 year old children with methamphetamine and tobacco exposure showed significantly reduced caudate volume following control for tobacco exposure[95]. A trend towards reduction in volume was observed in the caudates of children aged 3-16 years with prenatal methamphetamine exposure[94]. In an investigation of children aged 8-11 years with multiple substance exposure, including methamphetamine, a trend towards reduced caudate volume was observed, with significantly decreased total volume[149]. By contrast, increased striatal volume was found in 6-year-olds with *in utero* methamphetamine exposure, findings which may reflect methodological effects[96]. This was one of only two studies that performed automated segmentation using FreeSurfer, but Derauf and colleagues, who noted reduced caudate volume, made use of a validated pediatric atlas[95], while Roos *et al*[96] do not specify which atlas was used for analysis. In adult users, volumetric alterations have been observed in a number of studies. A reduction in caudate

volume was noted in methamphetamine-dependent smokers[20]. Other research, however, observed increased caudate volume in recently abstinent methamphetamine users[18,150].

The loss of effect of methamphetamine in the left caudate after controlling for confounders was unexpected, but may be due to chance confounding in this sample. The association of methamphetamine with volume was weaker in the left caudate than in the right before the addition of the confounding variables, while the association of cigarette smoking with volume was considerably stronger in the left caudate than in the right. Given that the relative magnitudes of these effects might vary in different samples, it seems reasonable to suggest that both these exposures have bilateral impact. Cigarette smoking has been shown to be associated with volume reductions in a variety of brain structures in adult smokers[151] and children with prenatal exposure[152].

Previous studies of prenatal methamphetamine exposure reported volume reductions in additional regions, including the hippocampus[94] and thalamus[93] as well as in a number of frontal cortical regions[93]. These alterations were not observed in the current study. It is worth noting that the strength of the association between methamphetamine and thalamus volume in this study might well have proved significant with a larger sample size; the same can be said of the association of methamphetamine exposure with cerebellar volumes. The strength of the association of methamphetamine with caudate volume in the current study, however, lends support to the hypothesis that prenatal methamphetamine specifically targets dopamine-rich regions, such as the caudate. This is in striking contrast to alcohol, which has been shown to be teratogenic to multiple regions of the brain[153–156], and suggests that the mechanisms whereby methamphetamine and alcohol induce CNS damage are likely distinct from one another.

Reduced total brain volume has been observed previously in children with prenatal methamphetamine exposure[149]. While this was also observed in the current study, the right

caudate was disproportionately affected, with the volume reduction in this structure remaining significant after adjusting for total brain volume. Reduced birth weight and lower gestational age at birth have also been shown to be associated with prenatal methamphetamine exposure[63,74,141]. This may be due to the vasoconstrictive effect of methamphetamine, causing reduced blood flow across the placenta[57] and consequent restriction of nutrient and oxygen supply to the fetus[65,94]. Analysis of placental development in our cohort showed that methamphetamine use during pregnancy was associated with increased placental size, as well as increased placenta- to birth- weight ratio, lower gestational age at birth, and increased risk of intrauterine passing of meconium, which suggests that the exposed fetus may experience prolonged periods of hypoxia-ischemia[58].

The precise mechanisms whereby *in utero* methamphetamine exposure reduces caudate volume are not fully understood. Methamphetamine has been shown to be neurotoxic to dopaminergic and serotonergic axons and terminals in animal[157–160] and human studies[45,161], and in mature neurons appears to involve the production of reactive oxygen species (ROS), activation of P53 and subsequent apoptosis, and dysfunction of mitochondria[162]. Alterations in dopamine and dopamine metabolite concentrations have been observed in the striatum of rats prenatally exposed to methamphetamine[163,164]. Additionally, gene expression profiles are altered in rats with prenatal methamphetamine exposure, with substantial changes being observed in a number of genes coding for structural and guidance proteins which play vital roles in regulating normal neuronal development[165]. ROS production consequent to methamphetamine exposure *in utero* has been observed in animal studies[166,167], although the mechanisms by which this induces damage in the developing nervous system appear to be different from those in mature neurons[167]. Methamphetamine exposure appears to have differential effects on dopamine neurons depending on the age at which exposure occurs[168]; in non-human primates in the second gestational trimester, neurons of the nigrostriatal pathway

have been shown to be particularly vulnerable to methamphetamine-induced damage[168]. During this period primate dopamine neurons undergo natural cell death as part of the normal development and maturation of the neuronal population[169], and it has been hypothesised that this might render them more highly susceptible to damage[168].

To our knowledge, this is the first study in which reduction in caudate volume is demonstrated in neonates with prenatal methamphetamine exposure. Piper and colleagues have observed that children with prenatal methamphetamine exposure are very likely to be born into a poor postnatal environment[81]. Primary caregiver psychological symptoms and poor quality home environment were shown to increase behavioural problems assessed on the Child Behavior Checklist, in studies of preschool age children with prenatal methamphetamine exposure[79,170]. Neonatal evaluation of the effects of methamphetamine exposure allows for assessments relatively unconfounded by the effects of postnatal environment. Evaluation of methamphetamine exposure effects during the neonatal period allows for assessments of exposure prior to the effects of postnatal environment. This may also be a consideration in understanding why effects were observed in a greater number of regions in studies of prenatal methamphetamine exposure which used older cohorts.

The women whose children were scanned in this study were recruited during pregnancy. This provided the advantage of allowing a more accurate measure of methamphetamine use by means of the timeline follow-back approach as described above. This is a distinct advantage over studies of older children in which recall of precise drug use by the mother is all but impossible, and it allows a more valid quantitative analysis of the effects of methamphetamine exposure. To our knowledge, this is the first study that shows an association between increasing methamphetamine exposure and reduced caudate volume rather than group differences as reported in previous research[93,94,96,149].

An additional strength of this study is the use of manual tracing for segmentation of brain regions. Manual segmentation is regarded as the "gold standard" in volumetric analysis of brain structures[171–173]. Furthermore, automated segmentations of immature brains, such as those of infants and children, are likely to be inaccurate given that the atlases on which these methods are based are derived from adult brains. This is a particularly relevant issue when the subjects are neonates, as incomplete myelination of the neonatal brain[97] presents a challenge in correctly identifying regions of interest.

There are a number of limitations to this study. The greatest is the potential confounding effects of polysubstance exposure, with the methamphetamine-exposed infants also having higher exposure to alcohol, cigarette smoking and marijuana. This is, unfortunately, almost inevitable in studies of prenatal drug exposure[82,93]. These other exposures were, however, controlled in the multivariable analyses in this study. Moreover, as mentioned above, recruitment during pregnancy allowed for a more accurate measure of substance use. Previous studies[93,94,96] did not control for cigarette exposure, which was shown to be a significant confounding variable in the current study.

It should be considered that some unexamined additional factor, such as malnutrition or deprivation, may have played a role in these findings. However, both exposed and control groups were recruited from the same community, and socioeconomic status[174] did not differ between groups. Furthermore, neither birth weight nor crown-to-heel length, both of which might be considered measures of intrauterine nutritional status, was different between exposed and control children.

The sample size was small, but comparable to other studies[93,96] and sufficient to observe statistically significant effects. It is possible that with a larger cohort additional differences might have been significant. A potential concern, as in most such studies, is the issue of

multiple comparisons. Eleven ROIs were included in the final analysis. However, the association of methamphetamine with right caudate volume remained significant, prior to the addition of confounders, even after controlling for multiple comparisons. Furthermore, as mentioned previously, the significant exposure effect was predicted *a priori* and found precisely where it was expected, which provides additional support for its validity.

Given the rapid and heterochronous nature of early brain growth[175], regional volumes obtained in the first weeks of life are particularly challenging to measure. Segmentation of the newborn brain is more time-consuming due to lower contrast-to-noise ratio[176]. Although the brain stem and posterior limbs of the internal capsule are myelinated in the newborn with white to grey matter contrast that is similar to the adult brain, other regions are unmyelinated with the grey/ white contrast inverted in T1-weighted images relative to adult contrast[101,177]. Despite these difficulties, we were able to demonstrate reductions in caudate volume in methamphetamine-exposed newborns, consistent with previously published research in older children. These reductions are thus already detectable in exposed infants in the first month postpartum. Future research is warranted to examine whether reduced caudate in methamphetamine-exposed neonates is predictive of the cognitive, behavioural and affective impairments observed in older children.

CHAPTER 4

WHOLE-BRAIN WHITE MATTER CHANGES ARE ASSOCIATED WITH PRENATAL METHAMPHETAMINE EXPOSURE

4.1 INTRODUCTION

Methamphetamine abuse is one of the fastest growing drug problems worldwide, with estimates suggesting that its use may exceed the combined use of heroin and cocaine[178]. It functions primarily as a stimulant of the CNS, altering the release and activity of the neurotransmitters dopamine, norepinephrine and serotonin[179–181]. In current and abstinent users, it has been shown to be associated with damage in a range of brain areas. Changes in the striatum[19,46,182], hippocampus[23], amygdala[46] and several cortical areas[23,46,183] have been associated with methamphetamine abuse, with damage being seen to correlate with affective or cognitive alterations in a number of studies[23,46,183,184].

It has been estimated that over 5% of women in the United States have used methamphetamine while pregnant[54]. Methamphetamine has been shown to cause vasoconstriction and reduced blood flow to the placenta[57]; this has deleterious effects on the placenta itself[58], and can result in fetal hypoxia[67]. Methamphetamine use during pregnancy is associated with increased risk of hypertensive diseases of pregnancy[142], increased risk of fetal and neonatal death[142] and of preterm birth[59,65,141], reduced birth weight[141] and size[142] and increased incidence of congenital abnormalities[60,185].

Given the demonstrated neurotoxicity of methamphetamine in adult users, it is to be expected that exposure during the vulnerable prenatal period would have severe and potentially long-lasting effects on the infants concerned. The CNS undergoes rapid development and growth during gestation[72] and it is reasonable to hypothesise that exposure to methamphetamine will produce significant neural modifications.

DTI provides a non-invasive means to visualise and characterise white matter[120,125]. It measures signal changes resulting from the diffusion of water molecules in the CNS and determines the various directionalities of this movement within fibre bundles, providing a number of measures of the structural integrity of the white matter and its component axons[123]. FA is the normalised standard deviation of the diffusivities parallel (AD) and perpendicular (RD) to the white matter fibres, and is the most widely-used DTI measure[123]. A high FA reflects diffusion that is chiefly parallel to the fibre bundles and restricted in the perpendicular direction, and is considered an indicator of more highly ordered, healthy or mature white matter[125].

In addition to the magnitude of the diffusivities, DT images contain information relating to the 3-dimensional direction and alignment of diffusion[123]. This information can be used to map the trajectories of white matter bundles in the CNS[120,123] by plotting fibre orientation from the directionality of sequential individual voxels[125]. The microstructure of these bundles, or of connections between defined regions of interest, can then be characterised by determining diffusion measures, such as FA, across the entire tract[125]. Alterations in diffusion characteristics are often related to functional changes[186]; many pathological processes induce changes in white matter microstructure, and DTI is thus a powerful tool for investigating the effects of these processes[122].

There is considerable evidence that methamphetamine induces alterations in white matter microstructure in adult users. Several studies have noted reduced FA in frontal regions of recently abstinent methamphetamine users[28,31,187]. Reduced FA in the CC, particularly in the genu, has also been observed in methamphetamine users[29,30,187]. Findings in the basal ganglia are more equivocal, with higher AD and RD observed in caudate and putamen in one study[31], while another observed no changes in these structures[188] relative to comparison subjects.

Given these findings in adult methamphetamine users, it is reasonable to hypothesise that *in utero* exposure to methamphetamine might have similar effects on the white matter of the exposed infants. The neuroimaging literature of children with prenatal methamphetamine exposure is sparse, however. In a study of children aged 6-7 years with prenatal methamphetamine exposure, reduced FA and higher RD, AD and MD were observed in tracts traversing striatal, limbic and frontal regions in comparison with control subjects[82]. Similarly, lower FA and increased AD and RD in the corona radiata were observed in infants exposed to methamphetamine and tobacco[90]. By contrast, higher FA was noted in the genu of the CC, the internal and external capsules and the corona radiata of 9-11 year old children with prenatal methamphetamine exposure[92]. Cloak and colleagues observed a similar trend in a voxel-based study of 3-4 year-olds with prenatal exposure, with lower diffusivity and higher FA in CC genu and splenium, frontal and parietal white matter, caudate, putamen, globus pallidus and thalamus[91].

The available literature thus demonstrates that prenatal methamphetamine exposure has significant and persistent effects on CNS microstructure, although the findings are not unanimous as to the exact direction of these changes. Further detailed investigations of white matter alterations associated with *in utero* methamphetamine exposure are highly warranted. Moreover, only one DTI study has to date been conducted with neonates, which investigated the combined effect of methamphetamine and tobacco exposure[90]. Investigations in neonates allow a greater separation of the effects of drug exposure from potential confounding post-natal influences. Given the sub-optimal environment into which children of mothers using methamphetamine are almost invariably born[65,81], these are likely to exert a significant effect on neural development.

The aim of this study was therefore to investigate the microstructural alterations, quantified by diffusion and anisotropy measures, in the three major classes of white matter tracts,

commissural, projection and association fibres, in the brains of neonates who had been exposed to methamphetamine prenatally, as compared to unexposed control infants from the same community.

4.2 METHODS

4.2.1 Study sample

The study sample comprised infants who were born to mothers from the Cape Coloured (mixed ancestry) community of Cape Town, South Africa. The rate of methamphetamine abuse in this community is the highest in South Africa[3]; 35-43% of patients seeking treatment for drug abuse report it as their primary drug[7,144]. Rates of methamphetamine use have been reported to be as high as 58% among women in this community[55]. The infants are a subset of a larger prospective longitudinal study of prenatal alcohol and drug exposure on infant development[58,132,135]. The exposed group consisted of infants with prenatal exposure to methamphetamine, while the control group consisted of infants from the same community who had not been exposed to methamphetamine in utero, and with minimal or no prenatal exposure to alcohol or other drugs of abuse.

Pregnant women were recruited following antenatal care visits at midwife obstetric care units in the community. They were interviewed at three time-points during pregnancy, once at recruitment, with regard to their methamphetamine, cigarette, alcohol and other drug use during pregnancy. The interviews used a timeline follow-back approach[130,131]. Women in the exposure group reported the use of methamphetamine on at least two occasions per month during pregnancy. Alcohol consumption, cigarette smoking and other drug use during pregnancy were recorded and controlled for in the later analyses. The control group consisted of women who abstained from methamphetamine, alcohol and other drugs of abuse, or who consumed no more

than 2 drinks on no more than 2 occasions during the pregnancy. Women were excluded if they met any of the following criteria: under 18 years of age, multiple pregnancy, HIV positive, or treatment for medical conditions such as hypertension, heart disease, epilepsy, or diabetes. Infant exclusion criteria were neural tube defects, seizures and chromosomal abnormalities[58].

Informed consent was obtained from each mother at recruitment and at the first laboratory visit. Ethics approval for the study was obtained from the ethics committee at Wayne State University and the Faculty of Health Sciences Human Research Ethics Committee at the University of Cape Town.

4.2.2 Scanning

Infants were scanned without sedation, at between 1 and 5 weeks of age, with the exception of 1 infant who was born at 31 weeks gestational age and scanned at 9 weeks of age. Scanning took place at the Cape Universities Brain Imaging Centre (CUBIC) at the Faculty of Health Sciences campus of the University of Stellenbosch, South Africa.

Infants were brought to the scanning facility at least 1 hour prior to scanning. Before scanning they were weighed, head circumference and crown-to-heel length were measured and neonatal behavioural characteristics[145] were assessed. The infant was then swaddled and placed in a deflatable vacuum cushion (VacFix®, S&S Par Scientific, Houston, TX). Earplugs were inserted to protect the infant from the noise of the scanner. The infant was fed and allowed to fall asleep.

The infant was placed in the scanner and immobilised by means of the VacFix® cushion, in accordance with a protocol developed by Laswad and colleagues[146]. A probe monitoring pulse and oxygen saturation was attached to the infant's foot, and this was monitored throughout the

scanning process by a developmental paediatrician or research nurse who remained in the scanning room for the duration of the procedure.

A Siemens 3T Allegra scanner was used for MRI scanning. A circularly polarised bird-cage coil, custom built for neonatal scanning, was used to transmit and receive the signal. Two diffusion weighted imaging (DWI) sets with opposite (AP/PA) phase encoding directions were acquired with a twice refocused spin echo EPI sequence. For 5 infants (1 exposed, 4 controls) the following scanning parameters were used: TR 9500 ms, TE 86 ms, 50 slices of 80x80 voxels (2x2x2 mm^3). For the remaining infants a navigated DTI sequence was used, which performs real-time motion detection and correction[189]. The parameters in the latter sequence were identical to the first, with the exception of TR = 10 026 ms. In both sequences, AP and PA acquisitions each contained four b = 0 $s.mm^{-2}$ reference scans and 30 DW gradient directions with b = 1000 $s.mm^{-2}$.

For anatomical imaging, a multiecho FLASH sequence[190] was used, with protocol parameters as follows: TR 20 ms, TE 1.46/ 3.14/ 4.82/ 6.5/ 8.18/ 9.86/ 11.54/ 13.22 ms, 128 x 144 x 144 voxels, 1 mm isotropic resolution. Two anatomical acquisitions were obtained with flip angles of 5° and 20° respectively.

4.2.3 Data processing and parameter estimation

DWI data were inspected visually for motion and dropout slices, and individual volumes of poor quality were discarded. A minimum of 12 DWIs remained for each infant. Motion and EPI distortion were corrected in each set using FSL's eddy_correct and topup tools[137], and DTs and tensor parameters such as FA, MD, eigenvalues (L_i, i = 1,2,3; AD = L_1; RD = [L_2+L_3]/2) and directional eigenvectors (e_i, i = 1,2,3) estimated using AFNI[191]. Freesurfer software

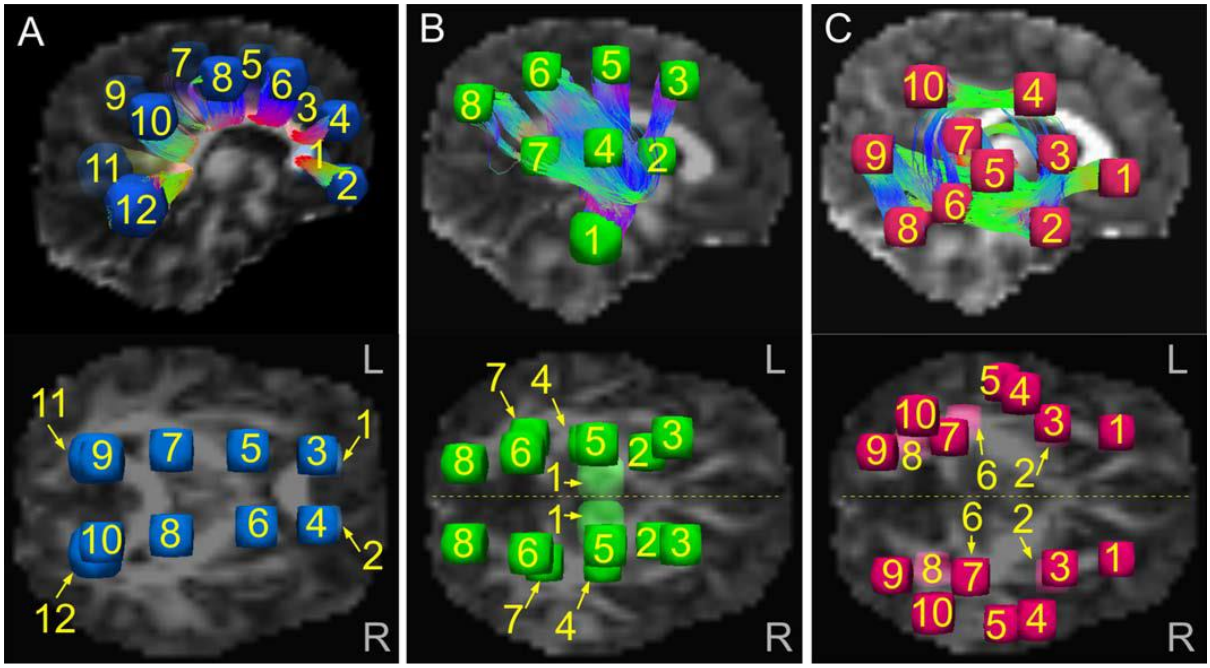

Figure 4.1. Locations of target ROIs, with WM-ROI connections shown in top panel. Mini-probabilistic tractography was used to create homologous target locations, following which ROIs were mapped to each subject's native DW space for tractography. **A**. Target ROIs for connections in the commissural network. **B**. The upper panel shows targets for right projection fibres in coronal view; the lower panel shows left and right projection targets in axial view. **C**. The upper panel shows targets for right association fibres in coronal view; the lower panel shows left and right association targets. (Figure reprinted from Ref[135]).

(http://surfer.nmr.mgh.harvard.edu/) was used to generate optimised anatomical images from the FLASH sequences, and T1 and PD images were estimated.

4.2.4 Selection of regions of interest and tractographic analysis

Five white matter network groups were analysed: commissural fibres, which included the CC, projection fibres in left and right hemispheres, and association fibres in left and right hemispheres. These networks were defined by placing spherical target ROIs in one control brain (see Fig. 4.1). Twelve ROIs were placed along the extent of the CC and corona radiata. Eight ROIs were placed in the left projection fibres and 8 homotopically located ROIs in the right projection fibres. Ten ROIs were placed in the left association fibres, and 10 homotopic ROIs in the right association fibres. Sphere location was decided based on an initial estimate

of likely white matter bundle locations, using a "mini-probabilistic" tractographic approach which combined deterministic tractography and DT uncertainty measures[135]. Once ROIs had been placed in the initial subject, they were mapped to the full study cohort to produce in each subject five networks of homologous target ROI sets.

Probabilistic tractography was then performed to find connections between ROIs in each network group and to determine quantitative measures of white matter properties in these connections. Using FATCAT software in AFNI[127], uncertainties in DT eigenvectors and FA were estimated. The FACTID algorithm[139] was then used to perform 5000 Monte Carlo iterations of brute force tractography. This algorithm finds fibres connecting pairs of targets at each iteration. The following propagation parameters were used: a maximum angle of propagation of 55°, between voxels with FA > 0.1, the standard FA threshold for white matter in infants[192]. All voxels through which a minimum (> 1% of Monte Carlo iterations) of tracts passed were included to define white matter regions of interest (WM-ROIs) associated with each pair of targets, and WM-ROIs found between the same target regions in every subject were included for further analysis. Mean and SD of the DTI parameters FA, AD, and RD were calculated for each WM-ROI.

4.2.5 Statistical analysis

Statistical analysis was performed using afex in R. SPSS (version 23; IBM, Armonk, NY) was used for analysis of demographic characteristics. Ten variables were considered as potential confounders: maternal marital status, parity, educational status (highest grade level completed) and socioeconomic status[174] (ses), maternal marijuana use (days per month during pregnancy), maternal smoking (number of cigarettes per day during pregnancy) and maternal alcohol use (oz AA consumed per day during pregnancy), and infant sex, birth weight (grams) and

gestational age at scan (weeks). Data were examined for skewness and outliers were recoded to one unit greater than the next highest value (methamphetamine, alcohol, marijuana and cigarette smoking; see[148]). *T*-tests, or chi-squared tests for categorical variables, were used to compare sample characteristics between exposed and control groups.

In each of the five WM networks, the association of prenatal methamphetamine exposure (number of days per month of pregnancy) with FA was examined. Acquisition sequence (DTI sequence used) was included in an initial multivariate general linear model analysis for each network. Potential confounding variables showing a weak association ($p < 0.1$) with FA were included in subsequent multiple linear regression analyses on a network-by-network basis. Following the network level analysis, the effect of methamphetamine exposure on each WM-ROI in each network was analysed, with the significant confounding variables for each network included in the multiple regression. The primary aim of the post hoc evaluation was not to investigate individual connections, but to analyse global patterns of white matter disturbance within the networks examined.

Potential associations of methamphetamine exposure with AD and RD were examined to determine whether significant associations of methamphetamine exposure on FA were related to either axial or radial diffusivity. Acquisition sequence was again included in an initial multivariate general linear model analysis for each network, followed by adjustment for the confounding variables used in the FA analysis. AD and RD in individual WM-ROIs were then analysed using the same procedure as described above.

4.3 RESULTS

4.3.1 Sample characteristics

The study sample consisted of 23 infants, 11 in the methamphetamine exposed group and 12 in the control group. Table 4.1 shows the demographic characteristics of the cohort. Maternal education, measured as the highest grade level achieved by the mother, was significantly lower in the exposed group than the controls.

The cohort included 12 male and 11 female infants, with the methamphetamine group including 5 males and the control group including 7 males. The number of male and female infants per group was not statistically different between groups. Although methamphetamine exposed infants tended to be born at a younger gestational age, the difference was not significant. There was no difference between groups in gestational age at scan (gestational age at birth + age in weeks) or birthweight.

Mothers of infants in the exposed group tended to smoke more than mothers of the control group. Control mothers did not use methamphetamine, but 67% smoked, 17% used marijuana and 1 mother drank alcohol within the acceptable limits set for inclusion in the cohort. By contrast, all of the mothers in the exposed group smoked cigarettes, 46% (n = 5) used marijuana and 46% drank alcohol during pregnancy.

4.3.2 Tractographic connections

Probabilistic tractography produced several WM-ROI connections between target ROIs that were common to all infants. In the commissural network, 3 connections were present in all infants. In the left and right projection fibre networks, 10 connections were present in each. In the left association fibre network, 12 connections were present, while in the right projection fibre network there were 9 connections common to all infants.

Table 4.1. Sample characteristics (*N*=23).

	Methamphetamine (PEM) (*n*= 11)			Control (Ctl) (*n* = 12)				
	Mean	**SD**	**Range**	**Mean**	**SD**	**Range**	**χ^2 or *t***	***p***
Maternal								
Age (years)	27.2	3.9	21.4 - 32.6	25.1	5.4	18.8 - 36.4	-1.05	0.305
Education	9.4	1.2	7.0 - 11.0	10.6	1.1	9.0 - 12.0	2.56	0.018
Parity	2.1	1.6	0 - 5	1.3	1.2	0 - 3	-1.44	0.165
Infant								
Sex (% male)	45.5			58.3			0.38	0.537
Birth weight (g)	2806.8	600.5	1370.0 - 3590.0	2795.8	485.2	1940.0 - 3470.0	-0.05	0.962
Gestational age at birth (weeks)	37.3	3.0	31.0 - 40.7	39.0	1.7	36.6 - 42.1	1.67	0.110
Gestational age at scan (weeks)	40.6	2.1	37.3 - 43.1	41.6	1.9	37.6 - 44.1	1.24	0.227
Substance use								
Methamphetamine (days/month)	7.1	3.5	1.5 - 12.0	0.0	0.0	0.0 - 0.0	-7.04	0.000
Smoking (number cigarettes/day)	6.5[a]	5.4	2.0 - 20.0	3.3[b]	2.8	0.0 - 7.7	-1.78	0.089
Marijuana (days/month)	4.4[c]	9.6	0.0 - 30.5	0.0[d]	0.1	0.0 - 0.2	-1.58	0.129
Alcohol (oz AA /day)	0.2[e]	0.4	0.0 - 1.4	0.0[f]	0.0	0.0 - 0.1	-1.26	0.222

[a]11/11 (100%) and [b]8/12 (66.7%) smoked cigarettes; [c]5/11 (45.5%) and [d]2/12 (16.7%) used marijuana; [e]5/11 (45.5%) and [f]1/12 (8.3%) drank alcohol during pregnancy.

Table 4.2. Association of methamphetamine exposure with FA in the five networks (*N*=23).

Network	β_{acq} (E-03)	p_{acq}	β_{conf} (E-03)	p_{conf}	Confounders added
Commissural	-1.90	0.087	**-1.49**	**0.034**	age, alcohol, ses, sex
Left projection	-1.54	0.051	**-1.79**	**0.001**	age, ses, marijuana, sex
Right projection	**-2.66**	**0.041**	**-2.86**	**0.009**	age, ses, sex
Left Association	**-1.75**	**0.032**	**-2.41**	**0.005**	age, education, ses, marijuana, sex
Right Association	**-2.11**	**0.017**	**-1.57**	**0.044**	age, sex

β values are non standardised. X_{acq} = value following regression with acquisition sequence. X_{conf} = value following regression with all significant confounding variables. Significant results are highlighted in boldface. Age = gestational age at scan (weeks); ses = Hollingshead socioeconomic status.

4.3.3 Association of prenatal methamphetamine exposure with FA in white matter networks

The association of methamphetamine exposure with FA in each of the five WM networks is shown in Table 4.2. Following an initial linear regression to control for acquisition sequence (DTI sequence used), FA was shown to be significantly associated with increasing methamphetamine exposure in the right projection fibre network and the left and right association fibre networks. Prenatal methamphetamine exposure was associated with FA at a trend-level ($p < 0.1$) in the commissural and left projection fibre networks. Confounding variables were included in the regression analysis of each network if they showed a weak association with FA in that network. Following the addition of confounding variables in the multivariate linear regression analysis, increasing methamphetamine exposure was observed to be significantly associated with FA reductions in all five WM networks.

The individual WM-ROIs within each network showing associations (at $p < 0.1$) of methamphetamine exposure with FA are listed in Table 4.3. In the projection fibre networks, increased methamphetamine exposure was significantly associated with decreased FA bilater-

Table 4.3. WM-ROIs showing associations of FA with methamphetamine exposure (*N*=23).

Network	WM-ROI	Methamphetamine FA (mean ± SD)	Control FA (mean ± SD)	β_{acq} (E-03)	p_{acq}	β (E-03)	p_{conf}	Confounders
Left Projection	001-007	0.244 ± 0.015	0.254 ± 0.025	-1.92	0.082	**-2.86**	**0.004**	age, ses, marijuana, sex
	004-006	0.253 ± 0.019	0.261 ± 0.022	**-2.41**	**0.005**	**-2.77**	**0.010**	
Right Projection	001-005	0.255 ± 0.014	0.277 ± 0.043	-3.01	0.099	**-3.93**	**0.023**	age, ses, sex
	002-003	0.185 ± 0.023	0.201 ± 0.032	-2.74	0.073	**-3.02**	**0.024**	
	004-005	0.249 ± 0.011	0.268 ± 0.024	**-2.27**	**0.036**	**-2.65**	**0.003**	
	004-006	0.251 ± 0.015	0.264 ± 0.026	**-2.76**	**0.005**	**-3.26**	**0.001**	
	004-007	0.253 ± 0.012	0.273 ± 0.036	-2.81	0.063	**-3.78**	**0.010**	
	007-008	0.183 ± 0.019	0.194 ± 0.023	**-2.76**	**0.011**	**-2.70**	**0.010**	
Left Association	001-003	0.174 ± 0.021	0.187 ± 0.020	**-2.28**	**0.040**	**-1.94**	**0.035**	age, education, ses, marijuana, sex
	003-007	0.235 ± 0.013	0.245 ± 0.027	-2.11	0.051	**-2.59**	**0.031**	
	005-007	0.188 ± 0.016	0.192 ± 0.021	-1.72	0.078	**-3.17**	**0.004**	
	006-007	0.215 ± 0.025	0.222 ± 0.019	**-2.25**	**0.047**	-2.55	0.074	
	007-009	0.232 ± 0.017	0.236 ± 0.017	**-2.01**	**0.010**	**-2.44**	**0.005**	
Right Association	001-002	0.197 ± 0.023	0.214 ± 0.026	**-3.06**	**0.018**	**-2.33**	**0.045**	age, sex
	005-007	0.176 ± 0.010	0.182 ± 0.016	**-1.33**	**0.044**	-1.21	0.098	
	006-007	0.232 ± 0.025	0.238 ± 0.038	**-3.07**	**0.028**	**-3.19**	**0.034**	
	006-008	0.217 ± 0.020	0.228 ± 0.023	**-2.88**	**0.006**	**-1.88**	**0.028**	

β values are non-standardised. X_{acq} = following regression with acquisition sequence. X_{conf} = following regression with all significant confounding variables. Significant results are highlighted in boldface. Age = gestational age at scan (weeks); ses = Hollingshead socioeconomic status.

ally in 1 WM-ROI, 004-006. In the left projection fibre network, increased methamphetamine exposure was significantly associated with decreased FA in the WM-ROI 001-007, while the right showed significant negative association between methamphetamine exposure and FA in five additional WM-ROIs (001-005, 002-003, 004-005, 004-007 and 007-008). In the association fibre networks, 2 WM-ROIs showed a negative association between methamphetamine exposure and FA which was significant in one hemisphere and at a trend-level in the other (005-007 and 006-007). Three additional WM-ROIs showed a significant association between increased methamphetamine exposure and reduced FA in the left hemisphere only (001-003, 003-007 and 007-009). In the right hemisphere, there was a significant association between methamphetamine exposure and FA in 2 additional connections (001-002 and 006-008).

4.3.4 Association of prenatal methamphetamine exposure with AD and RD in white matter networks

Networks which showed an association between methamphetamine exposure and FA were further analysed to investigate whether this association was driven by an association with methamphetamine of either AD or RD. Following multiple linear regression with acquisition sequence and significant confounding variables, AD was shown to be significantly associated with prenatal methamphetamine exposure in the commissural fibre network ($\beta = 4.42 \times 10^{-3}$, $p = 0.029$). AD was associated with methamphetamine exposure in the right association network but this result did not survive after it was adjusted for confounding variables. RD was observed to be significantly associated with methamphetamine exposure in the right projection fibre network ($\beta = 5.33 \times 10^{-3}$, $p = 0.033$).

Table 4.4. Association of methamphetamine exposure with RD in individual WM-ROIs (*N*=23).

Network	WM-ROI	Methamphetamine RD (mean ± SD)	Control RD (mean ± SD)	β_{acq} (E-03)	p_{acq}	β (E-03)	p_{conf}	Confounders
Right Projection	001-005	1.005 ± 0.048	0.964 ± 0.069	5.88	0.075	**5.46**	**0.024**	age, ses, sex
	002-003	1.231 ± 0.088	1.178 ± 0.104	**10.4**	**0.043**	**8.64**	**0.028**	
	004-005	1.071 ± 0.051	1.038 ± 0.070	5.92	0.073	5.19	0.055	
Left Association	001-003	1.256 ± 0.095	1.194 ± 0.079	**10.0**	**0.035**	**7.98**	**0.030**	age, education, ses, marijuana, sex
Right Association	001-002	1.202 ± 0.071	1.156 ± 0.075	**8.08**	**0.033**	**6.99**	**0.017**	age, sex
	005-007	1.204 ± 0.055	1.173 ± 0.067	**6.56**	**0.036**	4.94	0.098	

β values are non-standardised. X_{acq} = following regression with acquisition sequence. X_{conf} = following regression with all significant confounding variables. Significant results are highlighted in boldface. Age = gestational age at scan (weeks); ses = Hollingshead socioeconomic status.

Individual WM-ROIs within each network which showed an association between methamphetamine exposure and FA were similarly analysed to investigate whether this association was driven by AD or RD. Following multiple linear regression with acquisition sequence and confounding variables, no WM-ROIs showed any association between methamphetamine exposure and AD. Several connections showed a positive association between methamphetamine exposure and RD, and the results of these analyses are shown in Table 4.4. In the right projection fibre network, 001-005 and 002-003 showed a significant association, while the association in 004-005 just escaped significance. In the left association fibre network, RD in 001-003 was significantly associated with methamphetamine exposure. In the right association fibre network, RD in 001-002 was significantly associated with methamphetamine exposure, while 005-007 was associated at a trend-level.

4.4 DISCUSSION

This forms part of the first study to investigate the microstructural effects of prenatal methamphetamine in neonates using DTI tractography. Alterations were observed in the three major classes of white matter tracts in the CNS: commissural fibres, projection fibres (both hemispheres) and association fibres (both hemispheres). Following regression for significant confounding variables, increasing methamphetamine exposure was shown to be associated with reduced FA in all five networks. Methamphetamine was significantly correlated with increased AD and RD in one network each. Connections between individual ROIs within the projection and association fibre networks were observed to show a significant negative correlation between methamphetamine and FA. These included fibres in the corticospinal tracts, the internal capsule, the optic radiation and superior and posterior thalamic radiations in the projection networks; and the uncinate, occipitofrontal and superior and inferior longitudinal

fasciculi in the association networks (see [193]). At the individual connection level no effect of methamphetamine on AD was observed, but increased RD was associated with methamphetamine exposure in several WM-ROIs.

These results are in agreement with previous studies which examined white matter characteristics in an older cohort from the same geographic region. Roos and colleagues observed reduced FA in a number of white matter tracts in 6-7 year-old children, including the external capsule, sagittal stratum and fornix, which connect striatal, frontal and limbic regions[82]. RD was increased in the corresponding regions. Reduced FA and increased AD and RD were observed at 1 month in the corona radiata of 1 month-old infants with combined methamphetamine and tobacco exposure compared to infants with tobacco exposure only or controls[90]. Most studies of adult methamphetamine users have used a voxel-based approach to analyse DT images, and many have found reduced FA in frontal regions[28,31,187]. Not all findings in prenatally exposed children are in full agreement, however. An investigation in a cohort of 3-4 year-old children with methamphetamine exposure found reduced diffusivity and a trend for increased FA in frontal and parietal white matter[91]. Another group observed significantly increased FA in major white matter bundles including the CC, internal and external capsules and corona radiata, with increased AD and reduced RD[92]. The reasons for these inconsistencies are not fully apparent. One possible explanation may be methodological: the two studies which observed increased FA both used a voxel-wise method of analysis[91,92], while the current research used a tractographic approach. However, a voxel-wise approach was also used by Roos and colleagues, who found reduced FA[82].

Interpretation of the DT measurements and the changes therein is complex. FA is often interpreted as a measure of the structural integrity of white matter, with increased FA being representative of more organisation[135]. Reduced FA has been observed in white matter tracts of patients with a range of psychiatric and neurodegenerative disorders[194–197], but the exact

biochemical and structural nature of the pathology underlying the reductions is not directly apparent from this index alone[123]. FA alterations may be related to disruption in myelin structure or damage to the axons[198] or to changes in fluid content in the examined region[123]. Evaluation of additional diffusion measures such as AD and RD can provide a more complete picture. Reductions in FA may be the result of lower AD or increased RD[122], and these measures are differentially affected by the underlying pathology, with AD being sensitive to axonal degeneration and RD more severely affected by alterations in myelination[199,200]. Reduced FA was observed in the current study to be associated with methamphetamine exposure in all five major white matter networks examined. In all but one, increasing methamphetamine exposure was associated with increased RD, suggesting that the change in FA may be particularly the consequence of alterations in myelination, as the change in AD was less consistent or widespread. Prenatal methamphetamine exposure is associated with reduced myelination and myelin content in rats[201,202], and methamphetamine has been shown to induce oligodendroglial cell death *in vitro*[203]. In concert with findings of reduced FA and increased RD in adult methamphetamine users[30,31], these data suggest that methamphetamine exposure is associated with reduced white matter integrity particularly as a result of damage or alterations to myelin structure. The changes in AD, albeit to a lesser extent, should not be ignored, however. Previous studies of prenatal exposure in older children[82,92] and of methamphetamine abuse in adults[30,31] demonstrated AD alterations. There is some evidence that methamphetamine exposure induces axonal damage. Prenatal treatment with methamphetamine resulted in a higher percentage of smaller axons in rats[202], while treatment with amphetamines induced significant terminal and axonal loss in the striatum of rats[204] and baboons[205] and reduction of axon density in the medial prefrontal cortex[206]. The precise mechanisms of methamphetamine damage to white matter are thus likely multifactorial.

Interpretation of diffusion measures in neonates is further complicated by the fact that the neonatal brain is far from fully developed. Axonal connections are organised into fibre bundles in the last trimester of gestation, but the myelination process is ongoing from the second half of pregnancy and is significantly incomplete at birth[101]. In addition, the maturation of white matter in the infant brain is considerably regionally variable, with a general progression of maturation in posterior-to-anterior and central-to-peripheral directions[207]. Diffusion indices change with white matter maturation such that FA increases while AD, RD and MD decrease[124], which has been suggested to be the result of reduced brain water, increases in fibre diameter and myelination, more cohesive fibre tract arrangement and greater axonal packing[208]. Alterations in diffusion indices in the current study might therefore be considered to be an indication of delayed maturation in the white matter of exposed neonates. Lending credence to this interpretation are a number of preclinical studies which have found delays in somatic development[209], locomotor control[210] and sensory-motor development[211], and slowed maturation of frontal cortical density[212] in rats following amphetamine administration during gestation. Furthermore, the trajectories of FA and diffusivity measures were shown to be altered in corona radiata of infants with combined methamphetamine and tobacco exposure compared to controls[90].

White matter microstructure and connectivity are highly functionally significant. White matter pathways in the CNS are responsible for the transmission of information across networks and the integration and coordination of the activity of multiple individual regions[213]. A substantial body of literature supports the role of white matter in cognition. FA was shown to be associated with visuospatial information processing and sustained intelligence in school-age children[208,214]. The latter study additionally found that FA across multiple white matter regions was positively associated with IQ. The current study investigated changes in three major classes of white matter fibre tracts: callosal or commissural fibres connect cortical regions

across hemispheres; projection fibres connect cortical regions with spinal cord, brain stem, cerebellum and deep nuclei; and association fibres provide connections between cortical regions within the same hemisphere[193]. A number of studies have shown associations between specific fibre tracts and cognition in various domains. Higher white matter integrity, as measured by diffusion parameters, in the corona radiata, superior longitudinal fasciculus, posterior thalamic radiation and cerebral peduncle was associated with greater cognitive control, selective attention and interference suppression in school-age children[215]. Verbal ability was significantly associated with FA in the superior longitudinal fasciculus bilaterally and the left anterior thalamic radiation, and negatively with RD in the superior longitudinal fasciculi, the inferior longitudinal fasciculus and uncinate fasciculus in the left hemisphere and in forceps major[216]. Increased FA in fronto-parietal connections, particularly in the superior longitudinal fasciculus, was associated with better performance in a test of spatial working memory[217]. In infants, higher FA and reduced RD in anterior and superior thalamic radiations, anterior cingulum, arcuate fasciculus and temporo-parietal connections was related to better performance on a test of working memory[218]. Prenatal methamphetamine exposure in the current study was associated with poorer white matter integrity in a number of the above-mentioned connections, and might therefore reasonably be assumed to be related to dysfunction in a number of domains. This assumption is borne out by previous literature which has shown alterations in white matter structure as a consequence of methamphetamine exposure to be associated with a number of functional deficits. In adult users, FA was associated with several clinical indices of depression and affective disorder[187], with impairments in executive function[28] and with poorer measures of cognitive control[29]. In children with prenatal exposure, altered FA in several white matter regions was significantly associated with poorer motor coordination and with cognitive control and executive function[82]. Further investigations into

the effects of prenatal exposure in cognitive domains relating to specific white matter tracts is highly warranted.

To our knowledge, this is the first study to use DTI tractography to investigate white matter changes in neonates with prenatal exposure to methamphetamine. Studies in neonates of drug exposure effects have a significant advantage over studies in older cohorts. Children of women who abuse methamphetamine during pregnancy are almost invariably born into a suboptimal and disadvantageous environment[81], which has been shown to exert further damaging influences on development[79,170]. Evaluation of prenatal methamphetamine exposure in neonates permits an assessment relatively free of the potential confounding influences associated with the post-natal environment.

The women whose infants were scanned in the current study were recruited during pregnancy, allowing a more accurate measure of frequency of methamphetamine use. The timeline follow-back approach to determining substance use[130,131] provided a significant advantage in the current investigation over studies of older children in which precise measurement of drug use by the mother is almost impossible. A more informed quantitative analysis of methamphetamine exposure is thus feasible; of the limited previous studies of prenatal methamphetamine exposure, only one investigated potential associations between methamphetamine and diffusion properties[91]. As mentioned above, development of the CNS is far from complete at birth. This raises the possibility that effects observed during the neonatal period may be transient and resolve with maturation. Longitudinal investigations which follow cohorts from infancy as they mature will be invaluable in this regard. Given that our findings agree with previous results in both infants and older children, however, it is likely that the observed alterations will not resolve with age.

There are a number of limitations to this study. A significant limitation, almost inevitable in any study of prenatal drug exposure, is the potential confounding effects of polysubstance exposure[93]. The current study observed alcohol, cigarette and marijuana use by both control and methamphetamine-using mothers, with more in the methamphetamine group using each substance than in the control group, although a significant group difference was approached only for cigarette use. Prenatal exposure to all three has been demonstrated in animal and human studies to induce alterations in CNS structure and function[135,152,155,219–223]. However, as mentioned above, recruitment during pregnancy permits a far more accurate measure of substance use, so that alcohol, tobacco and marijuana use were included as confounding variables in the statistical analysis. A previous study of methamphetamine exposure which observed increased FA in frontal white matter, in contrast to the present findings, did not control for either cigarette or marijuana exposure[92]. Given that prenatal exposure to tobacco smoke has been shown to be associated with increased FA in frontal white matter[223], this could explain the contradiction with the results of the current study. Chang and colleagues noted that methamphetamine-using women smoked more cigarettes than women who smoked but did not use methamphetamine[90], suggesting that the effect of nicotine is likely to be higher in methamphetamine-exposed children. An additional limitation is the fairly small sample size. However, it is comparable to previous work[82] and alterations were observed in regions which have been noted previously. It is possible that with a larger cohort some of the trend-level associations would have reached significance. As mentioned above, development of the CNS is far from complete at birth. This raises the possibility that effects observed during the neonatal period may be transient and resolve with maturation. Longitudinal investigations which follow cohorts from infancy as they mature will be invaluable in this regard. Given that our findings agree with previous results in both infants and older children, however, it is likely that the observed alterations will not resolve with age.

Literature on white matter alterations in prenatally methamphetamine exposed children is not unanimous, but the findings presented here agree with previously published results showing reduced anisotropy and increased radial diffusion in a significant number of major white matter connections. The current study extends previous findings to show that these alterations are associated with increased methamphetamine exposure in exposed infants, investigated by tractographic analysis in the first month postpartum. Given that the affected tracts have considerable functional significance, it is to be assumed that these changes will have a serious impact on the exposed children. Further research into the precise cognitive changes associated with such findings will be essential to inform the necessary therapeutic interventions.

CHAPTER 5

CORTICOSTRIATAL WHITE MATTER CHANGES ARE ASSOCIATED WITH PRENATAL METHAMPHETAMINE EXPOSURE

5.1 INTRODUCTION

The abuse of methamphetamine is one of the most rapidly growing drug problems worldwide[13], with studies suggesting that it is second only to marijuana in global use[117,224]. It is a potent psychostimulant, exerting its effects primarily on the CNS by altering the release and activity of the monoaminergic neurotransmitters, dopamine, norepinephrine and serotonin[181,225,226]. Although the mechanisms of action of methamphetamine are not fully understood, a large body of preclinical and clinical literature has demonstrated its neurotoxic capabilities. Alterations in a number of brain areas, including the basal ganglia[18,19,227], hippocampus[23], amygdala[25], thalamus[228,229] and a range of cortical regions[21,228,230,231], have been observed in both current and abstinent users, and several studies have shown an association between methamphetamine-induced damage and altered cognitive or affective function[23,46,51,183].

The incidence of methamphetamine use by pregnant women has been estimated at over 5%[54,67]. Methamphetamine causes vasoconstriction and reduced placental blood flow[57], resulting in damage to the placenta[58] and hypoxia in the fetus[67]. A range of adverse perinatal effects on both mother and infant have been associated with methamphetamine use in pregnancy, including higher incidence of gestational hypertension and preeclampsia and increased risk of fetal and neonatal death[142]. Gestational age at birth has been observed to be lower in exposed infants[59,65], with an increased risk of preterm birth[141]. Methamphetamine exposure has also been shown to be associated with smaller size at birth[63–65,75,141] and lower birth weight[64,141].

In the light of the above-mentioned effects and the well-documented neurotoxicity of methamphetamine in adult abusers, it is logical to conclude that exposure during the neurologically vulnerable prenatal period would induce potentially severe and long-term

alterations. CNS growth and development is rapid and complex during gestation[72,101], and the influence of a highly neuroactive drug such as methamphetamine might well be expected to induce significant modifications.

DTI is a neuroimaging modality that enables visualisation and characterisation of white matter within the CNS by analysing the three-dimensional diffusion of water molecules within fibre bundles[125,192]. From the extracted data various measures of the structural integrity of the white matter bundles and their component axons can be determined. AD is a measure of the diffusion of water molecules in the direction parallel to the white matter fibres, while RD measures perpendicular movement. The most widely used measure of water movement is FA, which represents the normalised standard deviation of the total diffusivities[123]. Higher FA is a reflection of diffusion that is primarily in a direction parallel to the longitudinal axis of the white matter fibre bundles[125], and is generally regarded as a marker of more healthy, highly structured or mature white matter[122].

Information from DT images relating to the directionality and alignment of water diffusion can be used to map the trajectories of white matter fibre bundles within the brain[120,123] by determining fibre orientation from the principal diffusion vector in sequential voxels[101]. By defining regions of interest, the path of fibres within connecting tracts can then be defined[232] and the microstructure of the fibre bundles determined by analysing the diffusion measures across the entire tract[125]. Changes in diffusion measures within a fibre bundle are frequently an indication of functional alterations[186], with many pathologies affecting the microstructure and organisation of CNS white matter[122], and DTI is a valuable tool for investigating and quantifying the extent and nature of these changes.

An appreciable body of evidence shows significant effects of methamphetamine use on diffusion measures. Recently abstinent methamphetamine users exhibit reduced FA in frontal

cortical regions[28,31,187] and in the genu of the CC[29,30,187]. Higher AD and RD have been noted in the caudate and putamen of methamphetamine users[31], although no such striatal effects were observed by Lin and colleagues[188].

In the light of these findings, it is reasonable to hypothesise that prenatal methamphetamine exposure would exert similar deleterious effects on CNS structure in the exposed fetus. There is a sparsity of DT imaging literature examining such effects, however, and the results are not unanimous. Lower FA and increased MD, AD and RD were observed in white matter tracts passing through striatal, limbic and frontal cortical regions of 6-7 year old children with prenatal methamphetamine exposure[82]. Similarly, lower FA and increased AD and RD in the corona radiata were observed in infants exposed to methamphetamine and tobacco[90]. In a study of 9-11 year old children, however, exposure was associated with higher FA in the genu of the CC, corona radiata and internal and external capsules[92], while similar results were observed in a voxel-based study of a 3-4 year old cohort, which noted increased FA and reduced diffusivity in genu and splenium of the CC, frontal and parietal white matter and the basal ganglia[91].

There is thus agreement in the literature that *in utero* exposure to methamphetamine induces significant and enduring effects on CNS white matter, but the precise nature of these changes bears further investigation. Moreover, to date there are no published studies of DT tractography of methamphetamine exposure in neonates. Children born to women who abuse methamphetamine are almost invariably exposed to a suboptimal environment[65,81], and this is likely to have strong effects on neural development. Investigations of neonatal cohorts permit a cleaner separation of substance exposure effects from the potential confounding influences of the postnatal environment.

A previous 'whole-brain' analysis of the current cohort revealed altered diffusivity and reduced FA in three major classes of white matter tracts, commissural, projection and association fibres,

indicating a generalised effect of methamphetamine exposure on white matter microstructure (unpublished work). The aim of the current study was to investigate potential changes in white matter fibre bundles forming part of the corticostriatal and mesolimbic connections between OFC and subcortical ROIs which were previously manually defined in this cohort. It was hypothesised that prenatal methamphetamine exposure would be associated with microstructural alterations in these regions.

5.2 METHODS

5.2.1 Study sample

The study sample consisted of infants born to women from the Cape Coloured (mixed ancestry) community from Cape Town, South Africa, who form part of a larger prospective longitudinal study of prenatal alcohol and drug exposure on infant development[58,132,135]. The exposed group comprised infants with prenatal exposure to methamphetamine, while the control group comprised infants from the same community without methamphetamine exposure and with minimal or no exposure to alcohol or other drugs of abuse *in utero*.

Pregnant mothers were recruited following antenatal care bookings at midwife obstetric care units in the community. They were interviewed three times during pregnancy with regard to their methamphetamine and alcohol consumption by means of a time-line follow-back approach[130,131], as well as about cigarette and other drug use during pregnancy. The current study group consisted of women in the cohort who reported the use of methamphetamine on at least 2 occasions per month during pregnancy. The control group included women who abstained from alcohol and other drugs of abuse, or who consumed no more than 2 drinks on no more than 2 occasions during their pregnancy.

Informed consent was obtained from each mother at recruitment and at the first laboratory visit. Ethics approval for the study was obtained from the ethics committees at Wayne State University and the Faculty of Health Sciences of the University of Cape Town.

5.2.2 Scanning

Infants were scanned without use of sedation, between 1 and 5 weeks postpartum, with the exception of one infant, born at 31 weeks gestational age, who was scanned at 9 weeks of age. Scanning took place at the Cape Universities Brain Imaging Centre (CUBIC) at the Faculty of Health Sciences campus of the University of Stellenbosch, South Africa.

The infants were brought to the centre a minimum of 1 hour prior to scanning. During the pre-scan period the infants were weighed, head circumference and crown-to-heel length were measured, and neonatal behavioural characteristics[145] were assessed. The infant was then firmly swaddled and placed in a VacFix® vacuum cushion (S&S Par Scientific, Houston, TX). Earplugs were used to protect the infant from scanner noise. The infant was fed by the mother and allowed to fall asleep.

The infant was placed in the scanner and immobilised using the VacFix® cushion, following an adapted protocol for neuroimaging of nonsedated neonates[146]. A pulse and oxygen saturation monitor probe was secured to the infant's foot, and this was monitored during the scanning process by a developmental paediatrician, or by a research nurse, who remained in the scanner room with the infant throughout the procedure.

MRI scanning was performed using a Siemens 3T Allegra scanner. A circularly polarised bird-cage coil, custom-built for use with neonates, was used for transmission and reception of the signal. Two DWI sets with opposite (AP/PA) phase encoding directions were acquired with a twice refocused spin echo EPI sequence. For 5 infants (1 with methamphetamine exposure, 4

controls), the scanning parameters were as follows: TR 9500 ms, TE 86 ms, matrix 50 slices of 80x80 voxels, voxel size 2x2x2 mm^3. The remaining infants were scanned using a similar DTI sequence which included navigation for performing real-time motion detection and correction[189]; this had the same scanning parameters as above, but with TR = 10 026 ms. In both navigated and non-navigated sequences, AP and PA acquisitions each contained four b = 0 $s.mm^{-2}$ reference scans and 30 DW gradient directions with b = 1000 $s.mm^{-2}$.

For anatomical imaging, a motion-navigated multiecho gradient echo sequence[190] was used, with protocol parameters as follows: FOV 114 mm, 128 slices of 144x144 voxels, voxel size 1x1x1 mm^3, TR 20 ms, TE 1.46/ 3.14/ 4.82/ 6.5/ 8.18/ 9.86/ 11.54/ 13.22 ms. Two sets were acquired, with flip angles of 5° and 20° respectively.

5.2.3 Data processing and parameter estimation

DWI data were inspected visually for motion artifacts and dropout slices, and individual poor quality volumes were discarded. At least 12 DWIs remained for each infant. Motion and EPI distortion were corrected using FSL's eddy correct and topup tools[137]. DTs and tensor parameters such as FA, MD, eigenvalues (L_i, i=1,2,3; AD=L_1; RD=[L_2+L_3]/2) and directional eigenvectors (e_i, i=1,2,3) were estimated using AFNI[191].

For the anatomical images, individual echoes from the two flip angle acquisitions were combined using mri_ms_fitparms using FreeSurfer[147,233]. From this, tissue parameters were estimated and a single image volume, with an optimal contrast flip angle of 24°, was synthesised.

5.2.4 Manual tracing of target regions of interest

Regions of interest were viewed and manually delineated using Freeview software (the FreeSurfer image analysis suite http://surfer.nmr.mgh.harvard.edu/) run on a Lenovo ThinkPad X220 tablet (see Fig. 5.1). A subset of these traced ROIs were used as targets for tractographic analysis. The following previously traced ROIs were used bilaterally: caudate, nucleus accumbens, putamen, hippocampus and amygdala. Two additional regions were traced for the purposes of this study – the midbrain and the OFC.

5.2.4i Caudate nucleus and nucleus accumbens (NAcc)

An oblique line from the inferior tip of the lateral ventricle to the midpoint of the inferior boundary of the internal capsule was drawn to separate the caudate and nucleus accumbens, while a line descending from the middle of the inferior border of the anterior limb of the internal capsule was taken to define the boundary between the putamen and the nucleus accumbens.

Posteriorly, the caudate diminishes in size and eventually becomes difficult to define as the tail reaches the point where it curves inferiorly posterior to the thalamus. For this reason the posterior and inferior portions of the caudate were not traced.

5.2.4ii Putamen

The junction of putamen and pallidum was generally most clearly seen in axial sections, so that tracing was done in the axial or coronal planes on a slice by slice basis.

5.2.4iii Hippocampus

The hippocampus was traced chiefly in the coronal plane, with considerable guidance from views in the sagittal plane. It can be seen in sagittal sections within the temporal lobe as a sausage-shaped structure. More anteriorly in the coronal plane the hippocampal head appears, and the structure becomes large and rounded.

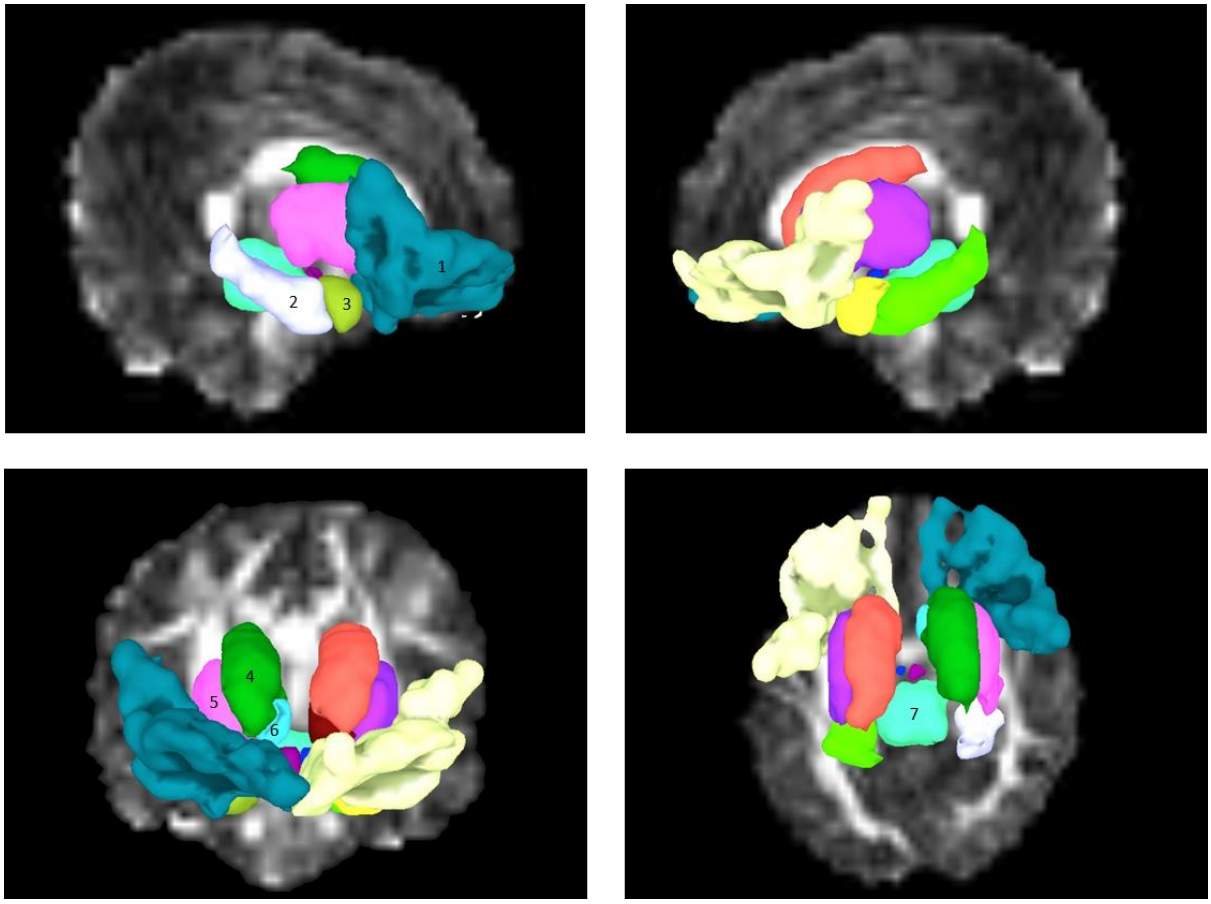

Figure 5.1. Traced ROIs used as seeds for probabilistic tractography, shown in sagittal view in upper panels, and coronal and axial views in left and right lower panels respectively. 1) orbitofrontal cortex; 2) hippocampus; 3) amygdala; 4) caudate nucleus; 5) putamen; 6) nucleus accumbens; 7) midbrain. Regions are numbered in one hemisphere only but were traced bilaterally.

5.2.4iv Amygdala

The amygdala is located anterior to the head of the hippocampus. It is bounded in its anterior, inferior and lateral aspects by white matter, and postero-inferiorly by the hippocampus and the tip of the lateral ventricle. The tracings of the amygdala were done in all three planes, as it was difficult to see in its entirety in any one plane.

5.2.4v Midbrain

The region described as midbrain included the complete midbrain (as defined anatomically), encompassing tectum, tegmentum, and crus cerebri. The lower border corresponded with the

mesencephalic/ pontine boundary at the upper border of the basilar pons. Superiorly, care was taken to exclude the subthalamic area which is easily identifiable in neonatal brains.

5.2.4vi Orbitofrontal cortex

The OFC was defined as that area of cortex situated on the inferior surface of the frontal lobe. Its anterior and lateral borders were defined by the hemispheric edge where the lateral and inferior frontal surfaces meet. Its posterior boundary was defined by the posterior edge of cortex on the inferior surface. The OFC was traced in one control subject, following which nonlinear registration was performed between the *b*0 reference volume of this subject and each of the others in the study using AFNI's 3dQwarp. The calculated transformation was then applied to map the ROIs into each subject's native diffusion space.

5.2.5 Tractographic analysis

Probabilistic tractography was performed using the FATCAT software in AFNI[127]. Local uncertainties in DT eigenvectors and FA were estimated with FATCAT, and probabilistic tractography was performed using the FACTID algorithm, which uses repeated iterations of whole brain tracking to estimate the most likely locations of white matter connections between pairs of targets[139]. The tract propagation parameters used were: maximum "turning" angle of propagation of 55 degrees, through voxels with FA > 0.1, which is the standard threshold for FA as a proxy for white matter in infants[129]. All voxels through which more than a minimum number of tracts passed to connect a pair of targets were included to create WM-ROIs associated with each pair of targets. Only WM-ROIs found between the same pairs of targets in all subjects were included for further analysis. The mean and standard deviation of the DTI parameters FA, AD and RD for each WM-ROI were automatically calculated by the tracking function.

5.2.6 Statistical analysis

Statistics were performed using IBM SPSS Statistics (version 23; IBM, Armonk, NY). Ten variables were examined as potential confounders: maternal alcohol use (in units of absolute alcohol consumed per day across pregnancy), maternal marijuana use (days per month during pregnancy), maternal cigarette smoking during pregnancy (number of cigarettes per day during pregnancy), maternal education (highest grade level completed), maternal marital status, parity, socioeconomic status (ses; see Ref. [174]), infant sex, gestational age at scan (measured in weeks), and birth weight (grams). Data were examined for skewness and outliers were "winsorised", that is, recoded to one unit greater than the next highest value[148]; this was applied to the methamphetamine, alcohol, marijuana and cigarette smoking exposure variables. Sample characteristics were compared between exposed and control groups using t-tests for continuous variables, or chi-squared tests for categorical variables.

ANCOVA was used to compare the mean FA of each WM-ROI between exposed and control groups, adjusting for acquisition sequence (navigated or non-navigated). Variables weakly ($p < 0.1$) associated with FA for each WM-ROI were added in subsequent ANCOVAs. For WM-ROIs in which group differences in FA had been observed, group differences (methamphetamine vs. control) in mean values of AD and RD were examined using the same procedure.

Linear regression analyses were used to investigate potential associations between methamphetamine exposure (number of days/ month of pregnancy that methamphetamine was used) and mean FA in each WM-ROI, adjusting for acquisition sequence. WM-ROIs in which FA showed a trend towards significant association with methamphetamine were then analysed by means of hierarchical multiple linear regression with best estimate approach. Confounding variables showing some relationship to FA ($p < 0.1$) were entered successively according to

their strength of association with FA in the tract of interest. Variables which altered β by less than 10% were excluded from further modeling. WM-ROIs in which a significant association between FA and methamphetamine exposure was observed were further analysed in terms of AD and RD.

5.3 RESULTS

5.3.1 Sample characteristics

The final study sample for analysis comprised 23 infants, 11 with methamphetamine exposure and 12 controls. The demographic characteristics of the sample are summarised in Table 5.1. Of the maternal characteristics, only maternal education, measured as the highest grade level completed by the mother, was significantly different between groups ($p < 0.05$), with the methamphetamine group achieving a lower level of education than controls.

The sample consisted of 12 male and 11 female infants, with 5 males and 7 males in the methamphetamine exposed and control groups, respectively. The number of male and female infants in each group was not statistically different between groups. Although infants with prenatal methamphetamine exposure tended to be born younger, there was no difference between the groups in gestational age at scan (gestational age at birth + age in weeks at scan) or in birth weight.

In comparing substance use between groups, mean cigarette use by the mothers of the exposed group tended to be higher than that of the control group. Control mothers did not use methamphetamine, but 67% smoked, 17% used marijuana and 1 mother drank alcohol, although the latter was within the acceptable limits set for inclusion in the cohort. By contrast, 100% of the mothers in the exposed group smoked, 46% ($n = 5$) used marijuana and 46% drank alcohol during pregnancy.

Table 5.1. Sample characteristics (*N*=23).

	Methamphetamine (PEM) (*n*= 11)			Control (Ctl) (*n* = 12)				
	Mean	**SD**	**Range**	**Mean**	**SD**	**Range**	**χ^2 or *t***	***p***
Maternal								
Age (years)	27.2	3.9	21.4 - 32.6	25.1	5.4	18.8 - 36.4	-1.05	0.305
Education	9.4	1.2	7.0 - 11.0	10.6	1.1	9.0 - 12.0	2.56	0.018
Parity	2.1	1.6	0 - 5	1.3	1.2	0 - 3	-1.44	0.165
Infant								
Sex (% male)	45.5			58.3			0.38	0.537
Birth weight (g)	2806.8	600.5	1370.0 - 3590.0	2795.8	485.2	1940.0 - 3470.0	-0.05	0.962
Gestational age at birth (weeks)	37.3	3.0	31.0 - 40.7	39.0	1.7	36.6 - 42.1	1.67	0.110
Gestational age at scan (weeks)	40.6	2.1	37.3 - 43.1	41.6	1.9	37.6 - 44.1	1.24	0.227
Substance use[a]								
Methamphetamine (days/month)	7.1	3.5	1.5 - 12.0	0.0	0.0	0.0 - 0.0	-7.04	0.000
Smoking (number cigarettes/day)	6.5[b]	5.4	2.0 - 20.0	3.3[c]	2.8	0.0 - 7.7	-1.78	0.089
Marijuana (days/month)	4.4[d]	9.6	0.0 - 30.5	0.0[e]	0.1	0.0 - 0.2	-1.58	0.129
Alcohol (oz AA /day)	0.2[f]	0.4	0.0 - 1.4	0.0[g]	0.0	0.0 - 0.1	-1.26	0.222

[a]mean, SD, range based on whole group (PEM, n=11; Ctl, n=12); [b]11/11 (100%) and [c]8/12 (66.7%) smoked cigarettes; [d]5/11 (45.5%) and [e]2/12 (16.7%) used marijuana; [f]5/11 (45.5%) and [g]1/12 (8.3%) drank alcohol during pregnancy.

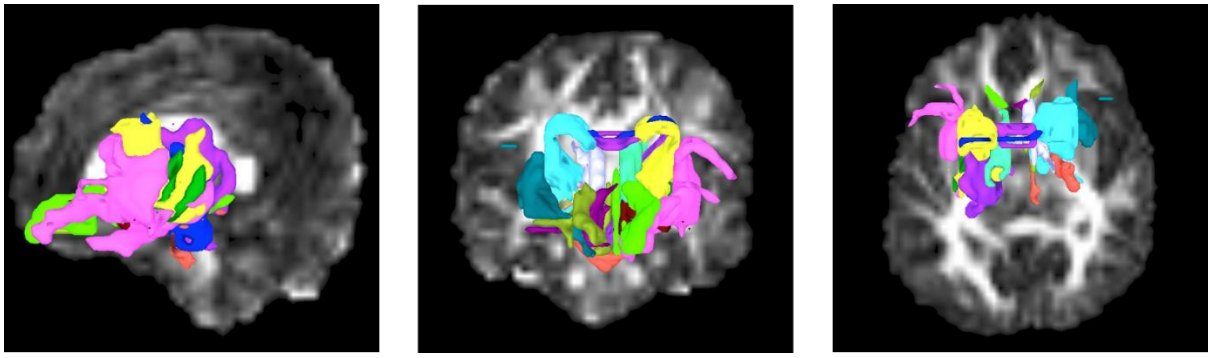

Figure 5.2. Volumetric depiction of WM-ROIs produced by probabilistic tractography between manually traced seed ROIs in one control infant brain.

5.3.2 Tractographic connections

Probabilistic tractography produced 31 WM-ROI connections between target ROIs that were common to all infants. These are shown in Table 5.2. (See also Fig. 5.2).

5.3.3 Comparison of mean WM-ROI parameters between methamphetamine and control groups

The results of the comparison of mean FA in WM-ROIs of methamphetamine exposed and control infants are shown in Table 5.3 (only regions showing at least trend-level significance, $p < 0.1$, in any of the tests are shown). Representative examples of tractographic connections between traced ROIs in control and methamphetamine-exposed infants are shown in Fig. 5.3. With the inclusion of acquisition sequence as a standard confounding variable, mean FA was observed to be significantly lower in the methamphetamine group in 4 WM-ROIs: midbrain – left putamen, left putamen – left OFC, right putamen – right OFC, and right putamen – right amygdala. Three more WM-ROIs showed a trend towards reduced mean FA in the methamphetamine group compared to controls (midbrain – right caudate; midbrain – right putamen; right putamen – right hippocampus).

Table 5.2. List of WM-ROIs which are present in all subjects (*N*=23) and their group means.

	Methamphetamine (*n*=11)						Control (*n*=12)					
	FA		AD ($x10^{-3}$ s/mm^2)		RD ($x10^{-3}$ s/mm^2)		FA		AD ($x10^{-3}$ s/mm^2)		RD ($x10^{-3}$ s/mm^2)	
WM-ROI	**mean**	**SD**	**mean**	**SD**	**mean**	**SD**	**mean**	**SD**	**mean**	**SD**	**mean**	**SD**
Midbrain - Left Hippocampus	0.223	0.031	1.699	0.068	1.211	0.068	0.220	0.036	1.683	0.124	1.208	0.118
Midbrain - Right Hippocampus	0.227	0.027	1.682	0.084	1.190	0.077	0.232	0.028	1.705	0.079	1.195	0.066
Midbrain - Left Caudate	0.235	0.014	1.486	0.075	1.029	0.043	0.240	0.018	1.440	0.060	0.988	0.056
Midbrain - Right Caudate	0.230	0.014	1.469	0.069	1.028	0.039	0.248	0.044	1.455	0.061	0.986	0.068
Midbrain - Left Putamen	0.243	0.018	1.466	0.044	1.002	0.045	0.258	0.025	1.472	0.076	0.982	0.067
Midbrain - Right Putamen	0.245	0.012	1.467	0.050	1.002	0.035	0.252	0.020	1.440	0.034	0.970	0.046
Left OFC - Left NAcc	0.160	0.020	1.618	0.122	1.275	0.100	0.165	0.016	1.555	0.120	1.217	0.098
Right OFC - Right NAcc	0.161	0.019	1.622	0.107	1.273	0.090	0.167	0.028	1.583	0.099	1.232	0.104
Left OFC - Left Amygdala	0.176	0.024	1.813	0.196	1.396	0.177	0.184	0.028	1.773	0.135	1.346	0.128
Right OFC - Right Amygdala	0.178	0.029	1.780	0.159	1.366	0.161	0.179	0.032	1.827	0.180	1.398	0.165
Left OFC - Left Caudate	0.191	0.013	1.689	0.084	1.263	0.074	0.192	0.017	1.640	0.090	1.231	0.091
Right OFC - Right Caudate	0.189	0.017	1.703	0.067	1.278	0.073	0.199	0.031	1.683	0.096	1.243	0.108
Left OFC - Left Putamen	0.181	0.013	1.605	0.054	1.229	0.050	0.191	0.013	1.588	0.070	1.196	0.061
Right OFC - Right Putamen	0.176	0.011	1.632	0.078	1.258	0.071	0.190	0.019	1.593	0.081	1.199	0.077
Left OFC - Left Hippocampus	0.232	0.021	1.762	0.113	1.238	0.070	0.239	0.020	1.801	0.151	1.252	0.120
Left OFC - Right OFC	0.197	0.015	1.755	0.105	1.298	0.093	0.203	0.022	1.694	0.127	1.240	0.094
Right OFC - Left Caudate	0.221	0.022	1.771	0.083	1.256	0.082	0.249	0.084	1.749	0.131	1.179	0.138
Left Caudate - Left NAcc	0.176	0.018	1.722	0.134	1.319	0.094	0.175	0.022	1.642	0.111	1.261	0.096

Right Caudate - Right NAcc	0.182	0.018	1.734	0.116	1.316	0.074	0.184	0.027	1.692	0.132	1.283	0.105
Left Caudate - Left Putamen	0.199	0.015	1.542	0.046	1.136	0.041	0.202	0.014	1.496	0.064	1.098	0.062
Right Caudate - Right Putamen	0.201	0.015	1.545	0.056	1.135	0.044	0.203	0.016	1.520	0.072	1.113	0.064
Left Caudate - Right Caudate	0.284	0.019	1.875	0.115	1.201	0.092	0.290	0.025	1.816	0.108	1.150	0.082
Left Caudate - Left Hippocampus	0.241	0.017	1.678	0.122	1.159	0.091	0.253	0.022	1.709	0.144	1.156	0.114
Left Putamen - Left NAcc	0.169	0.013	1.454	0.069	1.127	0.059	0.175	0.019	1.404	0.057	1.076	0.046
Right Putamen - Right NAcc	0.168	0.022	1.458	0.068	1.131	0.049	0.175	0.021	1.442	0.064	1.108	0.059
Left Hippocampus - Left Amygdala	0.198	0.023	1.564	0.070	1.151	0.054	0.197	0.025	1.567	0.074	1.156	0.083
Right Hippocampus - Right Amygdala	0.186	0.016	1.558	0.054	1.171	0.046	0.193	0.022	1.599	0.077	1.188	0.075
Left Putamen - Left Hippocampus	0.253	0.012	1.612	0.062	1.089	0.046	0.256	0.024	1.643	0.109	1.106	0.085
Right Putamen - Right Hippocampus	0.255	0.015	1.607	0.049	1.084	0.032	0.270	0.024	1.640	0.072	1.078	0.078
Left Putamen - Left Amygdala	0.220	0.030	1.478	0.063	1.052	0.081	0.242	0.027	1.499	0.053	1.029	0.078
Right Putamen - Right Amygdala	0.220	0.031	1.507	0.046	1.074	0.068	0.253	0.020	1.518	0.054	1.023	0.057

NAcc = nucleus accumbens; OFC = orbitofrontal cortex

Table 5.3. Group differences in FA in WM-ROIs (*N*=23).

	Methamphetamine (n=11)		Control (n=12)						
WM-ROI (target$_1$ – target$_2$)	**Mean**	**SD**	**Mean**	**SD**	F_{acq}	p_{acq}	F_{conf}	p_{conf}	**Confounders used**
Midbrain - Right Caudate	0.230	0.014	0.248	0.044	3.33	0.083	3.33	0.083	none
Midbrain - Right Putamen	0.245	0.012	0.252	0.020	3.49	0.077	3.49	0.077	none
Midbrain - Left Putamen	0.243	0.018	0.258	0.025	**4.39**	**0.049**	1.97	0.176	marijuana
Left Putamen - Left OFC	0.181	0.013	0.191	0.013	**5.65**	**0.028**	4.15	0.056	age
Right Putamen - Right OFC	0.176	0.011	0.190	0.019	**6.02**	**0.023**	**4.38**	**0.050**	age
Right Putamen - Right Amygdala	0.220	0.031	0.253	0.020	**7.48**	**0.013**	**6.73**	**0.019**	birthweight, alcohol, sex
Right Putamen - Right Hippocampus	0.255	0.015	0.270	0.024	3.95	0.061	2.72	0.116	age

NAcc = nucleus accumbens; OFC = orbitofrontal cortex X_{acq} = value when controlling for acquisition sequence in the analysis; X_{conf} = value following addition of acquisition sequence and significant confounding variables into analysis; significant effects (p<0.05) are highlighted in boldface. Age = gestational age at scan (weeks).

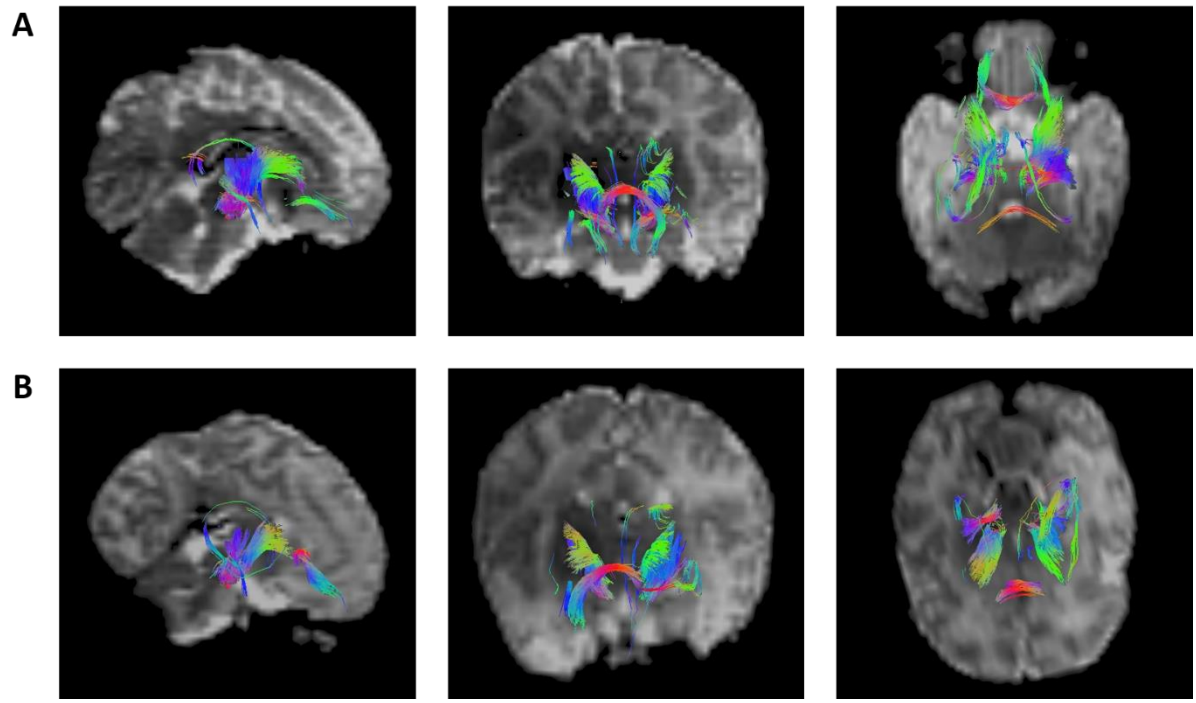

Figure 5.3. Examples of mini-probabilistic tractography connecting manually traced seed ROIs in one control (**A**) and one methamphetamine-exposed (**B**) infant brain. Colouration is by local tract direction, with left-right depicted in red, anterior-posterior in green, and inferior-superior in blue.

After controlling for additional confounding variables (listed in Table 5.3), the FA reductions in the right putamen – right OFC and right putamen – right amygdala survived. In 3 WM-ROIs a trend was observed towards reduced FA in the methamphetamine group compared to the controls (midbrain – right caudate; midbrain – right putamen; left putamen – left OFC). In 2 WM-ROIs (midbrain – left putamen; right putamen – right hippocampus) the group effect was lost once the confounding variables were included.

Tables 5.4 and 5.5 show the results of the comparison of mean AD and mean RD in WM-ROIs which showed significant or trend-level differences in mean FA between groups. No difference was observed in mean AD between methamphetamine exposed and control groups at any stage of the analysis in any WM-ROI. Increased RD in the methamphetamine group was observed in 2 WM-ROIs (midbrain – right caudate and right putamen – right OFC), and trend-level increases in another 2 WM-ROIs (midbrain – right putamen and right putamen – right

Table 5.4. Group differences in AD in WM-ROIs (*N*=23).

	Methamphetamine (n=11)		Control (n=12)						
WM-ROI (target$_1$ – target$_2$)	**Mean**	**SD**	**Mean**	**SD**	F_{acq}	p_{acq}	F_{conf}	p_{conf}	**Confounders used**
Midbrain - Right Caudate	1.469	0.069	1.455	0.061	0.218	0.646	0.218	0.646	none
Midbrain - Right Putamen	1.467	0.050	1.440	0.034	1.417	0.248	1.417	0.248	none
Midbrain - Left Putamen	1.466	0.044	1.472	0.076	0.178	0.677	0.215	0.648	marijuana
Left Putamen - Left OFC	1.605	0.054	1.588	0.070	0.558	0.464	0.059	0.811	age
Right Putamen - Right OFC	1.632	0.078	1.593	0.081	1.681	0.210	0.733	0.403	age
Right Caudate - Right Putamen	1.545	0.056	1.520	0.072	1.961	0.177	0.788	0.387	alcohol, age
Right Putamen - Right Amygdala	1.507	0.046	1.518	0.054	0.147	0.706	1.259	0.277	birthweight, alcohol, sex
Right Putamen - Right Hippocampus	1.607	0.049	1.640	0.072	0.959	0.339	1.258	0.276	age

NAcc = nucleus accumbens; OFC = orbitofrontal cortex; X_{acq} = value when controlling for acquisition sequence in the analysis; X_{conf} = value following addition of acquisition sequence and significant confounding variables into analysis. Age = gestational age at scan (weeks).

Table 5.5. Group differences in RD in WM-ROIs (*N*=23).

	Methamphetamine (*n*=11)		Control (*n*=12)						
WM-ROI (target$_1$ – target$_2$)	**Mean**	**SD**	**Mean**	**SD**	F_{acq}	p_{acq}	F_{conf}	p_{conf}	**Confounders used**
Midbrain - Right Caudate	1.028	0.039	0.986	0.068	**5.261**	**0.033**	**5.261**	**0.033**	none
Midbrain - Right Putamen	1.002	0.035	0.970	0.046	3.735	0.068	3.735	0.068	none
Left Putamen - Left OFC	1.229	0.050	1.196	0.061	2.737	0.114	1.434	0.246	age
Right Putamen - Right OFC	1.258	0.071	1.199	0.077	**4.456**	**0.048**	2.988	0.100	age
Right Caudate - Right Putamen	1.135	0.044	1.113	0.064	2.776	0.111	2.352	0.142	alcohol, age
Right Putamen - Right Amygdala	1.074	0.068	1.023	0.057	3.225	0.088	1.414	0.251	birthweight, alcohol, sex
Right Putamen - Right Hippocampus	1.084	0.032	1.078	0.078	0.276	0.605	0.040	0.844	age

NAcc = nucleus accumbens; OFC = orbitofrontal cortex; X_{acq} = value when controlling for acquisition sequence in the analysis; X_{conf} = value following addition of acquisition sequence and significant confounding variables into analysis. Significant results (p<0.05) are highlighted in boldface. Age = gestational age at scan (weeks).

amygdala). Following the addition of confounding variables, increased RD in the methamphetamine group only survived in the midbrain – right caudate connection, while RD in the methamphetamine group tended to be greater in the midbrain – right putamen.

5.3.4 Regression of tract parameters and methamphetamine exposure

The results of the regression analyses of FA and methamphetamine exposure are shown in Table 5.6. Linear regression including acquisition sequence as a standard confounding variable in all WM-ROIs showed that increasing methamphetamine exposure was significantly associated with reduced FA in 8 connections: midbrain – right caudate; midbrain – right putamen; left NAcc – left OFC; left putamen – left OFC; right NAcc – right OFC; right putamen – right OFC; midbrain – right hippocampus; and right putamen – right amygdala. A trend towards a significant association was observed in a further 7 connections (midbrain – left caudate; midbrain – left putamen; right caudate – right OFC; right putamen – right hippocampus; left caudate – right caudate; left caudate – left hippocampus; left hippocampus – left OFC).

Potential cofounding variables were included in subsequent regression analyses if they showed a correlation with FA in the relevant WM-ROI at $p < 0.1$. After control for confounders, associations of increased methamphetamine exposure with FA reductions in 7 of the eight WM-ROIs survived. The association in the right putamen – right OFC connection became a trend, while the associations in 2 WM-ROIs, namely right caudate – right OFC and left caudate – left hippocampus, which showed trend-like associations initially, became significant. Weak associations were no longer evident in most of the other regions that showed a trend towards association previously, other than in the left hippocampus – left OFC connection.

Table 5.6. Regression of FA in WM-ROIs with methamphetamine exposure (*N*=23).

	Methamphetamine (*n*=11)		Control (*n*=12)						
WM-ROI (target$_1$ – target$_2$)	**Mean**	**SD**	**Mean**	**SD**	β_{acq}	p_{acq}	β_{conf}	p_{conf}	**Confounders included**
Midbrain - Right Caudate	0.230	0.014	0.248	0.044	**-0.45**	**0.038**	**-0.45**	**0.038**	none
Midbrain - Right Putamen	0.245	0.012	0.252	0.020	**-0.41**	**0.048**	**-0.41**	**0.048**	none
Midbrain - Left Caudate	0.235	0.014	0.240	0.018	-0.38	0.089	-0.23	0.274	age
Midbrain - Left Putamen	0.243	0.018	0.258	0.025	-0.42	0.061	-0.31	0.181	marijuana
Left NAcc - Left OFC	0.160	0.020	0.165	0.016	**-0.51**	**0.009**	**-0.44**	**0.020**	marital status
Left Putamen - Left OFC	0.181	0.013	0.191	0.013	**-0.57**	**0.007**	**-0.42**	**0.027**	age
Right NAcc - Right OFC	0.161	0.019	0.167	0.028	**-0.50**	**0.010**	**-0.50**	**0.010**	none
Right Caudate - Right OFC	0.189	0.017	0.199	0.031	-0.41	0.061	**-0.37**	**0.043**	age, birthweight, ses
Right Putamen - Right OFC	0.176	0.011	0.190	0.019	**-0.49**	**0.029**	-0.364	0.094	age
Midbrain - Right Hippocampus	0.227	0.027	0.232	0.028	**-0.49**	**0.018**	**-0.49**	**0.018**	none
Right Putamen - Right Amygdala	0.220	0.031	0.253	0.020	**-0.47**	**0.035**	**-0.47**	**0.035**	none
Right Putamen - Right Hippocampus	0.255	0.015	0.270	0.024	-0.43	0.060	-0.34	0.150	age
Left Caudate - Right Caudate	0.284	0.019	0.290	0.025	-0.41	0.060	-0.16	0.352	age, sex
Left Caudate - Left Hippocampus	0.241	0.017	0.239	0.020	-0.44	0.054	**-0.44**	**0.049**	age, ses
Left Hippocampus - Left OFC	0.232	0.021	0.239	0.020	-0.43	0.054	-0.43	0.054	none

NAcc = nucleus accumbens; OFC = orbitofrontal cortex; X_{acq} = value controlling for acquisition sequence in the analysis; X_{conf} = value following addition of acquisition sequence and significant confounding variables into analysis. Significant effects (p<0.05) are highlighted in boldface. Age = gestational age at scan (weeks); ses = Hollingshead socioeconomic status.

Table 5.7. Regression of AD in WM-ROIs with methamphetamine exposure (*N*=23).

	Methamphetamine (*n*=11)		Control (*n*=12)						
WM-ROI (target$_1$ – target$_2$)	**Mean**	**SD**	**Mean**	**SD**	β_{acq}	p_{acq}	β_{conf}	p_{conf}	**Confounders included**
Midbrain - Right Caudate	1.469	0.069	1.455	0.061	-0.057	0.813	-0.057	0.813	none
Midbrain - Right Putamen	1.467	0.050	1.440	0.034	0.153	0.507	0.153	0.507	none
Midbrain - Left Caudate	1.486	0.075	1.440	0.060	0.129	0.589	0.021	0.932	age
Midbrain - Left Putamen	1.466	0.044	1.472	0.076	-0.193	0.411	-0.227	0.384	marijuana
Left NAcc - Left OFC	1.618	0.122	1.555	0.120	0.164	0.489	0.198	0.424	marital status
Left Putamen - Left OFC	1.605	0.054	1.588	0.070	0.146	0.539	-0.030	0.893	age
Right NAcc - Right OFC	1.622	0.107	1.583	0.099	0.146	0.540	0.146	0.540	none
Right Caudate - Right OFC	1.703	0.067	1.683	0.096	0.167	0.467	0.107	0.651	age, birthweight, ses
Right Putamen - Right OFC	1.632	0.078	1.593	0.081	0.271	0.248	0.113	0.612	age
Midbrain - Right Hippocampus	1.682	0.084	1.705	0.079	-0.331	0.148	-0.331	0.148	none
Right Putamen - Right Amygdala	1.507	0.046	1.518	0.054	-0.310	0.181	-0.310	0.181	none
Right Putamen - Right Hippocampus	1.607	0.049	1.640	0.072	-0.264	0.250	-0.337	0.169	age
Left Caudate - Right Caudate	1.875	0.115	1.816	0.108	0.383	0.097	0.277	0.226	age, sex
Left Caudate - Left Hippocampus	1.678	0.122	1.709	0.144	-0.221	0.348	-0.305	0.218	age, ses
Left Hippocampus - Left OFC	1.762	0.113	1.801	0.151	-0.189	0.425	-0.189	0.425	none

NAcc = nucleus accumbens; OFC = orbitofrontal cortex; X_{acq} = value controlling for acquisition sequence in the analysis; X_{conf} = value following addition of acquisition sequence and significant confounding variables into analysis. Age = gestational age at scan (weeks); ses = Hollingshead socioeconomic status.

Table 5.8. Regression of RD in WM-ROIs with methamphetamine exposure (*N*=23).

	Methamphetamine (*n*=11)		Control (*n*=12)						
WM-ROI (target$_1$ – target$_2$)	**Mean**	**SD**	**Mean**	**SD**	β_{acq}	p_{acq}	β_{conf}	p_{conf}	**Confounders included**
Midbrain - Right Caudate	1.028	0.039	0.986	0.068	0.422	0.059	0.422	0.059	none
Midbrain - Right Putamen	1.002	0.035	0.970	0.046	0.381	0.099	0.381	0.099	none
Midbrain - Left Caudate	1.029	0.043	0.988	0.056	0.319	0.166	0.144	0.494	age
Midbrain - Left Putamen	1.002	0.045	0.982	0.067	0.136	0.569	0.032	0.900	marijuana
Left NAcc - Left OFC	1.275	0.100	1.217	0.098	0.321	0.167	0.324	0.188	marital status
Left Putamen - Left OFC	1.229	0.050	1.196	0.061	0.382	0.096	0.166	0.367	age
Right NAcc - Right OFC	1.273	0.090	1.232	0.104	0.369	0.106	0.369	0.106	none
Right Caudate - Right OFC	1.278	0.073	1.243	0.108	0.323	0.143	0.264	0.160	age, birthweight, ses
Right Putamen - Right OFC	1.258	0.071	1.199	0.077	0.420	0.066	0.248	0.228	age
Midbrain - Right Hippocampus	1.190	0.077	1.195	0.066	0.113	0.633	0.113	0.633	none
Right Putamen - Right Amygdala	1.074	0.068	1.023	0.057	0.214	0.362	0.214	0.362	none
Right Putamen - Right Hippocampus	1.084	0.032	1.078	0.078	0.108	0.642	0.002	0.995	age
Left Caudate - Right Caudate	1.201	0.092	1.150	0.082	**0.531**	**0.016**	0.312	0.092	age, sex
Left Caudate - Left Hippocampus	1.159	0.091	1.156	0.114	-0.006	0.979	-0.084	0.719	age, ses
Left Hippocampus - Left OFC	1.238	0.070	1.252	0.120	0.023	0.921	0.023	0.921	none

NAcc = nucleus accumbens; OFC = orbitofrontal cortex; X_{acq} = value controlling for acquisition sequence in the analysis; X_{conf} = value following addition of acquisition sequence and significant confounding variables into analysis. Significant results (p<0.05) are highlighted in boldface. Age = gestational age at scan (weeks); ses = Hollingshead socioeconomic status.

Tables 5.7 and 5.8 show the results of the regression of AD and RD with methamphetamine exposure in the WM-ROIs that showed a significant or trend-level association between FA and methamphetamine exposure. No significant associations between AD and methamphetamine exposure were observed in any connection at any stage of the analysis.

Increasing methamphetamine exposure was significantly associated with increased RD in the left caudate – right caudate connection, which became a trend after control for confounders. Trend-level associations were additionally observed in a further 2 connections (midbrain – right caudate; midbrain – right putamen).

5.4 DISCUSSION

This investigation forms part of the first study to use DTI tractography to examine the effects of prenatal methamphetamine exposure on white matter in neonates. As hypothesised, methamphetamine exposure was shown to be associated with reduced FA in several white matter connections, chiefly involving striatal structures, the midbrain and the OFC. The right hemisphere appeared more strongly affected, with 7 right and 4 left hemisphere connections observed to show alterations in FA at either a significant or trend level. Effects of methamphetamine on other diffusion measures were less global. No effects on AD were observed at all. RD, however, was observed to be increased in association with methamphetamine exposure in a subset of connections showing reduced FA.

These results are in partial agreement with previous studies examining white matter alterations in children with prenatal methamphetamine exposure. In a study of 6-7 year-old children, methamphetamine exposed children had significantly reduced FA in left external capsule and fornix, measured in the putamen, pallidum, hippocampus, amygdala and OFC regions[82]. Similarly, infants with combined methamphetamine/ tobacco exposure were observed to have

reduced FA in superior, anterior and posterior corona radiata[90]. Both of these studies observed increased RD in the corresponding regions, in agreement with the findings of the current study. In the older cohort increased AD was also observed, although this was not found in the same regions which exhibited reduced FA[82]. Other studies of prenatal methamphetamine exposure, however, do not agree with these observations. Cloak and colleagues observed a trend towards increased FA in left frontal white matter in 3-4 year-olds with prenatal methamphetamine exposure, with significantly reduced diffusivity in frontal and parietal white matter. No alterations were observed in grey matter subcortical regions[91]. Similarly, increased FA was observed in older children (9-11 years) with prenatal exposure to methamphetamine and alcohol in a number of white matter tracts in the left hemisphere[92]. The latter study noted an overall reduction in diffusivity, including RD, in exposed children. In DTI studies of adult methamphetamine users, the findings are generally similar to those of the current study, with reduced FA noted in frontal white matter[28,31,187] and CC[29,30,187].

The precise structural and functional significance of alterations in diffusion indices is a matter of some complexity. Anisotropic water diffusion in neural tissue is primarily a product of intact axonal membranes, with the presence and integrity of the myelin sheath playing a modulating role[121]. FA is thus generally regarded as a measure of the structural coherence of the white matter under consideration[135], with higher FA reflecting greater restriction of diffusion and presumably more highly organised structure[125]. FA reductions have been shown to be associated with a number of neurodegenerative[194,197,234] and psychiatric[196,235,236] disorders. The nature of the white matter characteristics underlying changes in FA may, however, be multifactorial, and cannot be fully discerned from this measure alone. FA changes may be a consequence of altered myelin extent or structure[237], damage to the axon fibres[123] or changes in water content, such as in edema[192]. Reduced FA may be the result of increased RD or reduced AD, or a combination of alterations in both measures[122,237], and investigation of these indices

can provide some elucidation as to the nature of the underlying pathology, as AD is generally more sensitive to axonal damage[238], while RD changes have been shown to reflect changes in myelination[239].

As observed previously, *in utero* methamphetamine exposure was associated in the current study with reduced FA in a number of white matter connections. Investigation of the diffusion indices showed no changes in AD in any of the studied connections, while a subset exhibited increased RD in association with methamphetamine exposure. These findings indicate that the exposure to methamphetamine reduced the integrity of the white matter in the studied neonates, and suggests that this may be a result primarily of damage to or alterations in myelin. This pathology following methamphetamine exposure is supported by a variety of findings. *In vitro* methamphetamine treatment induces apoptosis in oligodendroglial cells in a dose- and time-dependent manner[203], and in animal studies prenatal exposure to methamphetamine has been shown to be associated with reduced myelination and myelin content of white matter[201,202]. Given that RD changes were observed in only a few connections, however, these conclusions should be drawn with caution. Methamphetamine has been associated with axonal degeneration in caudate, putamen[204] and hippocampus[240] and increased apoptosis of neurons in the olfactory bulb[241]. In DTI studies of methamphetamine abuse in adults, AD was shown to be decreased in the CC[30] and increased in caudate-putamen[31], while both studies showed an increase in RD. Studies of prenatal exposure have shown increased AD[82,92], and both increased[82,90] and decreased[92] RD. Despite the lack of unanimity as to the exact direction of the alterations in diffusion indices, however, it can be assumed that the damage to white matter is the result of several factors.

An additional consideration when interpreting diffusion data from infants, and one that adds considerable complexity, is that neural development is active and ongoing in neonates. Axonal organisation into fibre systems begins in the first trimester of pregnancy[101], and at birth most

of the major white matter tracts are in place[242]. The process of myelination, however, is far from complete at birth[129]. White matter maturation is, additionally, region specific: it appears to follow a caudal-to-rostral and central-to-peripheral progression[124], such that proximal pathways and central regions will be myelinated earlier and more rapidly than distal and polar ones[101]. Myelination also tends to occur earlier in functional systems that are used earlier in life than those that will be used later[243], so that sensory pathways and projection fibres will mature sooner than motor and association connections[129]. Anisotropy has been shown to be present in white matter prior to myelination[121], and is measurable even during gestation[244], but the rapid and anatomically non-uniform development of the white matter postnatally results in a natural shift in diffusion measures[121]. A variety of factors may play a role in this, including increased fibre diameter and cohesion of tracts, myelination, reduced brain water and denser axonal packing[208]. As the white matter tracts mature, FA tends to increase while AD and RD decrease[124,245]. Given that in the current study methamphetamine exposure was associated with reduced FA and, in some cases, increased RD, there is the additional possibility that these changes may be an indication of slower maturation of neonatal white matter. Delayed maturation of serotonergic neurons in the frontal cortex[246], and inhibited somatic and locomotor development[209,210,247] have been observed in rats following treatment with methamphetamine *in utero*. There is also precedence for this interpretation in a study of infants with prenatal methamphetamine and tobacco exposure, which noted reduced FA and increased diffusivity in the corona radiata at 1 month, and demonstrated that the developmental trajectories of these indices were altered in comparison to healthy comparison infants[90]. However, given that studies have observed diffusion and anisotropy differences in white matter of older children with prenatal exposure, it is unlikely that the changes observed are purely an indication of a delay in white matter development.

The basal ganglia are involved in regulating much of the activity of the frontal cortex, including motor function and a range of cognitive and emotional behaviours[96]. The OFC and its connections with the striatum and associated subcortical limbic regions are involved in motivation and reward[250], and alterations in these regions have been suggested to underlie some of the behavioural dysfunction observed in addiction[251]. Furthermore, children with prenatal exposure to methamphetamine exhibit structural and functional changes in striatal and limbic regions[87,89,94,96]. It is therefore unsurprising that methamphetamine exposure is associated with microstructural alterations in the white matter of the orbitofrontal-striatal circuit, as demonstrated in the current study.

There are certain limitations inherent in studies of prenatal drug exposure which may be addressed by investigating effects during the neonatal period. One such weakness is the influence of postnatal environment. Children who are exposed to methamphetamine in utero are almost invariably born into a suboptimal environment[81,84], which has itself been shown to exert a damaging influence on behavioural[77,170] and neurostructural[252–254] development. The potentially strong confounding effects of the postnatal environment can, however, be controlled to a substantial degree by investigating exposure effects in neonates, as in the current study. An additional advantage in an investigation of neonates is in the determination of exposure parameters. The women whose infants were studied here were recruited during pregnancy, and methamphetamine and poly-substance use was determined using a time-line follow-back method[130,131]. This provides a significant advantage over studies of older children, in which accurate determination of maternal drug use is difficult, and permits a more accurate measure of frequency of methamphetamine use and a more informed quantitative analysis of its effects. Only one previous study investigated the potential associations between increasing prenatal methamphetamine exposure and white matter diffusion properties[91].

There are a number of limitations in the current study. The potential confounding effects of polysubstance exposure is almost inevitable in any study investigating prenatal drug effects[93]. This is a significant concern, as exposure to alcohol, marijuana and tobacco has been shown in a range of both clinical and preclinical studies to be associated with altered structure and function of the CNS[135,220,222,255–258]. Individuals in both control and methamphetamine-using groups in the current study drank alcohol and used cigarettes and marijuana. More methamphetamine-using mothers used each substance during pregnancy, although only cigarette use was close to significantly different between groups. Prenatal exposure to tobacco has been shown to increase FA in the frontal white matter[223], and women using methamphetamine have been observed to smoke more cigarettes than women who smoke but do not use methamphetamine[90], so that the effect of cigarette smoking on infant white matter is likely to be compounded in the methamphetamine group. However, the accuracy of substance use recall permitted by recruitment and interview during pregnancy enabled a quantitatively reliable measurement of these variables, and they were analysed as potential confounders and included where statistically relevant. The sample size was fairly small, although comparable to previous work[82], and for this reason one must interpret the findings with a measure of caution. Alterations were, however, observed where they were expected, and in the hypothesized directions. In several WM-ROIs a trend was observed towards methamphetamine-associated changes, and with a larger cohort some might have reached significance. This should be inferred with caution, however[259]. As mentioned above, development of the CNS is far from complete at birth. This raises the possibility that effects observed during the neonatal period may be transient and resolve with maturation. Longitudinal investigations which follow cohorts from infancy as they mature will be invaluable in this regard. Given that our findings agree with previous results in both infants and older children, however, it is likely that the observed alterations will not resolve with age.

This is the first study, to our knowledge, to use DTI tractography to investigate methamphetamine-associated microstructural alterations in corticostriatal and limbic connections in neonates. The previous literature is equivocal, but the current results agree with findings of reduced anisotropy and increased RD in white matter connections in association with prenatal methamphetamine exposure, and extend them to show that these changes are measurable in infants in the first post-natal month. These alterations may well underlie a subset of the cognitive dysfunction exhibited by children with prenatal methamphetamine exposure. Further investigations will be essential to determine the extent to which methamphetamine-induced white matter damage is associated with cognitive deficits.

CHAPTER 6

DISCUSSION

Methamphetamine has long been known to be neurotoxic, with both animal studies and research in human users demonstrating a range of deleterious effects on the CNS. Exposure during the gestational period has been shown to be associated with increased risk of perinatal complications, and a range of cognitive, behavioural and affective changes have been observed in children with prenatal methamphetamine exposure. The current studies therefore aimed to investigate whether prenatal exposure to methamphetamine was associated with neurostructural changes in neonates. The women whose children were studied were drawn from the Cape Coloured community of Cape Town, South Africa, a region with high levels of abuse of methamphetamine.

The first study examined potential volumetric alterations of subcortical and cerebellar regions by means of manual segmentation of anatomical MR images. Reduction in volumes of the right and left caudate nuclei, in addition to reduced total brain volume, were observed to be associated with increased methamphetamine exposure, and this finding remained significant in the right caudate nucleus following adjustment for confounding variables.

The second part of the study used DTI to investigate possible white matter changes following prenatal methamphetamine exposure. Two analyses were used to assess changes in different aspects of white matter connections. Firstly, a whole-brain approach investigated possible changes in the three major classes of white matter connections, the commissural fibres and the projection and association fibres bilaterally. Methamphetamine exposure was shown to be associated with reduced FA in all five networks of white matter, and in individual WM-ROIs within the projection and association networks bilaterally. A subset of these regions also showed alterations in AD and – more frequently – in RD that were associated with methamphetamine exposure. The second DTI analysis examined the white matter that

connected regions which were traced in the anatomical study. Using a tractographic approach, the WM connections were assessed between the caudate, putamen and nucleus accumbens and the midbrain and OFC, and between these regions and the hippocampus and amygdala. In agreement with the findings of the first DTI analysis, reduced FA was observed to be associated with methamphetamine exposure in connections between the midbrain and striatal nuclei, and connections between these nuclei and the OFC. A small number of connections to the hippocampus and amygdala also exhibited FA changes in association with methamphetamine exposure. Increased RD was observed to be associated with methamphetamine exposure in a subset of these connections.

These findings are in agreement with previous investigations of children with prenatal methamphetamine exposure. Reduced volume of the caudate nucleus following methamphetamine exposure *in utero* has been observed in several studies of older children[93–95,149]. The literature is more equivocal as regards the effects of methamphetamine exposure on white matter, with some studies observing increased FA and reduced diffusivity in major white matter bundles[91,92], in contrast to the findings of the current study, while others have found reductions in FA and increased diffusivity in white matter regions[82,90], in agreement with our observations. Methodological differences may underlie these disparate findings, particularly as regards the tools of analysis of the structural and DT images. Despite these discrepancies, however, there is little doubt that prenatal methamphetamine is associated with neurostructural changes, at both volumetric and microstructural levels. As our findings have demonstrated, these effects are observable even in neonates.

The precise mechanisms whereby methamphetamine induces damage in monoaminergic neurons are not fully delineated, but are likely multifactorial. There is considerable evidence that oxidative stress plays a pivotal role in the neurotoxicity of methamphetamine. Levels of reactive oxygen and nitrogen species in dopaminergic neurons are increased following

exposure to methamphetamine[260,261], and lipid peroxidation products have been shown to be at higher levels in the caudate and prefrontal cortex of methamphetamine users[262–264]. These changes are likely the result of several processes[225]. The fundamental effect of methamphetamine is to increase dopamine levels, both at the extraneuronal level and within the cytosol of the presynaptic terminal[13,179]. Paradoxically, dopamine is thought to play a vital role in the neurotoxicity of methamphetamine. If not sequestered in presynaptic vesicles, dopamine is rapidly oxidised to form quinones, cysteinyls and other reactive species[265,266] which cause damage to proteins and lipids within the neuron[267]. Additionally, the products of dopamine oxidation appear to be at least partially responsible for inducing activation of microglia[268]. Microglial activation has been observed to be a significant response to methamphetamine exposure in both animal[269–271] and human[272] studies, and has been shown to play a role in its neurotoxicity[159,271]. It has been suggested that methamphetamine may exacerbate oxidative stress by promoting downregulation of cellular antioxidant mechanisms[273] and inducing mitochondrial dysfunction[274–276]. Oxidative stress may additionally be involved in promoting the activity of the transcription factor p53, which is responsible for inducing apoptosis[277].

The mechanisms of methamphetamine neurotoxicity are likely not completely limited to its effects on monoaminergic neurons, however. Methamphetamine has been shown to cause reduced blood flow across the placenta[57] and restricted supply of nutrients and oxygen to the developing fetus[70]. Analysis of placental development in the current cohort demonstrated that methamphetamine use during pregnancy was associated with greater placental size and increased intrauterine passing of meconium[58]. Both findings may be responses to chronic hypoxia, suggesting that the methamphetamine-exposed fetus may experience prolonged intervals of hypoxia-ischemia. White matter has been shown to be particularly vulnerable to hypoxic-ischemic insult[278–280], with late oligodendrocyte progenitor cells most highly

susceptible to ischemia-induced apoptosis[281–283]. This may be a consideration in the current findings of somewhat widespread white matter changes following methamphetamine exposure.

The basal ganglia are increasingly understood to be involved in the regulation of a diverse range of frontal cortical activities including motor function, cognition, executive function and decision-making, and reward-related and motivational processes[248,249]. Projections from frontal cortex to the basal ganglia are chiefly to the dorsal striatum, consisting of the caudate and putamen, and the ventral or limbic striatum, which includes the nucleus accumbens[284]. It has been postulated that corticostriatal connections exist in five parallel circuits, each projecting from a specific region of cortex to a defined area of striatum, which in turn projects back to that region of cortex via the thalamus[285]. Each circuit is then responsible for a specific set of motor, cognitive or affective functions based on its associated cortical region[284]. The motor and oculomotor circuits thus project from the supplementary motor area and the frontal eye fields respectively, while the dorsolateral, orbitofrontal and anterior cingulate circuits project from their eponymous cortical areas[285] and are involved in the planning, modulation and expression of goal-directed behaviours[106]. This understanding of closed, parallel corticostriatal circuits has been challenged, however, by a growing body of research suggesting that specific areas of the striatum receive afferents from several cortical regions, including the OFC, dorsolateral prefrontal cortex and parietal cortex[286–289]. The convergence of corticostriatal afferents within the striatum is postulated to underlie the integration of reward and executive control in reinforcement learning[290].

The OFC plays a fundamental role in stimulus-reinforcement and reversal learning and thus in modulating motivational, emotional and social behaviour[250], and is essential in the processes underlying inhibitory control and goal-directed behaviour[291]. It projects primarily to the ventral striatum, consisting of nucleus accumbens, ventral putamen and ventromedial caudate nucleus[292], as well as to the head and body of the caudate[292] and convergence zones within the

caudate and putamen in the dorsal striatum[286]. The ventral striatum receives input from the hippocampus and areas associated with the limbic regions such as the amygdala and ventral tegmental area in the midbrain[293]. As the primary circuit responsible for reinforcement, the striato-thalamo-orbitofrontal circuit and associated limbic-striatal areas has been postulated to be dysfunctional in drug addiction and to underlie the compulsive drug-seeking behaviour noted in addicted subjects[251,294].

A considerable body of evidence demonstrates alterations in components of this system following exposure to methamphetamine. In laboratory studies, methamphetamine administration has been shown to deplete dopamine levels[295–297] and dopamine transporter binding[298,299] and function[296] in the striatum, as well as to induce dopamine terminal degeneration[300] and apoptotic and necrotic cell death[301] in this region. In the basolateral amygdala, methamphetamine treatment resulted in increased dopamine fibre density[302]. Increased expression of c-fos[303] and GABA receptor subunit[304] mRNA have been observed in the OFC of rats pretreated with methamphetamine, and deficits in discrimination reversal learning, analogous to impairments observed following OFC damage in humans, were demonstrated to occur following methamphetamine treatment[299]. Similarly, damage to these regions has been observed in studies of adult methamphetamine users. Reduced volume of the OFC[22,183] and reduced activation of the OFC in decision-making tasks[51,52] have been shown to be associated with methamphetamine abuse. Altered glucose metabolism in OFC, amygdala and ventral striatum was associated with increased affective symptomatology in methamphetamine users[46], while in another study the severity of psychiatric symptoms was shown to correlate with reduced dopamine transporter density in the orbitofrontal and dorsolateral prefrontal cortices[48]. Reduced D_2 receptor availability in the caudate-putamen in methamphetamine abusers was associated with increased metabolic activity in the OFC[305].

Prenatal exposure to methamphetamine has been shown to produce similar results as exposure in adulthood. Animal studies of pre- or neo-natal methamphetamine treatment have demonstrated altered tyrosine hydroxylase and dopamine transporter mRNA levels in substantia nigra and ventral tegmental area[306–308], as well as altered dopamine and dopamine metabolite levels in the nucleus accumbens[163] and glutamate receptor expression in the hippocampus[309]. Mice exposed to methamphetamine in utero showed significantly increased impulsivity, reduced inhibitory control and heightened motivation for reward[310], behavioural characteristics which mimic core symptoms of addiction in humans and may indicate dysfunction in the striato-frontal cortex circuits. Similarly, children with prenatal methamphetamine exposure have been shown to have reduced caudate, putamen and hippocampal volumes[94,96] and altered metabolism in the striatum[89], and to exhibit lower activation in OFC and putamen in the performance of a working memory task[87].

The current findings of reduced volume of the caudate and decreased FA in the cortico-striatal circuits and associated limbic connections are thus unsurprising, and provide support for the consideration that the damage induced by methamphetamine exposure is not limited to cortex and subcortical structures but includes the white matter bundles connecting them. Furthermore, damage to these circuits has significant cognitive implications. Caudate volume has been shown to be a strong predictor of neurocognitive performance in children with fetal alcohol spectrum disorders[311] and autism[312]. In children with prenatal exposure to methamphetamine and alcohol, volume of the caudate was shown to be related to measures of intelligence[93]. Microstructural damage to the orbitofrontal-striatal circuit has repeatedly been demonstrated in individuals with a clinical diagnosis of ADHD[313–315]. Reduced generalised FA in the orbitofrontal-striatal connection has been associated with increased inattention[313,314], impaired executive function and severity of clinical symptoms[316] in children with ADHD. Children with prenatal methamphetamine exposure have a significantly increased incidence of ADHD[79,81]

and increased measures of ADHD clinical symptoms[85]. Prenatal methamphetamine exposure has been associated with significantly poorer performance on tasks of sustained attention[94,95] and inhibitory control[84] and increased risk of neurobehavioural disinhibition[83]. It is not unreasonable to speculate that alterations in the corticostriatal circuits such as those demonstrated in the current studies may, at least in part, underlie some of the cognitive deficits exhibited by methamphetamine-exposed children.

In the light of the current findings, there are multiple avenues for future investigation. The uncertainty as to the long-term nature of the findings warrants a scrutiny of the developmental trajectories of exposed children. It is additionally of importance to investigate whether the current structural findings are associated with or predictive of functional alterations in the specific modalities discussed above. These findings and future investigations arising from them are of vital significance for the development of appropriate and adequately informed interventions.

REFERENCES

1. Degenhardt L, Baxter AJ, Lee YY, et al. The global epidemiology and burden of psychostimulant dependence: Findings from the Global Burden of Disease Study 2010. *Drug Alcohol Depend*. 2014;137(1):36-47. doi:10.1016/j.drugalcdep.2013.12.025.

2. Degenhardt L, Whiteford HA, Ferrari AJ, et al. Global burden of disease attributable to illicit drug use and dependence: Findings from the Global Burden of Disease Study 2010. *Lancet*. 2013;382(9904):1564-1574. doi:10.1016/S0140-6736(13)61530-5.

3. Peltzer K, Ramlagan S, Johnson BD, Phaswana-Mafuya N. Illicit drug use and treatment in South Africa: a review. *Subst Use Misuse*. 2010;45(13):2221-2243. doi:10.3109/10826084.2010.481594.

4. Pasche S, Myers B. Substance misuse trends in South Africa. *Hum Psychopharmacol*. 2012;27(3):338-341. doi:10.1002/hup.2228.

5. Herman AA, Stein DJ, Seedat S, Heeringa SG, Moomal H, Williams DR. The South African Stress and Health (SASH) study: 12-month and lifetime prevalence of common mental disorders. *South African Med J*. 2009;99(5):339-344.

6. Parry CDH, Plüddemann A, Myers B, Wechsberg WM, Flisher AJ. Methamphetamine use and sexual risk behaviour in Cape Town, South Africa: a review of data from 8 studies conducted between 2004 and 2007. *Afr J Psychiatry*. 2011;14(5):372-376. doi:http://dx.doi.org/10.4314/ajpsy.v14i5.4.

7. Plüddemann A, Dada S, Parry CDH, et al. Monitoring the prevalence of methamphetamine-related presentations at psychiatric hospitals in Cape Town, South Africa. *Afr J Psychiatry*. 2013;16(1):45-49. doi:http://dx.doi.org/10.4314/ajpsy.v16i1.8.

8. Watt MH, Meade CS, Kimani S, et al. The impact of methamphetamine ("tik") on a peri-urban community in Cape Town, South Africa. *Int J Drug Policy*. 2014;25(2):219-225. doi:10.1016/j.drugpo.2013.10.007.

9. Jacobson SW, Jacobson JL, Stanton ME, Meintjes EM, Molteno CD. Biobehavioral markers of adverse effect in fetal alcohol spectrum disorders. *Neuropsychol Rev*. 2011;21(2):148-166. doi:10.1007/s11065-011-9169-7.

10. Meade CS, Watt MH, Sikkema KJ, et al. Methamphetamine use is associated with childhood sexual abuse and HIV sexual risk behaviors among patrons of alcohol-serving venues in Cape Town, South Africa. *Drug Alcohol Depend*. 2012;126(1-2):232-239. doi:10.1016/j.drugalcdep.2012.05.024.

11. Plüddemann A, Flisher AJ, McKetin R, Parry C, Lombard C. Methamphetamine use, aggressive behavior and other mental health issues among high-school students in Cape Town, South Africa. *Drug Alcohol Depend*. 2010;109(1-3):14-19. doi:10.1016/j.drugalcdep.2009.11.021.

12. Wechsberg WM, Luseno WK, Karg RS, et al. Alcohol, cannabis, and methamphetamine use and other risk behaviours among Black and Coloured South African women: a small randomized trial in the Western Cape. *Int J Drug Policy*. 2008;19(2):130-139. doi:10.1016/j.drugpo.2007.11.018.

13. Panenka WJ, Procyshyn RM, Lecomte T, et al. Methamphetamine use: a comprehensive review of molecular, preclinical and clinical findings. *Drug Alcohol Depend*. 2013;129(3):167-179. doi:10.1016/j.drugalcdep.2012.11.016.

14. Sulzer D, Sonders MS, Poulsen NW, Galli A. Mechanisms of neurotransmitter release by amphetamines: a review. *Prog Neurobiol*. 2005;75(6):406-433. doi:10.1016/j.pneurobio.2005.04.003.

15. Dela Peña I, Gevorkiana R, Shi WX. Psychostimulants affect dopamine transmission through both dopamine transporter-dependent and independent mechanisms. *Eur J Pharmacol*. 2015;764:562-570. doi:10.1016/j.ejphar.2015.07.044.

16. Kish SJ. Pharmacologic mechanisms of crystal meth. *CMAJ*. 2008;178(13):1679-1682. doi:10.1503/cmaj.071675.

17. Haber SN. The place of dopamine in the cortico-basal ganglia circuit. *Neuroscience*. 2014;282:248-257. doi:10.1016/j.neuroscience.2014.10.008.

18. Chang L, Cloak C, Patterson K, Grob C, Miller EN, Ernst T. Enlarged striatum in abstinent methamphetamine abusers: A possible compensatory response. *Biol Psychiatry*. 2005;57(9):967-974. doi:10.1016/j.biopsych.2005.01.039.

19. Jan RK, Lin JC, Miles SW, Kydd RR, Russell BR. Striatal volume increases in active methamphetamine-dependent individuals and correlation with cognitive performance. *Brain Sci*. 2012;2(4):553-572. doi:10.3390/brainsci2040553.

20. Morales AM, Lee B, Hellemann G, O'Neill J, London ED. Gray-matter volume in methamphetamine dependence: cigarette smoking and changes with abstinence from methamphetamine. *Drug Alcohol Depend*. 2012;125(3):230-238. doi:10.1016/j.drugalcdep.2012.02.017.

21. Aoki Y, Orikabe L, Takayanagi Y, et al. Volume reductions in frontopolar and left perisylvian cortices in methamphetamine induced psychosis. *Schizophr Res*. 2013;147(2-3):355-361. doi:10.1016/j.schres.2013.04.029.

22. Daumann J, Koester P, Becker B, et al. Medial prefrontal gray matter volume reductions in users of amphetamine-type stimulants revealed by combined tract-based spatial statistics and voxel-based morphometry. *Neuroimage*. 2011;54(2):794-801.

doi:10.1016/j.neuroimage.2010.08.065.

23. Thompson PM, Hayashi KM, Simon SL, et al. Structural abnormalities in the brains of human subjects who use methamphetamine. *J Neurosci*. 2004;24(26):6028-6036. doi:10.1523/JNEUROSCI.0713-04.2004.

24. Schwartz DL, Mitchell AD, Lahna DL, et al. Global and local morphometric differences in recently abstinent methamphetamine-dependent individuals. *Neuroimage*. 2010;50(4):1392-1401. doi:10.1016/j.neuroimage.2010.01.056.

25. Orikabe L, Yamasue H, Inoue H, et al. Reduced amygdala and hippocampal volumes in patients with methamphetamine psychosis. *Schizophr Res*. 2011;132(2-3):183-189. doi:10.1016/j.schres.2011.07.006.

26. Derauf C, Kekatpure M, Neyzi N, Lester B, Kosofsky B. Neuroimaging of children following prenatal drug exposure. *Semin Cell Dev Biol*. 2009;20(4):441-454. doi:10.1016/j.semcdb.2009.03.001.

27. Huang H, Vasung L. Gaining insight of fetal brain development with diffusion MRI and histology. *Int J Dev Neurosci*. 2014;32:11-22. doi:10.1016/j.ijdevneu.2013.06.005.

28. Chung A, Lyoo IK, Kim SJ, et al. Decreased frontal white-matter integrity in abstinent methamphetamine abusers. *Int J Neuropsychopharmacol*. 2007;10(6):765-775. doi:10.1017/S1461145706007395.

29. Salo R, Nordahl TE, Buonocore MH, et al. Cognitive control and white matter callosal microstructure in methamphetamine-dependent subjects: a diffusion tensor imaging study. *Biol Psychiatry*. 2009;65(2):122-128. doi:10.1016/j.biopsych.2008.08.004.

30. Kim I-S, Kim Y-T, Song H-J, et al. Reduced corpus callosum white matter microstructural integrity revealed by diffusion tensor eigenvalues in abstinent

methamphetamine addicts. *Neurotoxicology*. 2009;30(2):209-213. doi:10.1016/j.neuro.2008.12.002.

31. Alicata D, Chang L, Cloak C, Abe K, Ernst T. Higher diffusion in striatum and lower fractional anisotropy in white matter of methamphetamine users. *Psychiatry Res*. 2009;174(1):1-8. doi:10.1016/j.pscychresns.2009.03.011.

32. Salo R, Nordahl TE, Natsuaki Y, et al. Attentional control and brain metabolite levels in methamphetamine abusers. *Biol Psychiatry*. 2007;61(11):1272-1280. doi:10.1016/j.biopsych.2006.07.031.

33. Sekine Y, Minabe Y, Kawai M, et al. Metabolite alterations in basal ganglia associated with methamphetamine-related psychiatric symptoms. A proton MRS study. *Neuropsychopharmacology*. 2002;27(3):453-461. doi:10.1016/S0893-133X(02)00321-4.

34. Sung YH, Cho SC, Hwang J, et al. Relationship between N-acetyl-aspartate in gray and white matter of abstinent methamphetamine abusers and their history of drug abuse: a proton magnetic resonance spectroscopy study. *Drug Alcohol Depend*. 2007;88(1):28-35. doi:10.1016/j.drugalcdep.2006.09.011.

35. Ernst T, Chang L, Leonido-Yee M, Speck O. Evidence for long-term neurotoxicity associated with methamphetamine abuse: A 1H MRS study. *Neurology*. 2000;54(6):1344-1349. doi:10.1212/WNL.54.6.1344.

36. Nordahl TE, Salo R, Possin K, et al. Low N-acetyl-aspartate and high choline in the anterior cingulum of recently abstinent methamphetamine-dependent subjects: a preliminary proton MRS study. Magnetic resonance spectroscopy. *Psychiatry Res*. 2002;116(1-2):43-52. http://www.ncbi.nlm.nih.gov/pubmed/12426033.

37. Nordahl TE, Salo R, Natsuaki Y, et al. Methamphetamine users in sustained abstinence: a proton magnetic resonance spectroscopy study. *Arch Gen Psychiatry*. 2005;62(4):444-452. doi:10.1001/archpsyc.62.4.444.

38. Kim SJ, Lyoo IK, Hwang J, et al. Prefrontal grey-matter changes in short-term and long-term abstinent methamphetamine abusers. *Int J Neuropsychopharmacol*. 2006;9(2):221-228. doi:10.1017/S1461145705005699.

39. King G, Alicata D, Cloak C, Chang L. Neuropsychological deficits in adolescent methamphetamine abusers. *Psychopharmacology (Berl)*. 2010;212(2):243-249. doi:10.1007/s00213-010-1949-x.

40. Salo R, Nordahl TE, Moore C, et al. A dissociation in attentional control: evidence from methamphetamine dependence. *Biol Psychiatry*. 2005;57(3):310-313. doi:10.1016/j.biopsych.2004.10.035.

41. Nestor LJ, Ghahremani DG, Monterosso J, London ED. Prefrontal hypoactivation during cognitive control in early abstinent methamphetamine-dependent subjects. *Psychiatry Res*. 2011;194(3):287-295. doi:10.1016/j.pscychresns.2011.04.010.

42. Johanson C-E, Frey KA, Lundahl LH, et al. Cognitive function and nigrostriatal markers in abstinent methamphetamine abusers. *Psychopharmacology (Berl)*. 2006;185(3):327-338. doi:10.1007/s00213-006-0330-6.

43. Lewis SJG, Dove A, Robbins TW, Barker RA, Owen AM. Striatal contributions to working memory: a functional magnetic resonance imaging study in humans. *Eur J Neurosci*. 2004;19(3):755-760. doi:10.1111/j.1460-9568.2003.03108.x.

44. Uhlmann A, Fouche J-P, Lederer K, Meintjes EM, Wilson D, Stein DJ. White matter microstructure and impulsivity in methamphetamine dependence with and without a

history of psychosis. *Hum Brain Mapp*. 2016;37(6):2055-2067. doi:10.1002/hbm.23159.

45. Lee B, London ED, Poldrack RA, et al. Striatal dopamine d2/d3 receptor availability is reduced in methamphetamine dependence and is linked to impulsivity. *J Neurosci*. 2009;29(47):14734-14740. doi:10.1523/JNEUROSCI.3765-09.2009.

46. London ED, Simon SL, Berman SM, et al. Mood disturbances and regional cerebral metabolic abnormalities in recently abstinent methamphetamine abusers. *Arch Gen Psychiatry*. 2004;61(1):73-84. doi:10.1001/archpsyc.61.1.73.

47. Sekine Y, Iyo M, Ouchi Y, et al. Methamphetamine-related psychiatric symptoms and reduced brain dopamine transporters studied with PET. *Am J Psychiatry*. 2001;158(8):1206-1214. doi:10.1176/appi.ajp.158.8.1206.

48. Sekine Y, Minabe Y, Ouchi Y, et al. Association of dopamine transporter loss in the orbitofrontal and dorsolateral prefrontal cortices with methamphetamine-related psychiatric symptoms. *Am J Psychiatry*. 2003;160(9):1699-1701. doi:10.1176/appi.ajp.160.9.1699.

49. Volkow ND, Chang L, Wang GJ, et al. Association of dopamine transporter reduction with psychomotor impairment in methamphetamine abusers. *Am J Psychiatry*. 2001;158(3):377-382. doi:10.1176/appi.ajp.158.3.377.

50. Salo R, Fassbender C, Buonocore MH, Ursu S. Behavioral regulation in methamphetamine abusers: An fMRI study. *Psychiatry Res Neuroimaging*. 2013;211(3):234-238. doi:10.1016/j.pscychresns.2012.10.003.

51. Paulus MP, Hozack NE, Zauscher BE, et al. Behavioral and functional neuroimaging evidence for prefrontal dysfunction in methamphetamine-dependent subjects.

Neuropsychopharmacology. 2002;26(1):53-63. doi:10.1016/S0893-133X(01)00334-7.

52. Paulus MP, Hozack N, Frank L, Brown GG, Schuckit MA. Decision making by methamphetamine-dependent subjects is associated with error-rate-independent decrease in prefrontal and parietal activation. *Biol Psychiatry*. 2003;53(1):65-74. http://www.ncbi.nlm.nih.gov/pubmed/12513946.

53. Terplan M, Smith EJ, Kozloski MJ, Pollack HA. Methamphetamine use among pregnant women. *Obstet Gynecol*. 2009;113(6):1285-1291. doi:10.1097/AOG.0b013e3181a5ec6f.

54. Arria AM, Derauf C, Lagasse LL, et al. Methamphetamine and other substance use during pregnancy: preliminary estimates from the Infant Development, Environment, and Lifestyle (IDEAL) study. *Matern Child Health J*. 2006;10(3):293-302. doi:10.1007/s10995-005-0052-0.

55. Wechsberg WM, Jones HE, Zule WA, et al. Methamphetamine ("tik") use and its association with condom use among out-of-school females in Cape Town, South Africa. *Am J Drug Alcohol Abuse*. 2010;36(4):208-213. doi:10.3109/00952990.2010.493592.

56. Jones HE, Browne FA, Myers BJ, et al. Pregnant and nonpregnant women in cape town, South Africa: drug use, sexual behavior, and the need for comprehensive services. *Int J Pediatr*. 2011;2011:353410. doi:10.1155/2011/353410.

57. Stek AM, Baker RS, Fisher BK, Lang U, Clark KE. Fetal responses to maternal and fetal methamphetamine administration in sheep. *Am J Obstet Gynecol*. 1995;173(5):1592-1598. http://www.ncbi.nlm.nih.gov/pubmed/7503206.

58. Carter RC, Wainwright H, Molteno CD, et al. Alcohol, methamphetamine, and

marijuana exposure have distinct effects on the human placenta. *Alcohol Clin Exp Res*. 2016;40(4):753-764. doi:10.1111/acer.13022.

59. Smith L, Yonekura ML, Wallace T, Berman N, Kuo J, Berkowitz C. Effects of prenatal methamphetamine exposure on fetal growth and drug withdrawal symptoms in infants born at term. *J Dev Behav Pediatr*. 2003;24(1):17-23. http://www.ncbi.nlm.nih.gov/pubmed/12584481.

60. Good MM, Solt I, Acuna JG, Rotmensch S, Kim MJ. Methamphetamine use during pregnancy: maternal and neonatal implications. *Obstet Gynecol*. 2010;116(2 Pt 1):330-334. doi:10.1097/AOG.0b013e3181e67094.

61. Oei J, Abdel-Latif ME, Clark R, Craig F, Lui K. Short-term outcomes of mothers and infants exposed to antenatal amphetamines. *Arch Dis Child Fetal Neonatal Ed*. 2010;95(1):F36-41. doi:10.1136/adc.2008.157305.

62. Wright TE, Schuetter R, Tellei J, Sauvage L. Methamphetamines and pregnancy outcomes. *J Addict Med*. 2013;9(2):111-117. doi:10.1097/ADM.0000000000000101.

63. Shah R, Diaz SD, Arria A, et al. Prenatal methamphetamine exposure and short-term maternal and infant medical outcomes. *Am J Perinatol*. 2012;29(5):391-400. doi:10.1055/s-0032-1304818.

64. Smith LM, LaGasse LL, Derauf C, et al. The infant development, environment, and lifestyle study: effects of prenatal methamphetamine exposure, polydrug exposure, and poverty on intrauterine growth. *Pediatrics*. 2006;118(3):1149-1156. doi:10.1542/peds.2005-2564.

65. Nguyen D, Smith LM, Lagasse LL, et al. Intrauterine growth of infants exposed to prenatal methamphetamine: results from the infant development, environment, and

lifestyle study. *J Pediatr*. 2010;157(2):337-339. doi:10.1016/j.jpeds.2010.04.024.

66. Phupong V, Darojn D. Amphetamine abuse in pregnancy: the impact on obstetric outcome. *Arch Gynecol Obstet*. 2007;276(2):167-170. doi:10.1007/s00404-007-0320-x.

67. LaGasse LL, Wouldes T, Newman E, et al. Prenatal methamphetamine exposure and neonatal neurobehavioral outcome in the USA and New Zealand. *Neurotoxicol Teratol*. 2011;33(1):166-175. doi:10.1016/j.ntt.2010.06.009.

68. Paz MS, Smith LM, LaGasse LL, et al. Maternal depression and neurobehavior in newborns prenatally exposed to methamphetamine. *Neurotoxicol Teratol*. 2009;31(3):177-182. doi:10.1016/j.ntt.2008.11.004.

69. Smith LM, Lagasse LL, Derauf C, et al. Prenatal methamphetamine use and neonatal neurobehavioral outcome. *Neurotoxicol Teratol*. 2008;30(1):20-28. doi:10.1016/j.ntt.2007.09.005.

70. Burchfield DJ, Lucas VW, Abrams RM, Miller RL, DeVane CL. Disposition and pharmacodynamics of methamphetamine in pregnant sheep. *JAMA*. 1991;265(15):1968-1973. http://www.ncbi.nlm.nih.gov/pubmed/2008026.

71. Rambousek L, Kacer P, Syslova K, Bumba J, Bubenikova-Valesova V, Slamberova R. Sex differences in methamphetamine pharmacokinetics in adult rats and its transfer to pups through the placental membrane and breast milk. *Drug Alcohol Depend*. 2014;139:138-144. doi:10.1016/j.drugalcdep.2014.03.023.

72. Salisbury AL, Ponder KL, Padbury JF, Lester BM. Fetal effects of psychoactive drugs. *Clin Perinatol*. 2009;36(3):595-619. doi:10.1016/j.clp.2009.06.002.

73. Frederick AL, Stanwood GD. Drugs, biogenic amine targets and the developing brain.

Dev Neurosci. 2009;31(1-2):7-22. doi:10.1159/000207490.

74. Wouldes TA, Lagasse LL, Huestis MA, Dellagrotta S, Dansereau LM, Lester BM. Prenatal methamphetamine exposure and neurodevelopmental outcomes in children from 1 to 3 years. *Neurotoxicol Teratol*. 2014;42:77-84. doi:10.1016/j.ntt.2014.02.004.

75. Smith LM, LaGasse LL, Derauf C, et al. Motor and cognitive outcomes through three years of age in children exposed to prenatal methamphetamine. *Neurotoxicol Teratol*. 2011;33(1):176-184. doi:10.1016/j.ntt.2010.10.004.

76. Billing L, Eriksson M, Steneroth G, Zetterström R. Predictive indicators for adjustment in 4-year-old children whose mothers used amphetamine during pregnancy. *Child Abuse Negl*. 1988;12(4):503-507. doi:10.1016/0145-2134(88)90067-1.

77. Billing L, Eriksson M, Jonsson B, Steneroth G, Zetterström R. The influence of environmental factors on behavioural problems in 8-year-old children exposed to amphetamine during fetal life. *Child Abuse Negl*. 1994;18(1):3-9. doi:10.1016/0145-2134(94)90091-4.

78. Eze N, Smith LM, Lagasse LL, et al. School-Aged Outcomes following Prenatal Methamphetamine Exposure: 7.5-Year Follow-Up from the Infant Development, Environment, and Lifestyle Study. *J Pediatr*. 2016;170:34-38e1. doi:10.1016/j.jpeds.2015.11.070.

79. LaGasse LL, Derauf C, Smith LM, et al. Prenatal methamphetamine exposure and childhood behavior problems at 3 and 5 years of age. *Pediatrics*. 2012;129(4):681-688. doi:10.1542/peds.2011-2209.

80. Abar B, LaGasse LL, Derauf C, et al. Examining the relationships between prenatal methamphetamine exposure, early adversity, and child neurobehavioral disinhibition.

Psychol Addict Behav. 2013;27(3):662-673. doi:10.1037/a0030157.

81. Piper BJ, Acevedo SF, Kolchugina GK, et al. Abnormalities in parentally rated executive function in methamphetamine/polysubstance exposed children. *Pharmacol Biochem Behav*. 2011;98(3):432-439. doi:10.1016/j.pbb.2011.02.013.

82. Roos A, Kwiatkowski MA, Fouche J, et al. White matter integrity and cognitive performance in children with prenatal methamphetamine exposure. *Behav Brain Res*. 2015;279:62-67. doi:10.1016/j.bbr.2014.11.005.

83. Himes SK, LaGasse LL, Derauf C, et al. Risk of neurobehavioral disinhibition in prenatal methamphetamine-exposed young children with positive hair toxicology results. *Ther Drug Monit*. 2014;36(4):535-543. doi:10.1097/FTD.0000000000000049.

84. Derauf C, Lagasse LL, Smith LM, et al. Prenatal methamphetamine exposure and inhibitory control among young school-age children. *J Pediatr*. 2012;161(3):452-459. doi:10.1016/j.jpeds.2012.02.002.

85. Kiblawi ZN, Smith LM, LaGasse LL, et al. The effect of prenatal methamphetamine exposure on attention as assessed by continuous performance tests: results from the Infant Development, Environment, and Lifestyle study. *J Dev Behav Pediatr*. 2013;34(1):31-37. doi:10.1097/DBP.0b013e318277a1c5.

86. Lu LH, Johnson A, O'Hare ED, et al. Effects of prenatal methamphetamine exposure on verbal memory revealed with functional magnetic resonance imaging. *J Dev Behav Pediatr*. 2009;30(3):185-192. doi:10.1097/DBP.0b013e3181a7ee6b.

87. Roussotte FF, Bramen JE, Nunez SC, et al. Abnormal brain activation during working memory in children with prenatal exposure to drugs of abuse: the effects of methamphetamine, alcohol, and polydrug exposure. *Neuroimage*. 2011;54(4):3067-

3075. doi:10.1016/j.neuroimage.2010.10.072.

88. Chang L, Cloak C, Jiang CS, et al. Altered neurometabolites and motor integration in children exposed to methamphetamine in utero. *Neuroimage*. 2009;48(2):391-397. doi:10.1016/j.neuroimage.2009.06.062.

89. Smith LM, Chang L, Yonekura ML, Grob C, Osborn D, Ernst T. Brain proton magnetic resonance spectroscopy in children exposed to methamphetamine in utero. *Neurology*. 2001;57(2):255-260. doi:10.1212/WNL.57.2.255.

90. Chang L, Oishi K, Skranes J, et al. Sex-specific alterations of white matter developmental trajectories in infants with prenatal exposure to methamphetamine and tobacco. *JAMA psychiatry*. 2016;73(12):1217-1227. doi:10.1001/jamapsychiatry.2016.2794.

91. Cloak CC, Ernst T, Fujii L, Hedemark B, Chang L. Lower diffusion in white matter of children with prenatal methamphetamine exposure. *Neurology*. 2009;72(24):2068-2075. doi:10.1212/01.wnl.0000346516.49126.20.

92. Colby JB, Smith L, O'Connor MJ, Bookheimer SY, Van Horn JD, Sowell ER. White matter microstructural alterations in children with prenatal methamphetamine/polydrug exposure. *Psychiatry Res*. 2012;204(2-3):140-148. doi:10.1016/j.pscychresns.2012.04.017.

93. Sowell ER, Leow AD, Bookheimer SY, et al. Differentiating prenatal exposure to methamphetamine and alcohol versus alcohol and not methamphetamine using tensor-based brain morphometry and discriminant analysis. *J Neurosci*. 2010;30(11):3876-3885. doi:10.1523/JNEUROSCI.4967-09.2010.

94. Chang L, Smith LM, LoPresti C, et al. Smaller subcortical volumes and cognitive

deficits in children with prenatal methamphetamine exposure. *Psychiatry Res*. 2004;132(2):95-106. doi:10.1016/j.pscychresns.2004.06.004.

95. Derauf C, Lester BM, Neyzi N, et al. Subcortical and cortical structural central nervous system changes and attention processing deficits in preschool-aged children with prenatal methamphetamine and tobacco exposure. *Dev Neurosci*. 2012;34(4):327-341. doi:10.1159/000341119.

96. Roos A, Jones G, Howells FM, Stein DJ, Donald KA. Structural brain changes in prenatal methamphetamine-exposed children. *Metab Brain Dis*. 2014;29(2):341-349. doi:10.1007/s11011-014-9500-0.

97. Rivkin MJ. Developmental neuroimaging of children using magnetic resonance techniques. *Ment Retard Dev Disabil Res Rev*. 2000;6(1):68-80. doi:10.1002/(SICI)1098-2779(2000)6:1<68::AID-MRDD9>3.0.CO;2-9.

98. de Graaf-Peters VB, Hadders-Algra M. Ontogeny of the human central nervous system: What is happening when? *Early Hum Dev*. 2006;82(4):257-266. doi:10.1016/j.earlhumdev.2005.10.013.

99. Kandel ER, Schwartz JH, Jessell TM. *Principles of Neural Science*. 4th Ed. The McGraw-Hill Companies, Inc; 2000.

100. Prayer D, Kasprian G, Krampl E, et al. MRI of normal fetal brain development. *Eur J Radiol*. 2006;57(2):199-216. doi:10.1016/j.ejrad.2005.11.020.

101. Dubois J, Dehaene-Lambertz G, Kulikova S, Poupon C, Hüppi PS, Hertz-Pannier L. The early development of brain white matter: A review of imaging studies in fetuses, newborns and infants. *Neuroscience*. 2014;276:48-71. doi:10.1016/j.neuroscience.2013.12.044.

102. Stiles J, Jernigan TL. The basics of brain development. *Neuropsychol Rev*. 2010;20(4):327-348. doi:10.1007/s11065-010-9148-4.

103. Pierre WC, Smith PLP, Londono I, Chemtob S, Mallard C, Lodygensky GA. Neonatal microglia: The cornerstone of brain fate. *Brain Behav Immun*. 2017;59:333-345. doi:10.1016/j.bbi.2016.08.018.

104. Herlenius E, Lagercrantz H. Development of neurotransmitter systems during critical periods. *Exp Neurol*. 2004;190 Suppl(SUPPL. 1):S8-21. doi:10.1016/j.expneurol.2004.03.027.

105. Clark DL, Boutros NN, Mendez MF. *The Brain and Behavior: An Introduction to Behavioral Neuroanatomy*. 3rd Ed. Cambridge University Press; 2010.

106. Haber SN. The primate basal ganglia: parallel and integrative networks. *J Chem Neuroanat*. 2003;26(4):317-330. doi:10.1016/j.jchemneu.2003.10.003.

107. Keeler JF, Pretsell DO, Robbins TW. Functional implications of dopamine D1 vs. D2 receptors: A "prepare and select" model of the striatal direct vs. indirect pathways. *Neuroscience*. 2014;282:156-175. doi:10.1016/j.neuroscience.2014.07.021.

108. Beaulieu J-M, Gainetdinov RR. The physiology, signaling, and pharmacology of dopamine receptors. *Pharmacol Rev*. 2011;63(1):182-217. doi:10.1124/pr.110.002642.

109. Fleckenstein AE, Hanson GR. Impact of psychostimulants on vesicular monoamine transporter function. *Eur J Pharmacol*. 2003;479(1-3):283-289. doi:10.1016/j.ejphar.2003.08.077.

110. Sulzer D, Cragg SJ, Rice ME. Striatal dopamine neurotransmission: regulation of release and uptake. *Basal Ganglia*. 2016;6(3):123-148. doi:10.1016/j.baga.2016.02.001.

111. Uhl GR. Dopamine transporter: basic science and human variation of a key molecule for dopaminergic function, locomotion, and parkinsonism. *Mov Disord*. 2003;18 Suppl 7(SUPPL. 7):S71-80. doi:10.1002/mds.10578.

112. Ganong WF. *Review of Medical Physiology*. 21st Ed. The McGraw-Hill Companies, Inc; 2003.

113. Cruickshank CC, Dyer KR. A review of the clinical pharmacology of methamphetamine. *Addiction*. 2009;104(7):1085-1099. doi:10.1111/j.1360-0443.2009.02564.x.

114. Mendelson J, Uemura N, Harris D, et al. Human pharmacology of the methamphetamine stereoisomers. *Clin Pharmacol Ther*. 2006;80(4):403-420. doi:10.1016/j.clpt.2006.06.013.

115. Natarajan R, Yamamoto BK. The Basal Ganglia as a Substrate for the Multiple Actions of Amphetamines. *Basal Ganglia*. 2011;1(2):49-57. doi:10.1016/j.baga.2011.05.003.

116. Kahlig KM, Galli A. Regulation of dopamine transporter function and plasma membrane expression by dopamine, amphetamine, and cocaine. *Eur J Pharmacol*. 2003;479(1-3):153-158. doi:10.1016/j.ejphar.2003.08.065.

117. Barr AM, Panenka WJ, MacEwan GW, et al. The need for speed: an update on methamphetamine addiction. *J Psychiatry Neurosci*. 2006;31(5):301-313. http://www.ncbi.nlm.nih.gov/pubmed/16951733.

118. Hashemi RH, Bradley WG, Lisanti CJ. *MRI: The Basics*. 3rd Ed. Philadelphia, PA: Lippincott Williams & Wilkins; 2010.

119. Silk TJ, Wood AG. Lessons about neurodevelopment from anatomical magnetic

resonance imaging. *J Dev Behav Pediatr*. 2011;32(2):158-168. doi:10.1097/DBP.0b013e318206d58f.

120. Le Bihan D, Mangin JF, Poupon C, et al. Diffusion tensor imaging: concepts and applications. *J Magn Reson Imaging*. 2001;13(4):534-546. http://www.ncbi.nlm.nih.gov/pubmed/11276097.

121. Beaulieu C. The basis of anisotropic water diffusion in the nervous system - a technical review. *NMR Biomed*. 2002;15(7-8):435-455. doi:10.1002/nbm.782.

122. Alexander AL, Lee JE, Lazar M, Field AS. Diffusion tensor imaging of the brain. *Neurotherapeutics*. 2007;4(3):316-329. doi:10.1016/j.nurt.2007.05.011.

123. Assaf Y, Pasternak O. Diffusion tensor imaging (DTI)-based white matter mapping in brain research: a review. *J Mol Neurosci*. 2008;34(1):51-61. doi:10.1007/s12031-007-0029-0.

124. Qiu A, Mori S, Miller MI. Diffusion tensor imaging for understanding brain development in early life. *Annu Rev Psychol*. 2015;66:853-876. doi:10.1146/annurev-psych-010814-015340.

125. Feldman HM, Yeatman JD, Lee ES, Barde LHF, Gaman-Bean S. Diffusion tensor imaging: a review for pediatric researchers and clinicians. *J Dev Behav Pediatr*. 2010;31(4):346-356. doi:10.1097/DBP.0b013e3181dcaa8b.

126. Smith SM, Jenkinson M, Johansen-Berg H, et al. Tract-based spatial statistics: voxelwise analysis of multi-subject diffusion data. *Neuroimage*. 2006;31(4):1487-1505. doi:10.1016/j.neuroimage.2006.02.024.

127. Taylor PA, Saad ZS. FATCAT: (an efficient) Functional and Tractographic Connectivity Analysis Toolbox. *Brain Connect*. 2013;3(5):523-535.

doi:10.1089/brain.2013.0154.

128. Miller JH, McKinstry RC, Philip J V, Mukherjee P, Neil JJ. Diffusion-tensor MR imaging of normal brain maturation: a guide to structural development and myelination. *AJR Am J Roentgenol*. 2003;180(3):851-859. doi:10.2214/ajr.180.3.1800851.

129. Dubois J, Hertz-Pannier L, Dehaene-Lambertz G, Cointepas Y, Le Bihan D. Assessment of the early organization and maturation of infants' cerebral white matter fiber bundles: a feasibility study using quantitative diffusion tensor imaging and tractography. *Neuroimage*. 2006;30(4):1121-1132. doi:10.1016/j.neuroimage.2005.11.022.

130. Jacobson SW, Chiodo LM, Sokol RJ, Jacobson JL. Validity of maternal report of prenatal alcohol, cocaine, and smoking in relation to neurobehavioral outcome. *Pediatrics*. 2002;109(5):815-825. doi:10.1542/peds.109.5.815.

131. Jacobson SW, Stanton ME, Molteno CD, et al. Impaired eyeblink conditioning in children with fetal alcohol syndrome. *Alcohol Clin Exp Res*. 2008;32(2):365-372. doi:10.1111/j.1530-0277.2007.00585.x.

132. Jacobson SW, Jacobson JL, Molteno CD, et al. Heavy prenatal alcohol exposure is related to smaller corpus callosum in newborn MRI scans. *Alcohol Clin Exp Res*. 2017;41(5):965-975. doi:10.1111/acer.13363.

133. Freeview Guide - Freesurfer Wiki. https://surfer.nmr.mgh.harvard.edu/fswiki/FreeviewGuide.

134. de Macedo Rodrigues K, Ben-Avi E, Sliva DD, et al. A FreeSurfer-compliant consistent manual segmentation of infant brains spanning the 0-2 year age range. *Front*

Hum Neurosci. 2015;9(February):21. doi:10.3389/fnhum.2015.00021.

135. Taylor PA, Jacobson SW, van der Kouwe A, et al. A DTI-based tractography study of effects on brain structure associated with prenatal alcohol exposure in newborns. *Hum Brain Mapp*. 2015;36(1):170-186. doi:10.1002/hbm.22620.

136. Pannek K, Guzzetta A, Colditz PB, Rose SE. Diffusion MRI of the neonate brain: Acquisition, processing and analysis techniques. *Pediatr Radiol*. 2012;42(10):1169-1182. doi:10.1007/s00247-012-2427-x.

137. Smith SM, Jenkinson M, Woolrich MW, et al. Advances in functional and structural MR image analysis and implementation as FSL. *Neuroimage*. 2004;23 Suppl 1(SUPPL. 1):S208-19. doi:10.1016/j.neuroimage.2004.07.051.

138. Andersson JLR, Skare S, Ashburner J. How to correct susceptibility distortions in spin-echo echo-planar images: Application to diffusion tensor imaging. *Neuroimage*. 2003;20(2):870-888. doi:10.1016/S1053-8119(03)00336-7.

139. Taylor PA, Cho K, Lin C, Biswal BB. Improving DTI tractography by including diagonal tract propagation. *PLoS One*. 2012;7(9):e43415. doi:10.1371/journal.pone.0043415.

140. Mori S, Crain BJ, Chacko VP, van Zijl PC. Three-dimensional tracking of axonal projections in the brain by magnetic resonance imaging. *Ann Neurol*. 1999;45(2):265-269. http://www.ncbi.nlm.nih.gov/pubmed/9989633.

141. Ladhani NNN, Shah PS, Murphy KE, Knowledge Synthesis Group on Determinants of Preterm/LBW Births. Prenatal amphetamine exposure and birth outcomes: a systematic review and metaanalysis. *Am J Obstet Gynecol*. 2011;205(3):219.e1-7. doi:10.1016/j.ajog.2011.04.016.

142. Gorman MC, Orme KS, Nguyen NT, Kent EJ, Caughey AB. Outcomes in pregnancies complicated by methamphetamine use. *Am J Obstet Gynecol*. 2014;211(4):429.e1-7. doi:10.1016/j.ajog.2014.06.005.

143. Buchthal S, Ernst T, Anderson L, Cloak C, Kitamura R, Chang L. Brain Metabolite Changes in Infants Exposed in Utero to Methamphetamine and/or Nicotine. In: *Proceedings 17th Scientific Meeting, International Society for Magnetic Resonance in Medicine*. Vol Honolulu. ; 2009:1244. /MyPathway2009/1244.

144. Meade CS, Towe SL, Watt MH, et al. Addiction and treatment experiences among active methamphetamine users recruited from a township community in Cape Town, South Africa: A mixed-methods study. *Drug Alcohol Depend*. 2015;152:79-86. doi:10.1016/j.drugalcdep.2015.04.016.

145. Brazelton TB. *Neonatal Behavioral Assessment Scale*. 2nd ed. J.B. Lippincott Co; 1984.

146. Laswad T, Wintermark P, Alamo L, Moessinger A, Meuli R, Gudinchet F. Method for performing cerebral perfusion-weighted MRI in neonates. *Pediatr Radiol*. 2009;39(3):260-264. doi:10.1007/s00247-008-1081-9.

147. Fischl B, Salat DH, van der Kouwe AJW, et al. Sequence-independent segmentation of magnetic resonance images. *Neuroimage*. 2004;23 Suppl 1(SUPPL. 1):S69-84. doi:10.1016/j.neuroimage.2004.07.016.

148. Winer B. *Statistical Principles in Experimental Design*. 2nd ed. McGraw-Hill; 1971.

149. Walhovd KB, Moe V, Slinning K, et al. Volumetric cerebral characteristics of children exposed to opiates and other substances in utero. *Neuroimage*. 2007;36(4):1331-1344. doi:10.1016/j.neuroimage.2007.03.070.

150. Jernigan TL, Gamst AC, Archibald SL, et al. Effects of methamphetamine dependence and HIV infection on cerebral morphology. *Am J Psychiatry*. 2005;162(8):1461-1472. doi:10.1176/appi.ajp.162.8.1461.

151. Gallinat J, Meisenzahl E, Jacobsen LK, et al. Smoking and structural brain deficits: a volumetric MR investigation. *Eur J Neurosci*. 2006;24(6):1744-1750. doi:10.1111/j.1460-9568.2006.05050.x.

152. Ekblad M, Korkeila J, Parkkola R, et al. Maternal smoking during pregnancy and regional brain volumes in preterm infants. *J Pediatr*. 2010;156(2):185-90.e1. doi:10.1016/j.jpeds.2009.07.061.

153. Astley SJ, Aylward EH, Olson HC, et al. Magnetic resonance imaging outcomes from a comprehensive magnetic resonance study of children with fetal alcohol spectrum disorders. *Alcohol Clin Exp Res*. 2009;33(10):1671-1689. doi:10.1111/j.1530-0277.2009.01004.x.

154. Coles CD, Goldstein FC, Lynch ME, et al. Memory and brain volume in adults prenatally exposed to alcohol. *Brain Cogn*. 2011;75(1):67-77. doi:10.1016/j.bandc.2010.08.013.

155. Meintjes EM, Narr KL, van der Kouwe AJW, et al. A tensor-based morphometry analysis of regional differences in brain volume in relation to prenatal alcohol exposure. *NeuroImage Clin*. 2014;5:152-160. doi:10.1016/j.nicl.2014.04.001.

156. Sowell ER, Mattson SN, Kan E, Thompson PM, Riley EP, Toga AW. Abnormal cortical thickness and brain-behavior correlation patterns in individuals with heavy prenatal alcohol exposure. *Cereb Cortex*. 2008;18(1):136-144. doi:10.1093/cercor/bhm039.

157. Cappon GD, Pu C, Vorhees C V. Time-course of methamphetamine-induced neurotoxicity in rat caudate-putamen after single-dose treatment. *Brain Res*. 2000;863(1-2):106-111. doi:10.1016/S0006-8993(00)02107-7.

158. Castner SA, Vosler PS, Goldman-Rakic PS. Amphetamine sensitization impairs cognition and reduces dopamine turnover in primate prefrontal cortex. *Biol Psychiatry*. 2005;57(7):743-751. doi:10.1016/j.biopsych.2004.12.019.

159. LaVoie MJ, Card JP, Hastings TG. Microglial activation precedes dopamine terminal pathology in methamphetamine-induced neurotoxicity. *Exp Neurol*. 2004;187(1):47-57. doi:10.1016/j.expneurol.2004.01.010.

160. Marshall JF, Belcher AM, Feinstein EM, O'Dell SJ. Methamphetamine-induced neural and cognitive changes in rodents. *Addiction*. 2007;102 Suppl:61-69. doi:10.1111/j.1360-0443.2006.01780.x.

161. McCann UD, Wong DF, Yokoi F, Villemagne V, Dannals RF, Ricaurte GA. Reduced striatal dopamine transporter density in abstinent methamphetamine and methcathinone users: evidence from positron emission tomography studies with [11C]WIN-35,428. *J Neurosci*. 1998;18(20):8417-8422. http://www.ncbi.nlm.nih.gov/pubmed/9763484.

162. Quinton MS, Yamamoto BK. Causes and consequences of methamphetamine and MDMA toxicity. *AAPS J*. 2006;8(2):E337-47. doi:10.1208/aapsj080238.

163. Bubenikova-Valesova V, Kacer P, Syslova K, et al. Prenatal methamphetamine exposure affects the mesolimbic dopaminergic system and behavior in adult offspring. *Int J Dev Neurosci*. 2009;27(6):525-530. doi:10.1016/j.ijdevneu.2009.06.012.

164. Heller A, Bubula N, Freeney A, Won L. Elevation of fetal dopamine following

exposure to methamphetamine in utero. *Brain Res Dev Brain Res*. 2001;130(1):139-142. doi:10.1016/S0165-3806(01)00222-X.

165. Noailles PAH, Becker KG, Wood WH, Teichberg D, Cadet JL. Methamphetamine-induced gene expression profiles in the striatum of male rat pups exposed to the drug in utero. *Brain Res Dev Brain Res*. 2003;147(1-2):153-162. doi:10.1016/j.devbrainres.2003.11.003.

166. Wells PG, Bhuller Y, Chen CS, et al. Molecular and biochemical mechanisms in teratogenesis involving reactive oxygen species. *Toxicol Appl Pharmacol*. 2005;207(2 Suppl):354-366. doi:10.1016/j.taap.2005.01.061.

167. Wong AW, McCallum GP, Jeng W, Wells PG. Oxoguanine glycosylase 1 protects against methamphetamine-enhanced fetal brain oxidative DNA damage and neurodevelopmental deficits. *J Neurosci*. 2008;28(36):9047-9054. doi:10.1523/JNEUROSCI.2557-08.2008.

168. Morrow BA, Roth RH, Redmond DE, Elsworth JD. Impact of methamphetamine on dopamine neurons in primates is dependent on age: implications for development of Parkinson's disease. *Neuroscience*. 2011;189:277-285. doi:10.1016/j.neuroscience.2011.05.046.

169. Morrow BA, Roth RH, Redmond DE, Sladek JR, Elsworth JD. Apoptotic natural cell death in developing primate dopamine midbrain neurons occurs during a restricted period in the second trimester of gestation. *Exp Neurol*. 2007;204(2):802-807. doi:10.1016/j.expneurol.2007.01.009.

170. Twomey J, LaGasse L, Derauf C, et al. Prenatal methamphetamine exposure, home environment, and primary caregiver risk factors predict child behavioral problems at 5 years. *Am J Orthopsychiatry*. 2013;83(1):64-72. doi:10.1111/ajop.12007.

171. Pardoe HR, Pell GS, Abbott DF, Jackson GD. Hippocampal volume assessment in temporal lobe epilepsy: How good is automated segmentation? *Epilepsia*. 2009;50(12):2586-2592. doi:10.1111/j.1528-1167.2009.02243.x.

172. Rodionov R, Chupin M, Williams E, Hammers A, Kesavadas C, Lemieux L. Evaluation of atlas-based segmentation of hippocampi in healthy humans. *Magn Reson Imaging*. 2009;27(8):1104-1109. doi:10.1016/j.mri.2009.01.008.

173. Sánchez-Benavides G, Gómez-Ansón B, Sainz A, Vives Y, Delfino M, Peña-Casanova J. Manual validation of FreeSurfer's automated hippocampal segmentation in normal aging, mild cognitive impairment, and Alzheimer Disease subjects. *Psychiatry Res*. 2010;181(3):219-225. doi:10.1016/j.pscychresns.2009.10.011.

174. Hollingshead AB. Four factor index of social status. *Yale J Sociol*. 2011;8:21-52. http://elsinore.cis.yale.edu/sociology/yjs/yjs_fall_2011.pdf#page=21.

175. Oishi K, Faria A V., Yoshida S, Chang L, Mori S. Quantitative evaluation of brain development using anatomical MRI and diffusion tensor imaging. *Int J Dev Neurosci*. 2013;31(7):512-524. doi:10.1016/j.ijdevneu.2013.06.004.

176. Gousias IS, Edwards AD, Rutherford MA, et al. Magnetic resonance imaging of the newborn brain: manual segmentation of labelled atlases in term-born and preterm infants. *Neuroimage*. 2012;62(3):1499-1509. doi:10.1016/j.neuroimage.2012.05.083.

177. Xue H, Srinivasan L, Jiang S, et al. Automatic segmentation and reconstruction of the cortex from neonatal MRI. *Neuroimage*. 2007;38(3):461-477. doi:10.1016/j.neuroimage.2007.07.030.

178. Rawson RA, Condon TP. Why do we need an Addiction supplement focused on methamphetamine? *Addiction*. 2007;102 Suppl(SUPPL. 1):1-4. doi:10.1111/j.1360-

0443.2006.01781.x.

179. Fleckenstein AE, Volz TJ, Riddle EL, Gibb JW, Hanson GR. New insights into the mechanism of action of amphetamines. *Annu Rev Pharmacol Toxicol*. 2007;47:681-698. doi:10.1146/annurev.pharmtox.47.120505.105140.

180. Kuhn DM, Angoa-Pérez M, Thomas DM. Nucleus accumbens invulnerability to methamphetamine neurotoxicity. *ILAR J*. 2011;52(3):352-365. doi:10.1093/ilar.52.3.352.

181. Haughey HM, Fleckenstein AE, Metzger RR, Hanson GR. The effects of methamphetamine on serotonin transporter activity: role of dopamine and hyperthermia. *J Neurochem*. 2000;75(4):1608-1617. doi:10.1046/j.1471-4159.2000.0751608.x.

182. Chang L, Alicata D, Ernst T, Volkow N. Structural and metabolic brain changes in the striatum associated with methamphetamine abuse. *Addiction*. 2007;102 Suppl(SUPPL. 1):16-32. doi:10.1111/j.1360-0443.2006.01782.x.

183. Tanabe J, Tregellas JR, Dalwani M, et al. Medial orbitofrontal cortex gray matter is reduced in abstinent substance-dependent individuals. *Biol Psychiatry*. 2009;65(2):160-164. doi:10.1016/j.biopsych.2008.07.030.

184. Kim SJ, Lyoo IK, Hwang J, et al. Frontal glucose hypometabolism in abstinent methamphetamine users. *Neuropsychopharmacology*. 2005;30(7):1383-1391. doi:10.1038/sj.npp.1300699.

185. Elliott L, Loomis D, Lottritz L, Slotnick RN, Oki E, Todd R. Case-control study of a gastroschisis cluster in Nevada. *Arch Pediatr Adolesc Med*. 2009;163(11):1000-1006. doi:10.1001/archpediatrics.2009.186.

186. Thomason ME, Thompson PM. Diffusion imaging, white matter, and psychopathology. *Annu Rev Clin Psychol*. 2011;7(1):63-85. doi:10.1146/annurev-clinpsy-032210-104507.

187. Tobias MC, O'Neill J, Hudkins M, Bartzokis G, Dean AC, London ED. White-matter abnormalities in brain during early abstinence from methamphetamine abuse. *Psychopharmacology (Berl)*. 2010;209(1):13-24. doi:10.1007/s00213-009-1761-7.

188. Lin JC, Jan RK, Kydd RR, Russell BR. Investigating the microstructural and neurochemical environment within the basal ganglia of current methamphetamine abusers. *Drug Alcohol Depend*. 2015;149:122-127. doi:10.1016/j.drugalcdep.2015.01.026.

189. Alhamud A, Tisdall MD, Hess AT, Hasan KM, Meintjes EM, van der Kouwe AJW. Volumetric navigators for real-time motion correction in diffusion tensor imaging. *Magn Reson Med*. 2012;68(4):1097-1108. doi:10.1002/mrm.23314.

190. van der Kouwe AJW, Benner T, Salat DH, Fischl B. Brain morphometry with multiecho MPRAGE. *Neuroimage*. 2008;40(2):559-569. doi:10.1016/j.neuroimage.2007.12.025.

191. Cox RW. AFNI: software for analysis and visualization of functional magnetic resonance neuroimages. *Comput Biomed Res*. 1996;29(3):162-173. doi:10.1006/cbmr.1996.0014.

192. Hüppi PS, Dubois J. Diffusion tensor imaging of brain development. *Semin Fetal Neonatal Med*. 2006;11(6):489-497. doi:10.1016/j.siny.2006.07.006.

193. Jellison BJ, Field AS, Medow J, Lazar M, Salamat MS, Alexander AL. Diffusion tensor imaging of cerebral white matter: a pictorial review of physics, fiber tract

anatomy, and tumor imaging patterns. *AJNR Am J Neuroradiol*. 2004;25(3):356-369. doi:10.1038/nrn2776.

194. Mayo CD, Mazerolle EL, Ritchie L, Fisk JD, Gawryluk JR, Alzheimer's Disease Neuroimaging Initiative. Longitudinal changes in microstructural white matter metrics in Alzheimer's disease. *NeuroImage Clin*. 2017;13:330-338. doi:10.1016/j.nicl.2016.12.012.

195. Gan J, Yi J, Zhong M, et al. Abnormal white matter structural connectivity in treatment-naïve young adults with borderline personality disorder. *Acta Psychiatr Scand*. 2016;134(6):494-503. doi:10.1111/acps.12640.

196. Won E, Choi S, Kang J, et al. Association between reduced white matter integrity in the corpus callosum and serotonin transporter gene DNA methylation in medication-naive patients with major depressive disorder. *Transl Psychiatry*. 2016;6(8):e866. doi:10.1038/tp.2016.137.

197. Akbar N, Giorgio A, Till C, et al. Alterations in Functional and Structural Connectivity in Pediatric-Onset Multiple Sclerosis. *PLoS One*. 2016;11(1):e0145906. doi:10.1371/journal.pone.0145906.

198. Wozniak JR, Lim KO. Advances in white matter imaging: a review of in vivo magnetic resonance methodologies and their applicability to the study of development and aging. *Neurosci Biobehav Rev*. 2006;30(6):762-774. doi:10.1016/j.neubiorev.2006.06.003.

199. Song S, Sun S, Ju W, Lin S, Cross AH, Neufeld AH. Diffusion tensor imaging detects and differentiates axon and myelin degeneration in mouse optic nerve after retinal ischemia. *Neuroimage*. 2003;20(3):1714-1722. doi:10.1016/j.neuroimage.2003.07.005.

200. Fjell AM, Westlye LT, Greve DN, et al. The relationship between diffusion tensor imaging and volumetry as measures of white matter properties. *Neuroimage*. 2008;42(4):1654-1668. doi:10.1016/j.neuroimage.2008.06.005.

201. Melo P, Moreno VZ, Vázquez SP, Pinazo-Durán MD, Tavares MA. Myelination changes in the rat optic nerve after prenatal exposure to methamphetamine. *Brain Res*. 2006;1106(1):21-29. doi:10.1016/j.brainres.2006.05.020.

202. Melo P, Pinazo-Durán MD, Salgado-Borges J, Tavares MA. Correlation of axon size and myelin occupancy in rats prenatally exposed to methamphetamine. *Brain Res*. 2008;1222:61-68. doi:10.1016/j.brainres.2008.05.047.

203. Genc K, Genc S, Kizildag S, et al. Methamphetamine induces oligodendroglial cell death in vitro. *Brain Res*. 2003;982(1):125-130. doi:10.1016/S0006-8993(03)02890-7.

204. Bowyer JF, Schmued LC. Fluoro-Ruby labeling prior to an amphetamine neurotoxic insult shows a definitive massive loss of dopaminergic terminals and axons in the caudate-putamen. *Brain Res*. 2006;1075(1):236-239. doi:10.1016/j.brainres.2005.12.062.

205. Villemagne V, Yuan J, Wong DF, et al. Brain dopamine neurotoxicity in baboons treated with doses of methamphetamine comparable to those recreationally abused by humans: evidence from [11C]WIN-35,428 positron emission tomography studies and direct in vitro determinations. *J Neurosci*. 1998;18(1):419-427. http://www.ncbi.nlm.nih.gov/pubmed/9412518.

206. Kadota T, Kadota K. Neurotoxic morphological changes induced in the medial prefrontal cortex of rats behaviorally sensitized to methamphetamine. *Arch Histol Cytol*. 2004;67(3):241-251. http://www.ncbi.nlm.nih.gov/pubmed/15570889.

207. Oishi K, Mori S, Donohue PK, et al. Multi-contrast human neonatal brain atlas: application to normal neonate development analysis. *Neuroimage*. 2011;56(1):8-20. doi:10.1016/j.neuroimage.2011.01.051.

208. Mabbott DJ, Noseworthy M, Bouffet E, Laughlin S, Rockel C. White matter growth as a mechanism of cognitive development in children. *Neuroimage*. 2006;33(3):936-946. doi:10.1016/j.neuroimage.2006.07.024.

209. McDonnell-Dowling K, Donlon M, Kelly JP. Methamphetamine exposure during pregnancy at pharmacological doses produces neurodevelopmental and behavioural effects in rat offspring. *Int J Dev Neurosci*. 2014;35:42-51. doi:10.1016/j.ijdevneu.2014.03.005.

210. Acuff-Smith KD, Schilling MA, Fisher JE, Vorhees C V. Stage-specific effects of prenatal d-methamphetamine exposure on behavioral and eye development in rats. *Neurotoxicol Teratol*. 1996;18(2):199-215. doi:10.1016/0892-0362(95)02015-2.

211. Slamberová R, Pometlová M, Charousová P. Postnatal development of rat pups is altered by prenatal methamphetamine exposure. *Prog Neuropsychopharmacol Biol Psychiatry*. 2006;30(1):82-88. doi:10.1016/j.pnpbp.2005.06.006.

212. Tavares MA, Silva MC. Differential effects of prenatal exposure to cocaine and amphetamine on growth parameters and morphometry of the prefrontal cortex in the rat. *Ann N Y Acad Sci*. 1996;801:256-273. http://www.ncbi.nlm.nih.gov/pubmed/8959039.

213. Turken A, Whitfield-Gabrieli S, Bammer R, Baldo J V, Dronkers NF, Gabrieli JDE. Cognitive processing speed and the structure of white matter pathways: convergent evidence from normal variation and lesion studies. *Neuroimage*. 2008;42(2):1032-1044. doi:10.1016/j.neuroimage.2008.03.057.

214. Muetzel RL, Mous SE, van der Ende J, et al. White matter integrity and cognitive performance in school-age children: A population-based neuroimaging study. *Neuroimage*. 2015;119:119-128. doi:10.1016/j.neuroimage.2015.06.014.

215. Chaddock-Heyman L, Erickson KI, Voss MW, et al. White matter microstructure is associated with cognitive control in children. *Biol Psychol*. 2013;94(1):109-115. doi:10.1016/j.biopsycho.2013.05.008.

216. Tamnes CK, Østby Y, Walhovd KB, Westlye LT, Due-Tønnessen P, Fjell AM. Intellectual abilities and white matter microstructure in development: a diffusion tensor imaging study. *Hum Brain Mapp*. 2010;31(10):1609-1625. doi:10.1002/hbm.20962.

217. Vestergaard M, Madsen KS, Baaré WFC, et al. White matter microstructure in superior longitudinal fasciculus associated with spatial working memory performance in children. *J Cogn Neurosci*. 2011;23(9):2135-2146. doi:10.1162/jocn.2010.21592.

218. Short SJ, Elison JT, Goldman BD, et al. Associations between white matter microstructure and infants' working memory. *Neuroimage*. 2013;64(1):156-166. doi:10.1016/j.neuroimage.2012.09.021.

219. Alpár A, Di Marzo V, Harkany T. At the Tip of an Iceberg: Prenatal Marijuana and Its Possible Relation to Neuropsychiatric Outcome in the Offspring. *Biol Psychiatry*. 2016;79(7):e33-45. doi:10.1016/j.biopsych.2015.09.009.

220. Willford JA, Chandler LS, Goldschmidt L, Day NL. Effects of prenatal tobacco, alcohol and marijuana exposure on processing speed, visual-motor coordination, and interhemispheric transfer. *Neurotoxicol Teratol*. 2010;32(6):580-588. doi:10.1016/j.ntt.2010.06.004.

221. Minnes S, Lang A, Singer L. Prenatal tobacco, marijuana, stimulant, and opiate

exposure: outcomes and practice implications. *Addict Sci Clin Pract*. 2011;6(1):57-70. http://www.ncbi.nlm.nih.gov/pubmed/22003423.

222. Rivkin MJ, Davis PE, Lemaster JL, et al. Volumetric MRI study of brain in children with intrauterine exposure to cocaine, alcohol, tobacco, and marijuana. *Pediatrics*. 2008;121(4):741-750. doi:10.1542/peds.2007-1399.

223. Jacobsen LK, Picciotto MR, Heath CJ, et al. Prenatal and adolescent exposure to tobacco smoke modulates the development of white matter microstructure. *J Neurosci*. 2007;27(49):13491-13498. doi:10.1523/JNEUROSCI.2402-07.2007.

224. Courtney KE, Ray LA. Methamphetamine: An update on epidemiology, pharmacology, clinical phenomenology, and treatment literature. *Drug Alcohol Depend*. 2014;143(1):11-21. doi:10.1016/j.drugalcdep.2014.08.003.

225. Riddle EL, Fleckenstein AE, Hanson GR. Mechanisms of methamphetamine-induced dopaminergic neurotoxicity. *AAPS J*. 2006;8(2):E413-8. http://www.ncbi.nlm.nih.gov/pubmed/16808044.

226. Rothman RB, Baumann MH, Dersch CM, et al. Amphetamine-type central nervous system stimulants release norepinephrine more potently than they release dopamine and serotonin. *Synapse*. 2001;39(1):32-41. doi:10.1002/1098-2396(20010101)39:1<32::AID-SYN5>3.0.CO;2-3.

227. Volkow ND, Chang L, Wang GJ, et al. Loss of dopamine transporters in methamphetamine abusers recovers with protracted abstinence. *J Neurosci*. 2001;21(23):9414-9418. http://www.ncbi.nlm.nih.gov/pubmed/11717374.

228. Volkow ND, Chang L, Wang GJ, et al. Higher cortical and lower subcortical metabolism in detoxified methamphetamine abusers. *Am J Psychiatry*.

2001;158(3):383-389. doi:10.1176/appi.ajp.158.3.383.

229. Chung YA, Peterson BS, Yoon SJ, et al. In vivo evidence for long-term CNS toxicity, associated with chronic binge use of methamphetamine. *Drug Alcohol Depend*. 2010;111(1-2):155-160. doi:10.1016/j.drugalcdep.2010.04.005.

230. Chang L, Ernst T, Speck O, et al. Perfusion MRI and computerized cognitive test abnormalities in abstinent methamphetamine users. *Psychiatry Res*. 2002;114(2):65-79. doi:10.1016/S0925-4927(02)00004-5.

231. London ED, Berman SM, Voytek B, et al. Cerebral metabolic dysfunction and impaired vigilance in recently abstinent methamphetamine abusers. *Biol Psychiatry*. 2005;58(10):770-778. doi:10.1016/j.biopsych.2005.04.039.

232. Kubicki M, Westin C-F, Maier SE, et al. Diffusion tensor imaging and its application to neuropsychiatric disorders. *Harv Rev Psychiatry*. 2002;10(6):324-336. doi:10.1080/10673220216231.

233. Deoni SCL, O'Muircheartaigh J, Elison JT, et al. White matter maturation profiles through early childhood predict general cognitive ability. *Brain Struct Funct*. 2016;221(2):1189-1203. doi:10.1007/s00429-014-0947-x.

234. Duan J-H, Wang H-Q, Xu J, et al. White matter damage of patients with Alzheimer's disease correlated with the decreased cognitive function. *Surg Radiol Anat*. 2006;28(2):150-156. doi:10.1007/s00276-006-0111-2.

235. Tang CY, Friedman J, Shungu D, et al. Correlations between Diffusion Tensor Imaging (DTI) and Magnetic Resonance Spectroscopy (1H MRS) in schizophrenic patients and normal controls. *BMC Psychiatry*. 2007;7:25. doi:10.1186/1471-244X-7-25.

236. Chen Q, Chen X, He X, Wang L, Wang K, Qiu B. Aberrant structural and functional connectivity in the salience network and central executive network circuit in schizophrenia. *Neurosci Lett*. 2016;627:178-184. doi:10.1016/j.neulet.2016.05.035.

237. Mori S, Zhang J. Principles of diffusion tensor imaging and its applications to basic neuroscience research. *Neuron*. 2006;51(5):527-539. doi:10.1016/j.neuron.2006.08.012.

238. Wu Q, Butzkueven H, Gresle M, et al. MR diffusion changes correlate with ultra-structurally defined axonal degeneration in murine optic nerve. *Neuroimage*. 2007;37(4):1138-1147. doi:10.1016/j.neuroimage.2007.06.029.

239. Song S, Yoshino J, Le TQ, et al. Demyelination increases radial diffusivity in corpus callosum of mouse brain. *Neuroimage*. 2005;26(1):132-140. doi:10.1016/j.neuroimage.2005.01.028.

240. Schmued LC, Bowyer JF. Methamphetamine exposure can produce neuronal degeneration in mouse hippocampal remnants. *Brain Res*. 1997;759(1):135-140. doi:10.1016/S0006-8993(97)00173-X.

241. Deng X, Ladenheim B, Jayanthi S, Cadet JL. Methamphetamine Administration Causes Death of Dopaminergic Neurons in the Mouse Olfactory Bulb. *Biol Psychiatry*. 2007;61(11):1235-1243. doi:10.1016/j.biopsych.2006.09.010.

242. Ouyang A, Jeon T, Sunkin SM, et al. Spatial mapping of structural and connectional imaging data for the developing human brain with diffusion tensor imaging. *Methods*. 2015;73:27-37. doi:10.1016/j.ymeth.2014.10.025.

243. Barkovich AJ. Magnetic resonance techniques in the assessment of myelin and myelination. *J Inherit Metab Dis*. 2005;28(3):311-343. doi:10.1007/s10545-005-5952-

z.

244. Mitter C, Prayer D, Brugger PC, Weber M, Kasprian G. In vivo tractography of fetal association fibers. *PLoS One*. 2015;10(3):e0119536. doi:10.1371/journal.pone.0119536.

245. Ouyang A, Yu Q, Mishra V, et al. Structural development of human brain white matter from mid-fetal to perinatal stage. *Proc SPIE--the Int Soc Opt Eng*. 2015;9417(4):389-400. doi:10.1117/12.2082418.

246. Tavares MA, Silva MC, Silva-Araújo A, Xavier MR, Ali SF. Effects of prenatal exposure to amphetamine in the medial prefrontal cortex of the rat. *Int J Dev Neurosci*. 1996;14(5):585-596. http://www.ncbi.nlm.nih.gov/pubmed/8930690.

247. Cho DH, Lyu HM, Lee HB, Kim PY, Chin K. Behavioral teratogenicity of methamphetamine. *J Toxicol Sci*. 1991;16 Suppl 1(Suppl 1):37-49. doi:10.2131/jts.16.SupplementI_37.

248. Bonelli RM, Cummings JL. Frontal-subcortical circuitry and behavior. *Dialogues Clin Neurosci*. 2007;9(2):141-151. doi:10.1001/archneur.1993.00540080076020.

249. Di Martino A, Scheres A, Margulies DS, et al. Functional connectivity of human striatum: A resting state fMRI study. *Cereb Cortex*. 2008;18(12):2735-2747. doi:10.1093/cercor/bhn041.

250. Rolls ET. The functions of the orbitofrontal cortex. *Brain Cogn*. 2004;55(1):11-29. doi:10.1016/S0278-2626(03)00277-X.

251. Volkow ND, Fowler JS. Addiction, a disease of compulsion and drive: involvement of the orbitofrontal cortex. *Cereb Cortex*. 2000;10(3):318-325. doi:10.1093/cercor/10.3.318.

252. Avants BB, Hackman DA, Betancourt LM, Lawson GM, Hurt H, Farah MJ. Relation of childhood home environment to cortical thickness in late adolescence: specificity of experience and timing. *PLoS One*. 2015;10(10):e0138217. doi:10.1371/journal.pone.0138217.

253. Rao H, Betancourt L, Giannetta JM, et al. Early parental care is important for hippocampal maturation: evidence from brain morphology in humans. *Neuroimage*. 2010;49(1):1144-1150. doi:10.1016/j.neuroimage.2009.07.003.

254. Sethna V, Pote I, Wang S, et al. Mother-infant interactions and regional brain volumes in infancy: an MRI study. *Brain Struct Funct*. December 2016:1-10. doi:10.1007/s00429-016-1347-1.

255. Liu J, Cohen RA, Gongvatana A, Sheinkopf SJ, Lester BM. Impact of prenatal exposure to cocaine and tobacco on diffusion tensor imaging and sensation seeking in adolescents. *J Pediatr*. 2011;159(5):771-775. doi:10.1016/j.jpeds.2011.05.020.

256. El Marroun H, Tiemeier H, Franken IHA, et al. Prenatal Cannabis and Tobacco Exposure in Relation to Brain Morphology: A Prospective Neuroimaging Study in Young Children. *Biol Psychiatry*. 2016;79(12):971-979. doi:10.1016/j.biopsych.2015.08.024.

257. Mychasiuk R, Muhammad A, Gibb R, Kolb B. Long-term alterations to dendritic morphology and spine density associated with prenatal exposure to nicotine. *Brain Res*. 2013;1499:53-60. doi:10.1016/j.brainres.2012.12.021.

258. Nardelli A, Lebel C, Rasmussen C, Andrew G, Beaulieu C. Extensive deep gray matter volume reductions in children and adolescents with fetal alcohol spectrum disorders. *Alcohol Clin Exp Res*. 2011;35(8):1404-1417. doi:10.1111/j.1530-0277.2011.01476.x.

259. Wood J, Freemantle N, King M, Nazareth I. Trap of trends to statistical significance: likelihood of near significant P value becoming more significant with extra data. *BMJ*. 2014;348(mar31 2):g2215. doi:10.1136/bmj.g2215.

260. Pubill D, Chipana C, Camins A, Pallàs M, Camarasa J, Escubedo E. Free radical production induced by methamphetamine in rat striatal synaptosomes. *Toxicol Appl Pharmacol*. 2005;204(1):57-68. doi:10.1016/j.taap.2004.08.008.

261. Thrash-Williams B, Karuppagounder SS, Bhattacharya D, Ahuja M, Suppiramaniam V, Dhanasekaran M. Methamphetamine-induced dopaminergic toxicity prevented owing to the neuroprotective effects of salicylic acid. *Life Sci*. 2016;154:24-29. doi:10.1016/j.lfs.2016.02.072.

262. Kitamura O, Tokunaga I, Gotohda T, Kubo S. Immunohistochemical investigation of dopaminergic terminal markers and caspase-3 activation in the striatum of human methamphetamine users. *Int J Legal Med*. 2007;121(3):163-168. doi:10.1007/s00414-006-0087-9.

263. Moszczynska A, Fitzmaurice P, Ang L, et al. Why is parkinsonism not a feature of human methamphetamine users? *Brain*. 2004;127(Pt 2):363-370. doi:10.1093/brain/awh046.

264. Gluck MR, Moy LY, Jayatilleke E, Hogan KA, Manzino L, Sonsalla PK. Parallel increases in lipid and protein oxidative markers in several mouse brain regions after methamphetamine treatment. *J Neurochem*. 2001;79(1):152-160. doi:10.1046/j.1471-4159.2001.00549.x.

265. Guillot TS, Shepherd KR, Richardson JR, et al. Reduced vesicular storage of dopamine exacerbates methamphetamine-induced neurodegeneration and astrogliosis. *J Neurochem*. 2008;106(5):2205-2217. doi:10.1111/j.1471-4159.2008.05568.x.

266. Cubells JF, Rayport S, Rajendran G, Sulzer D. Methamphetamine neurotoxicity involves vacuolation of endocytic organelles and dopamine-dependent intracellular oxidative stress. *J Neurosci*. 1994;14(4):2260-2271. http://www.ncbi.nlm.nih.gov/pubmed/8158268.

267. Larsen KE, Fon E a, Hastings TG, Edwards RH, Sulzer D. Methamphetamine-induced degeneration of dopaminergic neurons involves autophagy and upregulation of dopamine synthesis. *J Neurosci*. 2002;22(20):8951-8960. doi:22/20/8951 [pii].

268. Kuhn DM, Francescutti-Verbeem DM, Thomas DM. Dopamine disposition in the presynaptic process regulates the severity of methamphetamine-induced neurotoxicity. *Ann N Y Acad Sci*. 2008;1139:118-126. doi:10.1196/annals.1432.026.

269. Escubedo E, Guitart L, Sureda FX, et al. Microgliosis and down-regulation of adenosine transporter induced by methamphetamine in rats. *Brain Res*. 1998;814(1-2):120-126. doi:10.1016/S0006-8993(98)01065-8.

270. Pubill D, Canudas AM, Pallàs M, Camins A, Camarasa J, Escubedo E. Different glial response to methamphetamine- and methylenedioxymethamphetamine-induced neurotoxicity. *Naunyn Schmiedebergs Arch Pharmacol*. 2003;367(5):490-499. doi:10.1007/s00210-003-0747-y.

271. Thomas DM, Walker PD, Benjamins J a, Geddes TJ, Kuhn DM. Methamphetamine neurotoxicity in dopamine nerve endings of the striatum is associated with microglial activation. *J Pharmacol Exp Ther*. 2004;311(1):1-7. doi:10.1124/jpet.104.070961.

272. Sekine Y, Ouchi Y, Sugihara G, et al. Methamphetamine causes microglial activation in the brains of human abusers. *J Neurosci*. 2008;28(22):5756-5761. doi:10.1523/JNEUROSCI.1179-08.2008.

273. Li X, Wang H, Qiu P, Luo H. Proteomic profiling of proteins associated with methamphetamine-induced neurotoxicity in different regions of rat brain. *Neurochem Int*. 2008;52(1):256-264. doi:10.1016/j.neuint.2007.06.014.

274. Krasnova IN, Cadet JL. Methamphetamine toxicity and messengers of death. *Brain Res Rev*. 2009;60(2):379-407. doi:10.1016/j.brainresrev.2009.03.002.

275. Brown JM, Quinton MS, Yamamoto BK. Methamphetamine-induced inhibition of mitochondrial complex II: roles of glutamate and peroxynitrite. *J Neurochem*. 2005;95(2):429-436. doi:10.1111/j.1471-4159.2005.03379.x.

276. Bu Q, Lv L, Yan G, et al. NMR-based metabonomic in hippocampus, nucleus accumbens and prefrontal cortex of methamphetamine-sensitized rats. *Neurotoxicology*. 2013;36:17-23. doi:10.1016/j.neuro.2013.02.007.

277. Yu S, Zhu L, Shen Q, Bai X, Di X. Recent advances in methamphetamine neurotoxicity mechanisms and its molecular pathophysiology. *Behav Neurol*. 2015;2015. doi:10.1155/2015/103969.

278. Skoff RP, Bessert DA, Barks JD, Song D, Cerghet M, Silverstein FS. Hypoxic-ischemic injury results in acute disruption of myelin gene expression and death of oligodendroglial precursors in neonatal mice. *Int J Dev Neurosci*. 2001;19(2):197-208. doi:10.1016/S0736-5748(00)00075-7.

279. Back SA, Luo NL, Mallinson RA, et al. Selective vulnerability of preterm white matter to oxidative damage defined by F2-isoprostanes. *Ann Neurol*. 2005;58(1):108-120. doi:10.1002/ana.20530.

280. Nobuta H, Ghiani CA, Paez PM, et al. STAT3-mediated astrogliosis protects myelin development in neonatal brain injury. *Ann Neurol*. 2012;72(5):750-765.

doi:10.1002/ana.23670.

281. Back S a, Han BH, Luo NL, et al. Selective vulnerability of late oligodendrocyte progenitors to hypoxia-ischemia. *J Neurosci*. 2002;22(2):455-463. doi:22/2/455 [pii].

282. Volpe JJ, Kinney HC, Jensen FE, Rosenberg PA. Reprint of "The developing oligodendrocyte: key cellular target in brain injury in the premature infant". *Int J Dev Neurosci*. 2011;29(6):565-582. doi:10.1016/j.ijdevneu.2011.07.008.

283. Craig A, Ling Luo N, Beardsley DJ, et al. Quantitative analysis of perinatal rodent oligodendrocyte lineage progression and its correlation with human. *Exp Neurol*. 2003;181(2):231-240. doi:10.1016/S0014-4886(03)00032-3.

284. Postuma RB, Dagher A. Basal ganglia functional connectivity based on a meta-analysis of 126 positron emission tomography and functional magnetic resonance imaging publications. *Cereb Cortex*. 2006;16(10):1508-1521. doi:10.1093/cercor/bhj088.

285. Tekin S, Cummings JL. Frontal-subcortical neuronal circuits and clinical neuropsychiatry: an update. *J Psychosom Res*. 2002;53(2):647-654. http://www.ncbi.nlm.nih.gov/pubmed/12169339.

286. Jarbo K, Verstynen TD. Converging structural and functional connectivity of orbitofrontal, dorsolateral prefrontal, and posterior parietal cortex in the human striatum. *J Neurosci*. 2015;35(9):3865-3878. doi:10.1523/JNEUROSCI.2636-14.2015.

287. Choi EY, Yeo BTT, Buckner RL. The organization of the human striatum estimated by intrinsic functional connectivity. *J Neurophysiol*. 2012;108(8):2242-2263. doi:10.1152/jn.00270.2012.

288. Averbeck BB, Lehman J, Jacobson M, Haber SN. Estimates of projection overlap and

zones of convergence within frontal-striatal circuits. *J Neurosci*. 2014;34(29):9497-9505. doi:10.1523/JNEUROSCI.5806-12.2014.

289. Selemon LD, Goldman-Rakic PS. Common cortical and subcortical targets of the dorsolateral prefrontal and posterior parietal cortices in the rhesus monkey: evidence for a distributed neural network subserving spatially guided behavior. *J Neurosci*. 1988;8(11):4049-4068. http://www.ncbi.nlm.nih.gov/pubmed/2846794.

290. Haber SN, Knutson B. The reward circuit: linking primate anatomy and human imaging. *Neuropsychopharmacology*. 2010;35(1):4-26. doi:10.1038/npp.2009.129.

291. Cole DM, Beckmann CF, Searle GE, et al. Orbitofrontal connectivity with resting-state networks is associated with midbrain dopamine D3 receptor availability. *Cereb Cortex*. 2012;22(12):2784-2793. doi:10.1093/cercor/bhr354.

292. Haber SN, Kunishio K, Mizobuchi M, Lynd-Balta E. The orbital and medial prefrontal circuit through the primate basal ganglia. *J Neurosci*. 1995;15(7 Pt 1):4851-4867. http://www.ncbi.nlm.nih.gov/pubmed/7623116.

293. Nakano K. Neural circuits and topographic organization of the basal ganglia and related regions. *Brain Dev*. 2000;22 Suppl 1:S5-16. http://www.ncbi.nlm.nih.gov/pubmed/10984656.

294. Olausson P, Jentsch JD, Krueger DD, Tronson NC, Nairn AC, Taylor JR. Orbitofrontal cortex and cognitive-motivational impairments in psychostimulant addiction: evidence from experiments in the non-human primate. *Ann N Y Acad Sci*. 2007;1121(203):610-638. doi:10.1196/annals.1401.016.

295. Daberkow DP, Kesner RP, Keefe KA. Relation between methamphetamine-induced monoamine depletions in the striatum and sequential motor learning. *Pharmacol*

Biochem Behav. 2005;81(1):198-204. doi:10.1016/j.pbb.2005.03.010.

296. Hanson JE, Birdsall E, Seferian KS, et al. Methamphetamine-induced dopaminergic deficits and refractoriness to subsequent treatment. *Eur J Pharmacol*. 2009;607(1-3):68-73. doi:10.1016/j.ejphar.2009.01.037.

297. Sabol KE, Roach JT, Broom SL, Ferreira C, Preau MM. Long-term effects of a high-dose methamphetamine regimen on subsequent methamphetamine-induced dopamine release in vivo. *Brain Res*. 2001;892(1):122-129. http://www.ncbi.nlm.nih.gov/pubmed/11172757.

298. Gross NB, Duncker PC, Marshall JF. Striatal dopamine D1 and D2 receptors: widespread influences on methamphetamine-induced dopamine and serotonin neurotoxicity. *Synapse*. 2011;65(11):1144-1155. doi:10.1002/syn.20952.

299. Izquierdo A, Belcher AM, Scott L, et al. Reversal-specific learning impairments after a binge regimen of methamphetamine in rats: possible involvement of striatal dopamine. *Neuropsychopharmacology*. 2010;35(2):505-514. doi:10.1038/npp.2009.155.

300. Pereira FC, Cunha-Oliveira T, Viana SD, et al. Disruption of striatal glutamatergic/GABAergic homeostasis following acute methamphetamine in mice. *Neurotoxicol Teratol*. 2012;34(5):522-529. doi:10.1016/j.ntt.2012.07.005.

301. Tulloch I, Afanador L, Mexhitaj I, Ghazaryan N, Garzagongora AG, Angulo JA. A single high dose of methamphetamine induces apoptotic and necrotic striatal cell loss lasting up to 3 months in mice. *Neuroscience*. 2011;193:162-169. doi:10.1016/j.neuroscience.2011.07.020.

302. Busche A, Polascheck D, Lesting J, Neddens J, Teuchert-Noodt G. Developmentally induced imbalance of dopaminergic fibre densities in limbic brain regions of gerbils (

Meriones unguiculatus). *J Neural Transm*. 2004;111(4):451-463. doi:10.1007/s00702-004-0106-2.

303. Palmer LC, Hess US, Larson J, Rogers GA, Gall CM, Lynch G. Comparison of the effects of an ampakine with those of methamphetamine on aggregate neuronal activity in cortex versus striatum. *Brain Res Mol Brain Res*. 1997;46(1-2):127-135. http://www.ncbi.nlm.nih.gov/pubmed/9191086.

304. Wearne TA, Parker LM, Franklin JL, Goodchild AK, Cornish JL. GABAergic mRNA expression is differentially expressed across the prelimbic and orbitofrontal cortices of rats sensitized to methamphetamine: Relevance to psychosis. *Neuropharmacology*. 2016;111:107-118. doi:10.1016/j.neuropharm.2016.08.038.

305. Volkow ND, Chang L, Wang GJ, et al. Low level of brain dopamine D2 receptors in methamphetamine abusers: association with metabolism in the orbitofrontal cortex. *Am J Psychiatry*. 2001;158(12):2015-2021. doi:10.1176/appi.ajp.158.12.2015.

306. Gomes-da-Silva J, Perez-Rosado A, de Miguel R, Fernandez-Ruiz J, Silva MC, Tavares M a. Neonatal methamphetamine in the rat: evidence for gender-specific differences upon tyrosine hydroxylase enzyme in the dopaminergic nigrostriatal system. *Ann N Y Acad Sci*. 2000;914:431-438. http://www.ncbi.nlm.nih.gov/pubmed/11085342.

307. Gomes-da-Silva J, Pérez-Rosado A, de Miguel R, Fernández-Ruiz J, Silva MC, Tavares MA. Prenatal exposure to methamphetamine in the rat: ontogeny of tyrosine hydroxylase mRNA expression in mesencephalic dopaminergic neurons. *Ann N Y Acad Sci*. 2002;965:68-77. http://www.ncbi.nlm.nih.gov/pubmed/12105086.

308. Fukushiro DF, Olivera A, Liu Y, Wang Z. Neonatal exposure to amphetamine alters social affiliation and central dopamine activity in adult male prairie voles.

Neuroscience. 2015;307:109-116. doi:10.1016/j.neuroscience.2015.08.051.

309. Šlamberová R, Vrajová M, Schutová B, et al. Prenatal methamphetamine exposure induces long-lasting alterations in memory and development of NMDA receptors in the hippocampus. *Physiol Res*. 2014;63 Suppl 4:S547-58. http://www.ncbi.nlm.nih.gov/pubmed/25669686.

310. Lloyd SA, Oltean C, Pass H, et al. Prenatal exposure to psychostimulants increases impulsivity, compulsivity, and motivation for rewards in adult mice. *Physiol Behav*. 2013;119:43-51. doi:10.1016/j.physbeh.2013.05.038.

311. Fryer SL, Mattson SN, Jernigan TL, Archibald SL, Jones KL, Riley EP. Caudate volume predicts neurocognitive performance in youth with heavy prenatal alcohol exposure. *Alcohol Clin Exp Res*. 2012;36(11):1932-1941. doi:10.1111/j.1530-0277.2012.01811.x.

312. Voelbel GT, Bates ME, Buckman JF, Pandina G, Hendren RL. Caudate nucleus volume and cognitive performance: Are they related in childhood psychopathology? *Biol Psychiatry*. 2006;60(9):942-950. doi:10.1016/j.biopsych.2006.03.071.

313. Gau SS, Tseng W-L, Tseng W-YI, Wu Y-H, Lo Y-C. Association between microstructural integrity of frontostriatal tracts and school functioning: ADHD symptoms and executive function as mediators. *Psychol Med*. 2015;45(3):529-543. doi:10.1017/S0033291714001664.

314. Wu Y-H, Gau SS-F, Lo Y-C, Tseng W-YI. White matter tract integrity of frontostriatal circuit in attention deficit hyperactivity disorder: association with attention performance and symptoms. *Hum Brain Mapp*. 2014;35(1):199-212. doi:10.1002/hbm.22169.

315. Konrad A, Dielentheis TF, El Masri D, et al. Disturbed structural connectivity is related to inattention and impulsivity in adult attention deficit hyperactivity disorder. *Eur J Neurosci*. 2010;31(5):912-919. doi:10.1111/j.1460-9568.2010.07110.x.

316. Shang CY, Wu YH, Gau SS, Tseng WY. Disturbed microstructural integrity of the frontostriatal fiber pathways and executive dysfunction in children with attention deficit hyperactivity disorder. *Psychol Med*. 2013;43(5):1093-1107. doi:10.1017/S0033291712001869.